

FINAL REPORT  
U.S. Department of Energy  
Fundamental Thermodynamics of Actinide-Bearing Mineral Waste Forms

Principal Investigator: Mark A. Williamson<sup>a,\*</sup>  
Institution: Los Alamos National Laboratory

Collaborators: John Huang,<sup>a</sup> Robert L. Putnam,<sup>a,b,\*</sup> Alexandra Navrotsky<sup>b</sup>, and  
Bartley B. Ebbinghaus<sup>c</sup>

Institutions: <sup>a</sup> Los Alamos National Laboratory

<sup>b</sup> University of California, Davis

<sup>c</sup> Lawrence Livermore National Laboratory.

\* Report prepared for Mark A. Williamson by Robert L. Putnam.

Project Number: TTP# AL17SP23

Grant Number: Such as DE-FG07-9745673

Grant Project Officers: Mark Gilbertson, DOE EM50

Project Duration: September 1997 through September 2000

## Table of Contents

<b>1.0</b>	<b>Executive Summary</b>	<b>3</b>
<b>2.0</b>	<b>Research Objectives and findings</b>	<b>6</b>
<b>3.0</b>	<b>Calorimetric Methodology</b>	<b>10</b>
	3.1 Calorimeters	10
	3.2 Types of Experiments	11
<b>4.0</b>	<b>Summary of Project Results</b>	<b>12</b>
	4.1 Thermodynamic Quantities	13
	4.2 Publications	15
	4.3 Participation	16
<b>5.0</b>	<b>Summary of recent progress and future direction at individual institutions.</b>	<b>17</b>
	5.1 Los Alamos National Laboratory, LANL	17
	5.2 University of California at Davis, UCD	17
	5.3 Lawrence Livermore National Laboratory, LLNL	18
<b>6.0</b>	<b>References</b>	<b>19</b>
<b>7.0</b>	<b>Appendix</b>	<b>20</b>
	A. Plutonium Immobilization Project Baseline Formulation	
	B. Manuscripts submitted or in press at the time of this report.	
<b>Table Summary</b>		
	1. Summary of SYNROC and related variants	7
	2. High Temperature Calorimetric Experiments	11
	3. Key thermodynamic quantities obtained in this study.	13
	4. Publications resulting from this study.	14
	5. Individuals supported by / or contributing to this project.	15
<b>Figure Summary</b>		
	1. $\text{CaTiO}_3\text{-HfTiO}_4\text{-AnTi}_2\text{O}_6$ phase diagram at 1350°C in air.	9

## 1.0 Executive Summary:

The end of the Cold War raised the need for the technical community to be concerned with the disposition of surplus nuclear weapon material. The United States Department of Energy has determined that surplus weapons plutonium belonging to the United States will be either burned as a mixed-oxide fuel (MOX) or incorporated into a ceramic material and then placed in a geologic repository. (US DOE ROD 2000)

The form of that ceramic material is a solid solution between four end member phases;  $\text{CaHfTi}_2\text{O}_7$ ,  $\text{CaUTi}_2\text{O}_7$ ,  $\text{CaPuTi}_2\text{O}_7$ , and  $\text{Gd}_2\text{Ti}_2\text{O}_7$ . (Ebbinghaus 2000, see Appendix A). The stability and behavior of plutonium in the proposed ceramic end member materials has only begun to be understood. Our studies into the fundamental thermodynamics of actinide substitution into these phases have begun to provide a basis for technically sound solutions to the issue of a safe, secure, and environmentally acceptable waste material. Our work has found thermodynamic trends that are beginning to be illuminated which can assist in better understanding the chemistry and phase equilibria of actinide substitution into the proposed immobilization matrix.

High temperature oxide melt solution calorimetry, one of the most powerful techniques and sometimes the only technique for providing the fundamental thermodynamic data (enthalpies) needed to extend our understanding of the phase relationships, fabrication parameters, and predictability of the proposed ceramic waste form, has been used. When combined with low temperature heat capacity measurements (yielding entropies and heat capacities), solution calorimetry provides

a full understanding of the energetics of formation (e.g., enthalpy, entropy, and Gibbs free energy) of these materials and allows the accurate modeling of the phase relationships, chemical durability, and fabrication parameters needed to optimize their compositions. The purpose of this EMSP project was to experimentally determine the enthalpy, entropy, and Gibbs free energies of formation of phases that are key to the disposition matrix (Ebbinghaus 2000, see Appendix A) of surplus weapons plutonium and its potential decomposition products.

Collaboration in this project was three fold. Samples were synthesized at Lawrence Livermore National Laboratory, LLNL, (Ebbinghaus) and at the University of California, Davis, UCD, (Navrotsky and Putnam) with supplemental synthesis efforts on zircon,  $AnSiO_4$  (where  $An = Pu, U, \text{ and } Zr$ ) performed at Los Alamos National Laboratory, LANL, (Williamson and Huang). Solution calorimetry on successfully synthesized samples was performed at UCD (Navrotsky and Putnam) on non-radioactive materials and those materials containing uranium and thorium. A high-temperature solution calorimeter similar to those used at UCD but capable of use with actinide-containing materials was installed at Los Alamos National Laboratory, LANL, (Williamson and Putnam). Prior to the end of project funding, plutonium-containing samples had not been successfully synthesized or sufficiently characterized to determine that they were in a sufficiently phase-pure form to be examined on the solution calorimeter at LANL. However a suitable sample of Pu-pyrochlore,  $CaPuTi_2O_7$ , has recently been synthesized by Ebbinghaus at LLNL.

External collaboration at Brigham Young University, BYU, under non-EMSP funds (LLNL – Ebbinghaus) was initiated by Putnam and Navrotsky to determine the

heat capacities and entropies of several of the phases examined. This fruitful collaboration has extended the usefulness and value of this study considerably and is especially noteworthy.

In summary, this three-year project has yielded 90 measured and derived thermodynamic quantities with an additional 30 estimated quantities representing information on a total of 27 different mineral phases where no data existed prior to our study. To date, two graduate degrees have been (Ph.D. Putnam 1999) or will soon be awarded (Ph.D. Helean 2001) with 10 peer reviewed papers in print (see Table 4), three additional papers in press or undergoing peer review (Table 4 and appendix B), at least five other papers in preparation, and over 25 invited lectures, abstracts, and / or presentations have been given at national and international scientific meetings based on work from this project.

## 2.0 Research Objectives and findings

In September 2000, the U.S. and Russia reached an agreement to jointly disposition roughly 68 metric tons of weapons usable plutonium. (Agreement 2000) In Russia, 34 metric tonnes of weapons-grade plutonium will be dispositioned by burning the plutonium as mixed oxide (MOX) fuel. In the U.S., 25 metric tons of plutonium recovered from pits and clean metal will likewise be dispositioned by burning as mixed oxide (MOX) fuel and about 9 metric tonnes of plutonium stored throughout the DOE complex will be dispositioned by immobilization in a ceramic which will then be encapsulated in high-level waste (HLW) glass. In all cases, the plutonium will be made equal to or less attractive for reuse in nuclear weapons than the much larger and growing inventory of plutonium in spent nuclear fuel. This threshold of unattractiveness is commonly referred to as the "spent fuel standard." In the U.S., the final products from plutonium disposition, irradiated fuel and ceramic encapsulated HLW, will be emplaced in the Federal Waste Repository, which is assumed to be Yucca Mountain.

The ceramic form selected for the disposition of plutonium is composed of a series of titanate-based phases which are generally referred to as SYNROC (short for Synthetic Rock). The particular formulation that was selected is composed of about 80 vol % pyrochlore, about 15 vol % brannerite, and about 5 vol % rutile. If impurities are present in the  $\text{PuO}_2$  feed material, about a half a dozen other phases can also form. The most common of these are zirconolite and a silicate glass. A screening process conducted in 1995, resulted in the selection of borosilicate glasses and titanate-based ceramics (e.g. SYNROCs) as the best available options for immobilization of plutonium. In 1998, a pyrochlore-rich ceramic form was selected in preference to a boro-silicate glass form. More information about the development and selection of the ceramic formulation can be found in the Plutonium Immobilization Program's Baseline Formulation report. (Ebbinghaus 2000)

Although the pyrochlore-rich ceramic is the most current application for titanate-based ceramics, the concept of SYNROC has been around for some time. The idea was first proposed by Ringwood in 1978. (Ringwood 1978) The strategy of SYNROC is to immobilize the radioactive isotopes of HLW in a mixture of minerals that all have analogs in nature that

- have survived for periods exceeding 20 million years in a wide variety of geochemical environments
- have crystal chemical properties that allow them to accept a wide range of elements into their crystalline matrix
- are thermodynamically stable together

A wide range of minerals meet these three criteria. Titanate-rich minerals were selected by Ringwood because they not only meet the above criteria, but are based on one of the most insoluble oxides known, namely  $\text{TiO}_2$ . A wide variety of different SYNROC formulations have been proposed for different HLW and actinide feed materials. These formulations and the processes used to make them are summarized in Table 1. For immobilization of HLW, SYNROC-C has received the most study.

summarized in **Table 1**. For immobilization of HLW, SYNROC-C has received the most study.

**Table 1. Summary of SYNROC and related variants**

Form Name	Mineralogy*	"Waste" Loading	Fabrication Process
SYNROC-A	40% Ba-feldspar, 30% hollandite, 20% perovskite, 10% zirconia, kalsilite, and/or leucite	10% HLW	Melting and Crystallizing 1330°C
SYNROC-B	40% hollandite, 35% zirconolite, 25% perovskite,	None	Hot Pressing 1200-1400°C
SYNROC-C	33% hollandite, 28% zirconolite, 19% perovskite, 15% rutile, 5% noble metal alloy	20% HLW	Hot Pressing 1150°C
SYNROC-D	46% spinel solid solution, 19% zirconolite, 17% nepheline, 15% perovskite, 3% hollandite	63% HLW sludge	Hot Pressing 1050-1100°C
SYNROC-E	79% rutile, 7% zirconolite, 7% perovskite, 5% hollandite, 2% pyrochlore	7% HLW	Hot Pressing 1300°C
SYNROC-F	90% pyrochlore, 5% hollandite, 5% rutile	50% U-rich HLW	Hot Pressing 1250°C
SYNROC-FA	89% pyrochlore, 8% perovskite, 3% uraninite	50% U-rich HLW	Cold Pressing and Sintering 1250-1400°C
Mixed Waste Ceramic	36% nepheline, 31% spinel solid solution, 12% zirconolite, 12% perovskite, 5% rutile, 4% whitlockite	40% residue	Cold Pressing and Sintering 1150-1200°C
Pu Ceramic Zirconolite-rich	80% zirconolite (with some pyrochlore), 10% hollandite, 10% rutile, <1% PuO <sub>2</sub>	12% Pu	Cold Pressing and Sintering 1325-1400°C
Pu Ceramic Pyrochlore-rich	85% pyrochlore, 10% brannerite, 5% rutile, <1% uraninite solid solution	10% Pu and 21% U	Cold Pressing and Sintering 1275-1400°C

\*All percents are given in weight percent.

Most of this SYNROC work including a pilot scale demonstration has been conducted at the Australian Nuclear Science and Technology Organization (ANSTO). For the immobilization of actinides, namely plutonium, the pyrochlore-rich ceramic has received the most study. Most of this work has been conducted in the Plutonium Immobilization Program (PIP). This is a multi-site effort including a number of DOE laboratories (ANL, LLNL, PNNL, and WSRC) and related contract work with universities (BYU and UCD) and foreign laboratories (ANSTO)

For all of the minerals listed in **Table 1**, it is important that the radioactive materials are effectively retained and it is important that the relative stability of the minerals are understood. In the case of SYNROC-C, the primary minerals of interest are zirconolite, hollandite, and perovskite. In the case of the pyrochlore-rich ceramic, the primary minerals of interest are pyrochlore, brannerite, and rutile.

In addition to the pyrochlore-rich ceramic, a number of other mineral phases have been proposed for the immobilization of plutonium and other actinides. These have all received some degree of recognition and study. These mineral phases

include zircon (Webber 1996 and Burakov 1996), zirconia (Degueldre 1996), and monazite (Boatner 1988) which was originally proposed for the immobilization of HLW. More recently zirconate-based pyrochlores (Wang 1999 and Sickafus 2000) have been proposed. All of these immobilization forms have the capability to incorporate significant amounts of plutonium and neutron absorbers for criticality safety and offer high durability in geologic environments. Therefore, they are also of interest in this thermodynamic study.

In order for the radioactive constituents to be effectively retained, the constituent mineral phases in the immobilization form must be resistant to dissolution in aqueous environments. Dissolution is related at least in part to solubility, which can be determined from a knowledge of the thermodynamics of the aqueous species and solid phases. The solubility in a complex system is usually calculated with the assistance of a free energy minimization program such as EQ3/6 and the accuracy is only as good as the data that are used. Thermodynamics for most of the solid phases of interest were not available and in most cases have since been determined by this work and related work in the Plutonium Immobilization Program.

It is also valuable to understand the relative stability of the constituent phases so that processing conditions are designed in a way that the desired phases are always obtained. The relative stability of the constituent phases are given by the thermodynamics of the solid phases under the conditions of fabrication. Again, these thermodynamics were not available and have since been determined by this work and related work in the Plutonium Immobilization Program. As an example, **Figure 1** shows the relevant phase equilibria in the pyrochlore-rich ceramic, the diagram was determined from quantitative EDS analyses at ANSTO (A in the legend) and by electron microprobe analyses at LLNL (L in the legend). In this representation,  $\text{UO}_2$ ,  $\text{PuO}_2$ , and  $\text{GdO}_{1.5}$  are considered as a single component and plotted on the same axis.  $\text{TiO}_2$  is excluded from the plot since all compositions are in equilibrium with rutile and its activity is therefore fixed at unity. A considerable amount of work has been conducted in the Plutonium Immobilization Program on how the stability of the phases in **Figure 1** are affected by changes in the base composition, plutonium oxide feed impurities, and processing conditions. (Ebbinghaus 2000) Ultimately, these changes are determined by the thermodynamic stability of the individual phases, which is the subject of this work.

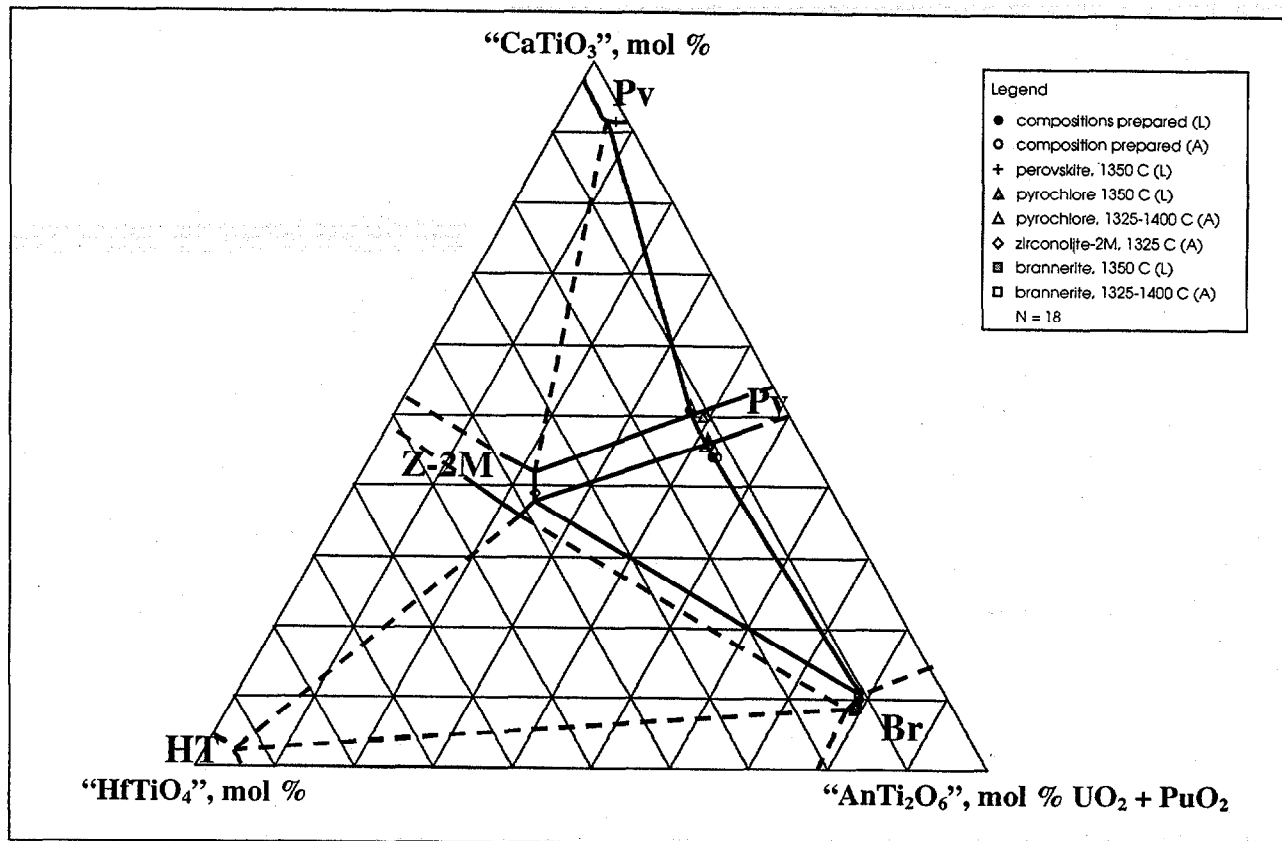


**Figure 1.**  $\text{CaTiO}_3\text{-HfTiO}_4\text{-AnTi}_2\text{O}_6$  phase diagram at  $1350^\circ\text{C}$  in air.  $\text{An} = \text{U} + \text{Pu} + \text{Gd}$ .  $\text{B} =$  brannerite,  $\text{HT} =$  hafnium titanate,  $\text{Py} =$  pyrochlore,  $\text{Pv} =$  perovskite,  $\text{Z-2M} =$  zirconolite-2M

In this work, the enthalpy of formation of the end-member phases of interest has been determined. These include end-members compositions of zirconolite, pyrochlore, brannerite, hafnium titanate, perovskite, zircon, and monazite. Related heat capacity work conducted at BYU and supported by the PIP allows one to determine the remaining thermodynamic parameters for many of these end-member.

Most immediately, the thermodynamic data provided by this work will be used by the Plutonium Immobilization Program. The data is likely to be provided to DOE-RW as part of a supplemental input for the licensing application for the Federal Waste Repository. If used in their analyses, the data will be added to their thermodynamic equilibrium codes, namely EQ3/6. The data will also be used by the PIP to better understand stability of the mineral phases during sample fabrication. In this application, the thermodynamic data will be added to a suitable free energy minimization program such as the FACT program and the phase equilibria will be calculated as a function of the composition, atmosphere, and processing temperature. Ultimately, it is hoped that these data will be incorporated into the standard databases for all the commonly used free energy minimization programs, EQ3/6, FACT, Thermocalc, HSC, and MTDData to name a few. Although the PIP has

the most immediate use of these data, similar ceramic forms continue to be proposed and developed for which the data obtained in this work will continue to be of value.

### 3.0 Calorimetric Methodology

#### 3.1 Calorimeters

High-temperature reaction calorimetry refers to the measurement of heats of chemical reactions at temperatures above 400°C. The reactions may be of direct interest (e.g., the melting of a silicate), the oxidation of a manganese oxide, the dehydration of a zeolite, or they may represent steps in a thermodynamic cycle needed to obtain the enthalpy of interest (e.g., enthalpy of solution in molten solvent to obtain the enthalpy of formation or phase transition). The latter approach, called high temperature oxide melt solution calorimetry, has been used widely (see Navrotsky 1977, 1997 for reviews). The advantages of calorimetry at high temperature generally lie in rapid and reproducible reactions of refractory materials.

The solution calorimeters used are of several types, but most have several features in common. They generally measure heat flow between a sample and heat sink maintained at an essentially constant temperature; thus they are of the isoperibol type. They are generally of the twinned variety, with two sample chambers, each surrounded by a Pt-PtRh thermopile linking it to a constant temperature metallic block. The thermopiles are linked in series opposition, and the twinned design both increases productivity and, more importantly, helps minimize the deleterious effects of small drifts in furnace and/or ambient temperature. Though no radical changes in calorimeter design have been made over the past twenty years, a number of incremental improvements have accumulated to improve the signal stability, the so called baseline, to increase the sensitivity by about a factor of seven. These improvements make routine the measurement of heat effects as small as 0.5 joule, and the use of 5-15 mg samples of silicates for solution calorimetry, in contrast with the 30-50 mg samples used in the late 1970's.

Adiabatic calorimeters are used to measure the constant pressure heat capacities ( $C_p$ ) of solids. The sample and sample holder (the calorimeter) are surrounded by thermal shields maintained at the same temperature as the sample. Unlike a reaction calorimeter, it is necessary that an adiabatic calorimeter cover a wide temperature range (from below 20 K to at least room temperature) in order to calculate third-law entropies from the heat capacity data using the relation

$$S_m^o = \int_0^T C_p / T dT . \text{ Enthalpy increments are also calculated from temperature}$$

dependent heat capacity data ( $\Delta_0^T H_m^o = \int_0^T C_p dT$ ) which, when combined with absolute

entropies and formation enthalpies measured using reaction calorimeters, can give the temperature dependence of the Gibbs free energy of formation for a particular material.

The adiabatic calorimeter at BYU is only one of two or three such instruments currently operational in the U.S. This apparatus has a demonstrated temperature range from 5 K to 400 K with an accuracy within  $\pm 0.1\%$  and a resolution better than 0.1%. Sample sizes are generally on the order of 10 g. Although the high-temperature limit of the adiabatic calorimeter is 400 K, it has clearly been shown (Woodfield 1999) that it is possible to extrapolate the heat capacity data to high-temperatures with reasonable accuracy for these ceramics.

### 3.2 Types of Experiments

**Table 2** summarizes the types of experiments that can be done in a high temperature reaction calorimeter. A transposed temperature drop experiment consists of dropping a sample from room temperature into the hot calorimeter with no solvent present. If no phase change or chemical reaction occurs, the heat content,  $H_{\text{cal temp}} - H_{\text{room temp}}$ , is measured. Its temperature derivative gives the average heat capacity. If a phase transition, solid-solid or solid-liquid, takes place, the enthalpy of that change is included in the measurement. Measurements at several different calorimeter temperatures map out the heat capacity and enthalpy of transition.

#### **Table 2. High Temperature Calorimetric Experiments**

Calorimeter is essentially isothermal

##### ***Solvent present***

- Solution calorimetry: sample equilibrated in hot calorimeter, then dissolved. Differences in heats of solution give heat of reaction at calorimeter T.
- Drop solution calorimetry: sample dropped from room T. Sample may be encapsulated in Au or Pt, pyrex or silica glass (which dissolves) or lead borate glass (same as solvent), or as unencapsulated pellets. Differences in heats of drop-solution give heat of reaction at room T.

##### ***Solvent absent***

- Transposed temperature drop calorimetry. No permanent changes in sample: heat content measurement, includes heat of any rapid and reversible phase change.
  - Sample changes oxidation state: difference between first and second drop related to heat of redox reaction.
  - Sample loses  $\text{H}_2\text{O}$ ,  $\text{CO}_2$  or other volatiles: difference related to heat of devolatilization.
  - Sample undergoes irreversible phase change: difference gives heats transformation at room T.
  - Sample undergoes change in degree of order or other structural parameters: difference gives ordering energy.

If the sample undergoes an irreversible chemical change (e.g., annealing, decomposition, dehydration, or oxidation reduction) upon dropping, the heat effect associated with that process is included in the measurement the first time the sample is dropped into the calorimeter. An example of such an application is the study of radiation damage in zircon (Ellsworth 1994).

Dropping the sample into a solvent is called drop-solution calorimetry. It measures the heat content of the sample plus its enthalpy of solution at the

calorimetric temperature. The difference in enthalpy of drop solution of reactants and products gives the enthalpy of transformation at room temperature.

In solution calorimetry, the sample is equilibrated in the calorimeter for several hours before being stirred into the solvent and dissolved. The difference in enthalpy of solution of reactants and products yields the enthalpy of the reaction at the calorimetric temperature.

If the sample persists at calorimetric temperature, then all three types of experiments can be done. Since the enthalpy of drop solution is the sum of heat content and heat of solution, confirming this equality experimentally is a powerful indication that the calorimeter calibration factors are correct for each type of experiment, that the dissolution reactions go to completion, and that no unsuspected decomposition reactions are occurring.

#### **4.0 Summary of Project Results**

**Table 3** contains an excerpt from Putnam et al. (Putnam 2001) which published a partial thermodynamic database for use in examining the stability, performance, and reliability of many of the proposed waste matrices for surplus weapon's plutonium.

**Table 4** lists the completed manuscripts that have resulted from this work. In some cases the manuscripts have not completed the peer review process. In these cases we include the full, as submitted, manuscripts in **appendix B**. **Table 5** contains a listing of individuals at each institution that were supported by or contributed to this project.

## 4.1 Thermodynamic Quantities

**Table 3. Key thermodynamic quantities obtained in this study.**

Fundamental standard molar thermodynamic functions valid at 298.15 K. Units are found in the table headings. The standard state pressure is 1 atm (101 325 Pa). Errors are reported in parenthesis () applicable notes are reported in braces {} (e.g., {ac} represents the application of notes a and c). Reported for each compound are: the molar mass ( $M_w$ ), the molar volume ( $V^\circ$ ), the standard molar entropy ( $S^\circ$ ), the standard molar enthalpy ( $\Delta_f H^\circ$ ), the standard molar Gibbs free energy ( $\Delta_f G^\circ$ ), and the enthalpies of reactions 1 ( $\Delta_r H^\circ(1)$ ) and 2 ( $\Delta_r H^\circ(2)$ ) which are: 1) the enthalpies of compound formation from the binary oxides and 2) the from the binary oxides plus perovskite,  $\text{CaTiO}_3$ , respectively. Data obtained in our current EMSP is **boldfaced** and estimated values are *italicized*. Literature values are referenced in Putnam 2001.

Compound name [phase, allotrope]	$M_w$ $\text{g} \cdot \text{mol}^{-1}$	$V^\circ$ $\text{cm}^3 \cdot \text{mol}^{-1}$	$S^\circ$ $\text{J} \cdot \text{K}^{-1} \cdot \text{mol}^{-1}$	$\Delta_f H^\circ$ $\text{kJ} \cdot \text{mol}^{-1}$	$\Delta_f G^\circ$ $\text{kJ} \cdot \text{mol}^{-1}$	$\Delta_r H^\circ(1)$ $\text{kJ} \cdot \text{mol}^{-1}$	$\Delta_r H^\circ(2)$ $\text{kJ} \cdot \text{mol}^{-1}$
<b>Zirconolite / Pyrochlore</b>							
$\text{CaZrTi}_2\text{O}_7$ [cr]	337.0558 {a}	76.00 {b}	<b>193.3</b> (0.38)	<b>-3713.7</b> (4.5)	<b>-3514.5</b> (4.5)	<b>-88.79</b> (4)	<b>-8.1</b> (4.6)
$\text{CaHfTi}_2\text{O}_7$ [cr]	424.3258 {a}	76.48 {b}	<b>194.4</b> (0.38)	<b>-3752.2</b> (4.9)	<b>-552.03</b> (4.9)	<b>-111.5</b> (4.4)	<b>-29.9</b> (5.3) {b}
$\text{CaCeTi}_2\text{O}_7$ [cr]	385.9558 {a}	79.63 {b}	{c}	<b>-3666.5</b> (6.3)	{c}	<b>-54.7</b> (5.5) {b}	<b>+26.9</b> (6.3) {bd}
$\text{CaPuTi}_2\text{O}_7$ [cr]	484.888 {a}	78.11 {b}		<i>-3636</i> (6) {e}		<i>-56.9</i> (5.6) {e}	<i>+25</i> (6) {de}
$\text{CaUTi}_2\text{O}_7$ [cr]	483.8647 {a}	79.34 {b}		<i>-3653</i> (9) {e}		<i>-44.9</i> (9.4) {e}	<i>+36.8</i> (9.8) {de}
$\text{CaThTi}_2\text{O}_7$ [cr]	477.8739 {a}			<i>-3782</i> (9) {e}		<i>-32.1</i> (9.6) {e}	<i>+49</i> (10) {de}
$\text{Gd}_2\text{Ti}_2\text{O}_7$ [cr]	522.2558 {a}	80.01 {b}	{c}	<b>-3820.9</b> (4.7) {b}	{c}	<b>-113.3</b> (2.7)	
<b>Brannerite</b>							
$\text{CeTi}_2\text{O}_6$ [cr]	329.8764 {a}	67.263 {b}	<i>174.7</i> (4.8) {bf}	<b>-2958.4</b> (5.1) {b}	<i>-2787.0</i> (5.5) {bf}	<b>+18.3</b> (4.7) {d}	
$\text{ThTi}_2\text{O}_6$ [cr]	421.7945 {a}	69.348 {b}	<i>168.5</i> (4.7) {bf}	<b>-3111</b> (6) {b}	<i>-2943.9</i> (6.1) {bf}	<b>+3.4</b> (4.6) {10d}	
$\text{PuTi}_2\text{O}_6$ [cr]	428.8086 {a}	66.155 {b}	<i>196.9</i> (20.1) {bf}	<b>-2896</b> (20.1) {b}	<i>-2736.6</i> (20.) {bf}	<b>+48</b> (20) {de}	
$\text{UTi}_2\text{O}_6$ [cr]	427.7853 {a}	67.249 {b}	<i>174.4</i> (4.3) {bcf}	<b>-2979.2</b> (4.5) {b}	<i>-2809.4</i> (4.5) {bf}	<b>-6.1</b> (4.1)	
<b>Zircon</b>							

Compound name [phase, allotrope]	Mw g • mol <sup>-1</sup>	V <sup>o</sup> cm <sup>3</sup> • mol <sup>-1</sup>	S <sup>o</sup> J • K <sup>-1</sup> • mol <sup>-1</sup>	$\Delta_f H^o$ kJ • mol <sup>-1</sup>	$\Delta_f G^o$ kJ • mol <sup>-1</sup>	$\Delta_r H^o$ (1) kJ • mol <sup>-1</sup>	$\Delta_r H^o$ (2) kJ • mol <sup>-1</sup>
ZrSiO <sub>4</sub> [cr]	183.3031 {a}	39.26 {b}	84.0 (1.3)	-2034.2 (3.1)	-1919.7 (3.1)	-22.9 (3.6) {b}	
HfSiO <sub>4</sub> [cr]	270.5731 {a}	38.79 {b}			-1973.36 {gh}		
CeSiO <sub>4</sub> [cr]	232.2031 {a}				-1874.59 {ghi}		
PuSiO <sub>4</sub> [cr]	331.1353 {a}	44.66 {b}			-1854.37 {gh}		
USiO <sub>4</sub> [cr]	330.112 {a}	45.84 {b}	118 (12)	-1991.3 (5.4)	-1883.6 (4.0)	+4.4 (5.5) {b}	
ThSiO <sub>4</sub> [cr]	324.1212 {a}	48.41 {b}			-2050.1 (4.3)		
AmSiO <sub>4</sub> [cr]	335.0831 {a}				-1764.77 {gh}		
<b>Monazite</b>							
LaPO <sub>4</sub> [cr]	233.8769 {a}	45.679 {k}		-1955.2 (2.1) {b}		-306 (2)	
CePO <sub>4</sub> [cr]	235.0914 {a}	44.695 {k}		-1959.5 (4.6) {b}		-309 (2)	
NdPO <sub>4</sub> [cr]	239.2114 {a}	43.554 {k}		-1960.4 (2.0) {b}		-304 (2)	
EuPO <sub>4</sub> [cr]	246.9314 {a}	42.02 {k}		-1850.1 (5.1) {b}		-272 (3)	
YbPO <sub>4</sub> [cr]	268.0114 {a}	41.73 {k}		-1966.1 (2.3) {b}		-261 (2)	
LuPO <sub>4</sub> [cr]	269.9384 {a}	41.33 {k}		-1582.6 (2.5)		-256 (2.5)	
PuPO <sub>4</sub> [cr]	334.0236 {a}			-1916 (14) {b}		-264 (14) {be}	
UPO <sub>4</sub> [cr]	333.0003 {a}			-1752 (17) {b}		-272.7 (14) {be}	
AmPO <sub>4</sub> [cr]	337.9714 {a}			-1888 (15) {b}		-273 (14) {be}	
<b>Other Phases</b>							
CaTiO <sub>3</sub> [cr, perovskite]	134.9582 {a}	33.69 {b}	93.3 (0.2)	-1660.8 (3.3)	-1575.3 (3.3)	-81.7 (2.9)	

Compound name [phase, allotrope]	Mw g • mol <sup>-1</sup>	V <sup>o</sup> cm <sup>3</sup> • mol <sup>-1</sup>	S <sup>o</sup> J • K <sup>-1</sup> • mol <sup>-1</sup>	$\Delta_f H^o$ kJ • mol <sup>-1</sup>	$\Delta_f G^o$ kJ • mol <sup>-1</sup>	$\Delta_r H^o$ (1) kJ • mol <sup>-1</sup>	$\Delta_r H^o$ (2) kJ • mol <sup>-1</sup>
ZrTiO <sub>4</sub> [cr]	202.0976 {a}	39.95 {b}	111.0 (0.2)	-2023.8 (4.2)	-1913.8 (4.3)	+20.5 (4.1) {d}	
HfTiO <sub>4</sub> [cr]	289.3676 {a}	40.07 {b}		{c}		{c}	

**Notes to table 3.**

- Value calculated by the authors from data found in a publication referenced by Putnam et al. (Putnam 2001).
- Value calculated by the authors for this work.
- Measured data forthcoming in a future publication.
- Metastability predicted or potential for metastability is predicted based on the value and its error margins.
- Estimated using systematic trends described by Putnam in (Ph.D. Putnam 1999).
- Values of S are estimated based on assumed sample stability at a synthesis temperature of 1623 K (synthesis temp of Ce, U, and Th brannerite samples). Values of G are calculated based on entropy stabilization from binary oxides at 1623 K.
- Published results corrected for improper conversion from calories to J. as noted by the authors through personal communication.
- Uses a linear free energy relationship to predict the Gibbs free energy of formation as noted by Xu (Xu1999).
- Predicted definitely to be metastable with respect to decomposition. Delta G for CeO<sub>2</sub> + SiO<sub>2</sub> = CeSiO<sub>4</sub> is calculated to be +7.1 (2.1) at 298.15 K.
- Predicted to possibly be metastable with respect to decomposition. Delta G for PuO<sub>2</sub> + SiO<sub>2</sub> = PuSiO<sub>4</sub> is calculated to be -0.11 (1.2) at 298.15 K.
- Calculated for this work from data found in another reference found in this work.

## 4.2 Publications

### Table 4. Publications resulting from this study.

- "Thermodynamics of Formation for Zirconolite, CaZrTi<sub>2</sub>O<sub>7</sub>, From T= 298 K to T= 1500 K." *J. Chem. Thermodynamics* **1999**, 31, 3, 229-243. R. L. Putnam, A. Navrotsky, B. F. Woodfield, J. Boerio-Goates, J. L. Shapiro.
- "Molar Heat Capacity and Thermodynamic Functions of Zirconolite, CaZrTi<sub>2</sub>O<sub>7</sub>." *J. Chem. Thermodynamics* **1999**, 31, 3, 245-253. B. F. Woodfield, J. Boerio-Goates, J. L. Shapiro. R. L. Putnam, A. Navrotsky.
- "Heat capacity, third law entropy, and formation energetics of zirconolite, CaZrTi<sub>2</sub>O<sub>7</sub>." R. L. Putnam, A. Navrotsky, B. F. Woodfield, J. L. Shapiro, and J. Boerio-Goates *Environmental Issues and Waste Management Technologies in the Ceramic and Nuclear Industries IV*; eds. J. C. Marra and G. T. Chandler; The American Ceramic Society; Westerville, OH **1999**, 93, 339-347.
- "Thermochemistry of Hf-zirconolite, CaHfTi<sub>2</sub>O<sub>7</sub>." R. L. Putnam, A. Navrotsky, B. F. Woodfield, J. L. Shapiro, R. Stevens, and J. Boerio-Goates *Mat. Res. Soc. Proc.* **1999**, 556, 11-18.
- "Molar Heat Capacity and Thermodynamic Functions for CaTiO<sub>3</sub>." *J. Chem. Thermodynamics* **1999**, 31, 12, 1573-1583. B. F. Woodfield, J. L. Shapiro, R. Stevens, J. Boerio-Goates. R. L. Putnam, K. B. Helean, A. Navrotsky.
- "Thermodynamics of formation for two cerium aluminum oxides, CeAlO<sub>3</sub> and CeAl<sub>12</sub>O<sub>19.918</sub>, and cerium sesquioxide, Ce<sub>2</sub>O<sub>3</sub> at T= 298.15 K." *J. Chem. Thermodynamics* **2000**, 32, 7, In Press. R. L. Putnam, A. Navrotsky, E. H. P. Cordfunke, M. E. Huntelaar.
- "Microstructure and Composition of Synroc Samples Crystallized from a CaCeTi<sub>2</sub>O<sub>7</sub> Chemical System: HRTEM/EELS Investigation." *Mat. Res. Soc. Proc.* **In Press - 2000** H. Xu, Y. Wang, R. L. Putnam, J. Gutierrez, A. Navrotsky.

8. "The Thermodynamics of Formations, Molar Heat Capacity, and Thermodynamic Functions of  $ZrTiO_4$  (cr)." *J. Chem. Thermodynamics* **In Press 2001**. B. K. Hom, R. Stevens, B. F. Woodfield, J. Boerio-Goates, R. L. Putnam, K. B. Helean, A. Navrotsky.
9. "Thermodynamics of Formation for Hf-Zirconolite,  $CaHfTi_2O_7$ (cr) and  $HfO_2$ (cr) from  $T= 0$  K to  $T= 1500$  K; Revised values of  $\Delta_f^T G_m^o$  for  $CaZrTi_2O_7$ (cr) over the same temperature." *J. Chem. Thermodynamics* **Submitted 12/00**. R. L. Putnam, J. Gutierrez, A. Navrotsky, R. Stevens, B. K. Hom, J. Boerio-Goates., and B. F. Woodfield.
10. "The Molar Heat Capacity and Thermodynamic Functions of  $CaHfTi_2O_7$ (cr) and the Solid Solution  $CaZr_{0.26}Hf_{0.74}Ti_2O_7$ (cr); New Values for the Entropy of  $CaZrTi_2O_7$ (cr)." *J. Chem. Thermodynamics* **Submitted 12/00** R. Stevens, B. K. Hom, J. Boerio-Goates., B. F. Woodfield, R. L. Putnam, J. Gutierrez, and A. Navrotsky.
11. "Formation energetics of ceramic phases related to surplus plutonium disposition." R. L. Putnam, B. B. Ebbinghaus, A. Navrotsky, K. B. Helean, S. V. Ushakov, B. F. Woodfield, J. Boerio-Goates *Ceramic Transactions* Proceedings of the 102<sup>nd</sup> American ceramic Society, symposium B5. St. Louis, MO April 2000. Volume edited by D. Spearing and R.L. Putnam. **In press for early 2001**.
12. "Systematic Trends and Prediction of Enthalpies of Formation of Refractory Lanthanide and Actinide Ternary Oxide Phases." A. Navrotsky. *Ceramic Transactions* Proceedings of the 102<sup>nd</sup> American ceramic Society, symposium B5. St. Louis, MO April 2000. Volume edited by D. Spearing and R.L. Putnam. **In press for early 2001**.
13. "Enthalpies of Formation of  $Gd_2(Ti_{2-x}Zr_x)O_7$  Pyrochlores", K. B. Helean, B. D. Begg, A. Navrotsky, B. Ebbinghaus, W. J. Webber, and R. C. Ewing, *Mat. Res. Soc. Proc.* (**submitted 12/2000**).
14. Ph.D. Dissertation: Princeton University **November 1999**, R. L. Putnam.

### 4.3 Participation

**Table 5. Individuals supported by / or contributing to this project.**

<b>Individual</b>	<b>Designation</b>	<b>Location</b>
Mark A. Williamson	Principle Investigator - Technical Staff Member	Los Alamos National Laboratory
John Huang	Co-Principle Investigator- Technical Staff Member	Los Alamos National Laboratory
Dane Spearing	Post Doctoral Staff Member	Los Alamos National Laboratory
Robert L. Putnam	Post Doctoral Staff Member – Technical Staff Member	Los Alamos National Laboratory
Ubaldo Gallegos	Technical Staff Member	Los Alamos National Laboratory
Alexandra Navrotsky	Co-Principle Investigator – Professor	University of California, Davis
Sergey Ushakov	Post Doctoral Researcher	University of California, Davis
Matia Howlader	Post Doctoral Researcher	University of California, Davis
Robert L. Putnam	Graduate Student	University of California, Davis
Katheryn B. Helean	Graduate Student	University of California, Davis
Vladimir Kodash	Graduate Student	University of California, Davis
Theresa Lee	Graduate Student	University of California, Davis
April Martinez	Graduate Student	University of California, Davis
Jose Gutierrez	High School Student	University of California, Davis
Bartley B. Ebbinghaus	Co-Principle Investigator	Lawrence Livermore National Laboratory
James M Lawson	Sample characterization	Lawrence Livermore National Laboratory
Robert P. Gomez	Technical staff - Sample Fabrication	Lawrence Livermore National Laboratory
Thomas E. Macari	Technical staff – Sample Fabrication	Lawrence Livermore National Laboratory
Walter L. Close III	Technical staff – Sample Fabrication	Lawrence Livermore National Laboratory

### 5.0 Summary of recent progress and future direction at individual institutions

#### 5.1 Los Alamos National Laboratory, LANL

The installation and initial prove-in process for the LANL high-temperature solution calorimeter has been completed by Putnam and the instrument is ready for the study of actinide-bearing materials. Funding is being sought to examine the Pu-pyrochlore which has recently been synthesized and characterized at LLNL by Ebbinghaus. Further studies in actinide-bearing oxide materials and pyrochlore structured materials have been started with collaboration with Sickafus (Sickafus 2000). Additionally, the calorimeter will be used in phase studies of actinide metal alloys.

#### 5.2 University of California at Davis, UCD

K.B. Helean's Ph.D. thesis is progressing well, and it is expected to be completed about a year from now. In order to provide reliable data on rare-earth containing

phases (pyrochlores, fluorite-based materials, phosphates, silicates) the enthalpies of solution of the rare earth oxides in our calorimetric solvents must be well known. Because of hygroscopicity, polymorphism, and somewhat slow solution kinetics, these values need to be crosschecked using several solvents and methods to assure accuracy and precision. This work is now complete and forms the basis of a number of papers to be written in the next few months. Similarly, calorimetric data for  $\text{UO}_2$  and  $\text{ThO}_2$  are now secure, and work on brannerites containing these elements is essentially complete. The experience gained in using the lanthanide and U and Th oxides is crucial before the Los Alamos calorimetry effort goes on to tackle oxides of Pu and other actinides. Work on cerium pyrochlore is complete and that on a nonstoichiometric U-pyrochlore is finished except for some additional electron microprobe analysis. A series of  $\text{Gd}_2\text{Zr}_2\text{O}_7$ - $\text{Gd}_2\text{Ti}_2\text{O}_7$  pyrochlores have been made, as well as a mainly disordered gadolinium titanate. Calorimetry on these samples is in the final stages and the energetics are being analyzed in terms of heats of mixing and order-disorder phenomena. The disordered pyrochlores are in fact cubic zirconia (fluorite structure) phases similar to those encountered as solid electrolytes. Theresa Lee, a postdoc, is working on their energetics. Because of the possible relation between ease of disordering and radiation resistance, as stressed by Sickafus at Los Alamos and Ewing at Michigan, understanding the energetics of both ordered pyrochlores and disordered fluorites is very important. A set of rare earth titanate pyrochlores, provided by Lynn Boatner at Oak Ridge, will explore this relation further, as well as studies on  $\text{Gd}_2\text{Hf}_2\text{O}_7$ , in collaboration with Putnam and Sickafus at Los Alamos. Postdoc Sergey Ushakov is involved in this work.

Rare earth phosphates,  $\text{REPO}_4$ , are potential actinide hosts and are important secondary phases in the corrosion of actinide bearing glasses and ceramics in the natural environment. Ushakov has completed a systematic study of their energetics using a set of single crystal samples provided by Boatner.

This next year will be one of completing calorimetry on pyrochlores and writing papers. What remains to be done at Davis is a systematic study relating order disorder, energetics, and radiation damage studies done elsewhere. This area, linking pyrochlore and fluorite studies, has impact both for the radiation resistance and durability of waste forms and for the use of the very similar disordered phases as solid electrolytes in oxide fuel cells and oxygen separation membranes. In both cases, fundamental thermochemical data are essential to assessing materials compatibility, degradation in use, and optimum synthesis routes. The thermodynamic data are necessary input into kinetic models of dissolution and decomposition. Without such fundamental data, commercial processes rest on uncertain ground as to the final states of the materials they produce and utilize.

### **5.3 Lawrence Livermore National Laboratory ,LLNL**

At LLNL the focus of the work was to fabricate two Pu-bearing minerals and send them to LANL for drop solution calorimetry. Under funding provided by the PIP, a number of other non-Pu bearing phases were also prepared and sent to UCD for drop solution calorimetry. The two Pu-bearing samples selected for this work are a Pu

brannerite, nominally  $\text{PuTi}_2\text{O}_6$ , and a Pu-pyrochlore, nominally  $\text{CaPuTi}_2\text{O}_7$ . Ultimately the preparation of the Pu brannerite was unsuccessful. The sample was lost after the sixth heat treatment when one of the crucibles of containment melted in the furnace. The preparation of the Pu pyrochlore was marginally successful. A sample containing greater than 90 vol % pyrochlore was obtained. The balance of the material was a quantifiable amount of essentially pure  $\text{PuO}_2$  and  $\text{TiO}_2$ . Although suitable for drop solution calorimetry, the sample was not fabricated in time to conduct the drop solution measurements as part of this work.

## 6.0 References

- US DOE ROD 2000.** "Record of decision for the Surplus Plutonium Disposition Final Environmental Impact Statement" January 2000.
- Ebbinghaus 2000.** B. Ebbinghaus, G. Armantrout, L. Gray, C. Herman, H. Shaw, R. VanKonynenburg, "Plutonium Immobilization Project Baseline Formulation," Lawrence Livermore National Laboratory Report, UCRL-ID-133089, Plutonium Immobilization Program, PIP-00-141 (September 2000)
- Ph.D. Putnam 1999.** "Formation Energetics of Ceramic Waste Materials for the Disposal of Surplus Weapons Plutonium" Ph.D. dissertation by Robert L. Putnam to the faculty of Princeton University, November 1999. Copies of this 253 page document can be obtained by contacting the author via email [rputnam@lanl.gov](mailto:rputnam@lanl.gov) or by regular post at Los Alamos National Laboratory; Mail Stop G721; Los Alamos, NM 87545.
- Ph.D. Helean 2001.** Ph.D. dissertation by Kathryn B. Helean to the faculty of the University of California, Davis. To be completed in early 2001.
- Agreement 2000.** "Agreement Between the Government of the United States of America and the Government of the Russian Federation Concerning the Management and Disposition of Plutonium Designated as no Longer Required for Defense Purposes and Related Cooperation," posted at [www.doe-md.com](http://www.doe-md.com) (September 2000)
- Ringwood 1978.** A. E. Ringwood, Safe Disposal of High Level Nuclear Reactor Wastes: A New Strategy, Australian Nuclear University Press, Canberra, Australia and Norwalk, Conn, USA (1978).
- Webber 1996.** W.J. Weber, R.C. Ewing, and W. Lutze, "Performance Assessment of Zircon as a Waste Form for Excess Weapons Plutonium Under Deep Borehole Burial Conditions," *Materials Research Society Symposium Proceedings*, **412**, pp. 25-32, Materials Research Society, Pittsburgh, PA (1996).
- Burakov 1996.** B. E. Burakov, E. B. Anderson, V. S. Rovsha, S. V. Ushakov, R. C. Ewing, W. Lutze, and W. J. Weber, "Synthesis of Zircon for Immobilization of Actinides," *Materials Research Society Symposium Proceedings*, **412**, pp. 33-39, Materials Research Society, Pittsburgh, PA (1996).
- Degueldre 1996.** C. Degueldre, U. Kasemeyer, F. Botta, and G. Ledergerber, "Plutonium Incineration in LWRs by a Once-through Cycle with a Rock-like Fuel," *Materials Research Society Symposium Proceedings*, **412**, pp. 15-23, Materials Research Society, Pittsburgh, PA (1996).
- Boatner 1988.** L. A. Boatner and B. C. Sales, "Monazite," pp. 495-564 in Radioactive Waste Forms for the Future, W. Lutze and R.C. Ewing, eds., North-Holland, New York (1988).
- Wang 1999.** S. X. Wang, B. D. Begg, L. M. Wang, R. C. Ewing, W. J. Weber, and K. V. Govidan Kutty, "Radiation Stability of Gadolinium Zirconate: A Waste Form for Plutonium Disposition," *J. Mater. Res.*, **14**(12), 4470-4473 (1999).
- Sickafus 2000.** K. E. Sickafus, L. Minervini, R. W. Grimes, J. A. Valdez, M. Ishimaru, F. Li, K. J. McClellan, and T. Hartmann, "Radiation Tolerance of Complex Oxides," *Science*, **289**, 748-751 (2000).
- Navrotsky 1977,1999.** A. Navrotsky (1977) *Phys. Chem. Min.* **2**: 89-104. and A. Navrotsky,

- (1997) *Phys. Chem. Min.* 24, 222-241.
- Woodfield 1999.** B. F. Woodfield, J. Boerio-Goates, J.L. Shapiro, R. L. Putnam, A. Navrotsky. *J. Chem. Thermodynamics* 1999, 31, 245-253.
- Ellsworth 1994.** S. Ellsworth, A. Navrotsky, R. C. Ewing. *Phys. Chem. Min.* 1994, 21: 140-149.
- Putnam 2001.** R.L. Putnam, B.B. Ebbinghaus, A. Navrotsky, K.B. Helean, S.V. Ushakov, B.F. Woodfield, J. Boerio-Goates, M.A. Williamson. "Formation energetics of ceramic phases related to surplus plutonium disposition." Submitted to *Ceramic Transactions*, for the 102<sup>nd</sup> American Ceramics Society Meeting in St. Louis, MO April 2000. Volume edited by D. Spearing and R.L. Putnam. In press for early 2001.
- Xu 1999.** H. Xu, and Y. Wang. *J. Nucl. Mat.* 1999, 275, 216-220.

## 7.0 Appendix

**Fissile Materials Disposition Program**

**Plutonium Immobilization Project  
Baseline Formulation**

**September 2000**

**Bartley B. Ebbinghaus, LLNL  
Guy A. Armantrout, LLNL  
Leonard Gray, LLNL  
Connie C. Herman, SRTC  
Henry F. Shaw, LLNL  
Richard A. Van Konynenburg, LLNL**

**Plutonium Immobilization Project**

**Lawrence Livermore National Laboratory  
Livermore, CA 94550**

This document was reviewed in accordance with LLNL D&T QA Implementing Procedure LQIP-6.2, Revision 0, *Document Review*. The data included or referenced in this report may have been collected before the approval of the LLNL PIP D&T QA Program (September 29, 2000). Therefore prior to use as qualified data, the contents and reference data should be subject to review as detailed in LLNL D&T QA Implementing Procedure YAP-SIII.1, Revision 3, *Qualification of Unqualified Data*.

## *Table of Contents*

---

1	Introduction and Summary	4
2	History and Programmatic Context	6
3	Form Development Strategy	13
3.1	Plutonium Feed Assumptions	13
3.1.1	Feed Material Categories	13
3.1.2	Impurities and Isotopics	14
3.2	Repository Considerations	16
3.2.1	Criticality Safety and Durability	17
3.2.2	Compatibility with High Level Waste	17
3.2.3	Other Repository Requirements	18
3.3	Selection of the Form and Process	19
3.3.1	Selection of the Formulation	19
3.3.2	Selection of the Fabrication Process	24
4	Development of the Ceramic Form	27
4.1	Overview	27
4.1.1	Form Development Tasks	27
4.1.2	Participants and Capabilities	28
4.2	Sample Test Matrices	29
4.2.1	The A Series Tests	31
4.2.2	The B Series Tests	31
4.2.3	Statistically Designed Tests	33
5	Immobilization Form Specifications	35
5.1	Baseline Formulation	35
5.1.1	Composition	35
5.1.2	Precursor and Actinide Feed Specifications	36
5.1.3	Product Phase Assemblage	39
5.2	Baseline Fabrication Process	44
5.2.1	Ceramic Precursor Preparation	45
5.2.2	Baseline Immobilization Process	47
5.3	Mixing Recipes	52
5.3.1	Attritor Mill/Mixer Recipe	52
5.3.2	Calculated Ceramic Compositions	53
6	References	56
	Appendix A – List of Acronyms	61

## *List of Figures*

---

3.1	Secondary electron image (SEI) of zirconolite-rich form	22
3.2	Backscattered electron image (BEI) of pyrochlore-rich form	23
4.1	Linkages between tasks and sample test matrices	30
5.1	Depiction of the processing regime	44
5.2	Recommended process for preparing ceramic precursors	46
5.3	The ceramic immobilization process flow diagram	48
5.4	The overall baseline firing schedule	51

## *List of Tables*

---

1.1	Composition of the baseline formulation	5
2.1	Summary of SYNROC and related variants	10
3.1	Actinide and estimated impurity contents of Pu feed materials	14
3.2	Average isotopics for various Pu feed materials	15
3.3	Average and extreme impurity contents in the PuO <sub>2</sub> feed	16
4.1	Readily available analytical capabilities for Pu-loaded samples	28
4.2	Surrogates for plutonium and americium	31
4.3	Summary of the B series sample test matrices	32
4.4	Impurity categories for statistical tests	33
5.1	Feed composition to produce the baseline ceramic form	36
5.2	Precursor feed compositions for the baseline formulation	37
5.3	Feed specifications for precursor preparation	37
5.4	Uranium and plutonium oxides feed specifications	37
5.5	Product acceptability criteria used to define feed impurity specifications	38
5.6	Limits on uncompensated impurities	39
5.7	Phase abundances in baseline and product extremes	39
5.8	Nominal composition of Pu ceramic and natural analog phases	42
5.9	Composition of phases in the ceramic	45
5.10	Baseline burn-out schedule	51
5.11	Baseline sintering schedule	51
5.12	Table of molecular weights	53
5.13	Calculated product compositions	54
5.14	Calculated isotopic compositions	55

## ***1. Introduction and Summary***

---

Since 1994 Lawrence Livermore National Laboratory (LLNL), with the help of several other laboratories and university groups, has been the lead laboratory for the Plutonium Immobilization Project (PIP). This involves, among other tasks, the development of a formulation and a fabrication process for a ceramic to be used in the immobilization of excess weapons-usable plutonium.

This report reviews the history of the project as it relates to the development of the ceramic form. It describes the sample test plan for the pyrochlore-rich ceramic formulation that was selected, and it specifies the baseline formulation that has been adopted. It also presents compositional specifications (e.g. precursor compositions and mixing recipes) and other form and process specifications that are linked or potentially linked to the baseline formulation.

The PIP traces its history to the end of the Cold War and agreements between the U.S. and the Russian Federation to reduce their stockpiles of excess fissile material. A study by a National Academy of Sciences committee recommended means for disposition of plutonium, including use in reactor fuel and immobilization in a geological repository. In the U.S., a selection process resulted in the choice of ceramic as the material to be used for the immobilization form. The extensive experience with the Synroc family of nuclear waste forms, together with the high durability of the titanate-based ceramics, led to selection of this type of ceramic for the immobilization of surplus plutonium. Consideration of the composition of the plutonium feed streams and the relative durability of natural analogs led to selection of a pyrochlore-rich Synroc formulation for the ceramic. Early testing in combination with previous experience led to the selection of cold pressing and reactive sintering as the process to be used in fabrication of the ceramic.

An extensive test plan was developed and executed to determine the effects of impurities and processing parameters on the properties of the ceramic, to develop an understanding of the phase equilibria involved, and to produce material for leach testing to provide a basis for repository acceptance. Based on this testing and the programmatic objectives, a baseline formulation was selected and is shown in **Table 1.1**.

Researchers from Lawrence Livermore National Laboratory, the Savannah River Technology Center (SRTC), the Australian Nuclear Science and Technology Organization (ANSTO), Argonne National Laboratory (ANL), and the Pacific Northwest National Laboratory (PNNL) were involved in the development of the ceramic formulation. Supporting calorimetric work was also performed at the University of California at Davis (UCD) and at Brigham Young University (BYU). Thanks to the cooperation and teamwork of this group, a large number of experimental ceramic samples have been fabricated and analyzed, making it possible to define the baseline formulation. This formulation has been shown to have several important attributes:

- Very resistant to chemical dissolution in repository-like environments
- Safe with respect to nuclear criticality in repository degradation analyses

- Able to accommodate PuO<sub>2</sub> feed impurities in the ranges expected
- Amenable to a variety of straight-forward and practical fabrication processes

For all of these reasons, the baseline formulation has been found to be suitable for the mission for which it has been developed.

**Table 1.1 Composition of the  
baseline formulation**

<b>Oxide</b>	<b>Weight Percent</b>
CaO	9.488
TiO <sub>2</sub>	37.775
Gd <sub>2</sub> O <sub>3</sub>	7.580
HfO <sub>2</sub>	11.100
UO <sub>2</sub>	23.286
PuO <sub>2</sub>	10.771
Pu (wt. % of the element)	9.500

## ***2. History and Programmatic Context***

---

The end of the Cold War left the United States and the Russian Federation with large numbers of stockpiled nuclear weapons. A series of arms reduction agreements and unilateral pledges resulted in the reduction of these stockpiles and the classification of large quantities of weapons-usable plutonium and highly enriched uranium as surplus to the needs of national defense. In the U.S., the weapons-usable plutonium is present in a number of chemical and physical forms, having a range of purities and chemical compositions. The more dilute forms of plutonium fall into the category of transuranic (TRU) waste, which is destined for disposal in the Waste Isolation Pilot Plant (WIPP) facility in Carlsbad, New Mexico. The more concentrated forms of plutonium are more attractive from the standpoint of nuclear weapons proliferation, and must be safeguarded. Because of the potential for use of this plutonium in nuclear weapons, as well as its radiological and chemical toxicity and nuclear criticality potential, the more concentrated forms of plutonium cannot be disposed of directly.

In March of 1992, after a briefing by the Committee on International Security and Arms Control (CISAC) of the U.S. National Academy of Sciences, General Brent Scowcroft, the National Security Advisor to President George Bush, asked for a full-scale study of the management and disposition options for plutonium. The Clinton administration confirmed the Committee's mandate in January 1993 [1].

On September 27, 1993, President Clinton announced that "the U.S. will initiate a comprehensive review of long-term options for plutonium disposition, taking into account technical, nonproliferation, environmental, budgetary and economic considerations. Russia and other nations with relevant interests and experience will be invited to participate in this study [2]." On January 24, 1994 Secretary of Energy Hazel O'Leary formed a small cross-cutting project organization within the Department of Energy (DOE) to oversee the U.S. effort on the disposition of excess fissile materials [3]. In October 1994 the Congress established this organization as a permanent office within the DOE by passing the National Defense Authorization Act for Fiscal Year 1995 (P.L.103-335), naming this organization the Office of Fissile Materials Disposition (MD).

Also in early 1994 the CISAC released its report [1] entitled "Management and Disposition of Excess Weapons Plutonium," which became the basis for the DOE-MD plutonium disposition program. The CISAC report identified the most promising disposition options to be (1) the incorporation of plutonium into reactor fuel for use in producing electricity, after which it would become part of the reactor spent fuel stream, and (2) vitrification together with high-level radioactive waste (HLW). Under the Nuclear Waste Policy Act both spent reactor fuel and HLW are destined for disposal in a deep geologic repository. The report also mentioned deep borehole disposal as a less thoroughly studied option. The deep borehole option subsequently was studied at LLNL and was found to be technically viable [4,5]. However, DOE subsequently judged that this option was not politically viable, because it lacked a supportive constituency and would require the siting of boreholes in numerous locations in the U.S., which would likely be unpopular [6].

An important guideline recommended in the CISAC report was that the excess weapons plutonium should be transformed "into a physical form that is at least as inaccessible for weapons use as the much larger and growing stock of plutonium that exists in spent fuel from commercial nuclear reactors [1]." This guideline was called the "spent fuel standard." The report emphasized that there should be radiological or physical barriers in addition to chemical barriers to the extraction of plutonium from the physical form to be used. The CISAC envisioned that plutonium could be added to the Defense High Level Waste (DHLW) glass already in production at the Defense Waste Processing Facility (DWPF) at Savannah River. The gamma radiation from the fission products (notably cesium-137) in this glass could then serve as a radiation barrier to deter theft and extraction of the plutonium. Although the process for incorporating the majority of the cesium-137 into the HLW glass was not yet operational, it was anticipated that it would become operational in time to meet the schedule for disposition of the plutonium.

DOE-MD later slightly modified the definition of the spent fuel standard to read "The surplus weapons-usable plutonium should be made as inaccessible and unattractive for weapons use as the much larger and growing quantity of plutonium that exists in spent nuclear fuel from commercial power reactors [7]." DOE-MD also expanded the term "vitrification" by changing it to "immobilization," recognizing that other immobilization forms beside glass should be considered.

LLNL was named by DOE-MD as the lead laboratory for development of the technologies to immobilize excess weapons-usable plutonium. Other laboratories, mainly SRTC, ANL, and PNNL, were also assigned roles in the immobilization program. The ANSTO was also involved in the program through contracts with LLNL.

In March 1995 President Clinton announced that approximately 50 metric tonnes (MT) of plutonium, including about 38 MT of weapons-grade material, was considered surplus to U.S. defense needs.

One of the early steps performed by LLNL (in 1995) was a screening study of waste forms previously considered for immobilizing high level radioactive waste, which technically is a similar problem [8]. This screening process resulted in the selection of glasses (more specifically boro-silicate glasses), as originally envisioned by the CISAC, and also crystalline ceramics (more specifically Synroc's) as the two classes of materials that would best exhibit the desirable characteristics of a plutonium immobilization form. The characteristics considered include the following:

- a. absence of materials proscribed by the Nuclear Regulatory Commission regulation 10CFR60 for waste forms to be emplaced in a geologic repository (organic materials, free liquids, explosive, pyrophoric, or combustible materials)
- b. absence of materials classified by the Environmental Protection Agency in regulations 40CFR261.30 through 40CFR261.33 as chemically hazardous materials
- c. high solid solubility of actinides in the immobilization form (to effectively bind them while minimizing the total amount of the immobilization form to minimize cost)

- d. high solid solubility of neutron absorbers (to adequately protect against nuclear criticality)
- e. ability to incorporate cesium-137 (This was important for the internal radiation barrier option, discussed later.)
- f. ability to incorporate plutonium oxide feed material into the immobilization form without a significant amount of non-reacted material, using a practical fabrication process and minimizing the necessity to reduce the particle size into the respirable range
- g. tolerance to the impurities in the existing weapons-grade plutonium feed streams without significantly affecting the durability or processability
- h. easy, safe and reliable handling and processing in a glovebox facility, with an experience base to support this assessment
- i. amenability to development of process controls and control models
- j. easy material control and accountability of the plutonium
- k. no adverse effect on the immobilization form from the heating and cooling involved in pouring molten DHLW glass around it (This became important because of the can-in-canister option, described later.)
- l. no adverse effect on the performance of the DHLW glass in the case of options in which the immobilized plutonium would be associated with this glass
- m. durability in a geologic repository environment at least as high as that of borosilicate glass and spent reactor fuels, which are the intended radioactive waste forms to be emplaced, taking into account expected temperatures, radiation damage, and aqueous corrosion
- n. existence of naturally occurring mineral analogues of the form to help in assessing long-term durability
- o. difficult extraction of plutonium for reuse in weapons (to promote nonproliferation goals as well as to assure Russia of serious U.S. intent to remove the plutonium from weapons use)
- p. high cost effectiveness
- q. compliance with environmental, safety, and health requirements
- r. ability to foster cooperation with Russia and other countries
- s. high public and institutional acceptance
- t. ability to be developed in a short time

LLNL and ANSTO engaged in the development of a ceramic immobilization form, based on their prior experience in the development of SYNROC-C [9] and SYNROC-D [10] and on ongoing work on a related mixed waste ceramic [11]. The other partner laboratories, ANL, PNNL, and SRTC, were directed to focus their attention on the development of glass immobilization forms, based on their corresponding experience and capabilities in this field.

As analyses proceeded, it became clear that there would be significant problems in mixing plutonium into the DHLW glass. The DHLW glass formulation had not been designed to incorporate plutonium. It was not clear that plutonium would dissolve fast enough in this glass at the processing temperature in use (1150°C), or that it would be sufficiently soluble in the glass. The boron neutron absorber would be much more soluble in repository water than would the plutonium, raising doubts about long-term criticality safety. The DWPF facility also had not

been designed for plutonium processing, in terms of criticality control (particularly in the large melter in use there) and materials control and accountability. Contamination control would be more difficult with the addition of plutonium, a significant alpha emitter. From a programmatic point of view, the plant was already in production accomplishing the mission of vitrifying DHLW, and changes would be disruptive.

In view of these considerations, other alternatives were explored, including the internal radiation barrier and the external radiation barrier concepts, the latter also known as the can-in-canister concept. The internal barrier scheme involved mixing cesium-137 (from Hanford) into the plutonium immobilization form to serve as a gamma radiation barrier to deter extraction and reuse of the plutonium. Accordingly, this was also called the homogeneous form. The can-in-canister concept involved production of the plutonium immobilization form in a separate facility from the DWPF, without added gamma emitters. This form was thus called the heterogeneous form. In this scheme, the form would be placed in relatively small sealed cans, the external surfaces of which would be uncontaminated. These cans in turn would be mounted on racks inside the empty DWPF canisters, and the molten DHLW glass from the DWPF would then be poured into the canisters and would encapsulate the cans of immobilized plutonium. In this way, the problems listed above would be circumvented, while the gamma-ray emission, physical size, and encapsulation available from the canisters of DHLW glass could still be used to meet the "spent fuel standard." After comparison of the advantages and disadvantages, the can-in-canister concept was shown to be superior on the basis of timeliness, higher technical viability, much lower costs, and to a lesser extent, lower environmental and health risks. The can-in-canister concept could be accomplished using a glove-box facility, whereas the homogeneous concept (using cesium-137) would need a hot cell facility. Fabrication of a plutonium immobilization form would be much simpler if the volatile cesium did not have to be incorporated into it during the fabrication process that occurred at high temperatures.

The CISAC [1] had declared that the existence of the surplus fissile material "constitutes a clear and present danger to national and international security." In response, DOE-MD established an urgent program schedule for the disposition of excess weapons plutonium. This tight schedule did not permit the developers of the immobilization forms to be given the charter, the time or the resources to study additional alternatives or different ceramic or glass formulations and arrive at an optimum choice. Instead, they were constrained to draw upon previous experience and choose what appeared to be the best of the alternative formulations already studied for other purposes. In the case of ceramics, the most developed mineral assemblages from past nuclear waste research and development was the titanate-based SYNROC series of ceramics. Van Konynenburg [12] and Oversby [13] had each independently suggested the use of a titanate mineral assemblage for U.S. plutonium immobilization in February 1994.

SYNROC (which is an abbreviation for SYNthetic ROCK) had been conceived by Ringwood [14]. Development had been carried out by he and his collaborators and later by the staff of the Australian Nuclear Science and Technology Organization (ANSTO) [15,16]. As mentioned above, LLNL had obtained experience with these formulations from its earlier work on SYNROC-D. The various types of SYNROC that have been developed, including those developed by the Plutonium Immobilization Program, are shown in **Table 2.1** [9,10,17-22].

**Table 2.1 Summary of SYNROC and related variants**

Form Name	Mineralogy*	"Waste" Loading	Fabrication Process
SYNROC-A	40% Ba-feldspar, 30% hollandite, 20% perovskite, 10% zirconia, kalsilite, and/or leucite	10% HLW	Melting and Crystallizing 1330°C
SYNROC-B	40% hollandite, 35% zirconolite, 25% perovskite,	None	Hot Pressing 1200-1400°C
SYNROC-C	33% hollandite, 28% zirconolite, 19% perovskite, 15% rutile, 5% noble metal alloy	20% HLW	Hot Pressing 1150°C
SYNROC-D	46% spinel solid solution, 19% zirconolite, 17% nepheline, 15% perovskite, 3% hollandite	63% HLW sludge	Hot Pressing 1050-1100°C
SYNROC-E	79% rutile, 7% zirconolite, 7% perovskite, 5% hollandite, 2% pyrochlore	7% HLW	Hot Pressing 1300°C
SYNROC-F	90% pyrochlore, 5% hollandite, 5% rutile	50% U-rich HLW	Hot Pressing 1250°C
SYNROC-FA	89% pyrochlore, 8% perovskite, 3% uraninite	50% U-rich HLW	Cold Pressing and Sintering 1250-1400°C
Mixed Waste Ceramic	36% nepheline, 31% spinel solid solution, 12% zirconolite, 12% perovskite, 5% rutile, 4% whitlockite	40% residue	Cold Pressing and Sintering 1150-1200°C
Pu Ceramic Zirconolite-rich	80% zirconolite (with some pyrochlore), 10% hollandite, 10% rutile, <1% PuO <sub>2</sub>	12% Pu	Cold Pressing and Sintering 1325-1400°C
Pu Ceramic Pyrochlore-rich	85% pyrochlore, 10% brannerite, 5% rutile, <1% uraninite solid solution	10% Pu and 21% U	Cold Pressing and Sintering 1275-1400°C

\*All percents are given in weight percent.

Of all the SYNROC formulations, SYNROC-C was by far the most studied and the most developed. The strategy of SYNROC is to immobilize the radioactive isotopes of HLW in a mixture of minerals that all have natural analogs in nature that

- have survived for periods exceeding 20 million years in a wide variety of geochemical environments
- have crystal chemical properties that allow them to accept a wide range of elements into their crystalline matrix

- are thermodynamically stable together

There is a wide range of minerals that meet these three criteria. Titanate-rich minerals were selected by Ringwood because they not only meet the above criteria, but are based on one of the most insoluble oxides known, namely  $\text{TiO}_2$ .

Actinides, which represent some of the components of HLW, are easily accommodated into SYNROC. Consequently, SYNROC was also an attractive candidate for the more specific problem of immobilizing excess plutonium. Although a very limited amount of work had been carried out on alternative mineral phases for plutonium immobilization, LLNL focused early on the titanate-based ceramics because of their prior successful history. LLNL entered into a contract with ANSTO for assistance with titanate ceramic development and to benefit from ANSTO's extensive experience and expertise.

Over the course of fiscal years 1995 through 1997, development was carried out on both the ceramic and glass candidate immobilization forms, including formulation, processing, some property measurements including thermal stability and corrosion behavior, preconceptual plant design, and nonproliferation evaluation of the can-in-canister concept. The ceramic formulation effort was led by Ebbinghaus, who with coworkers summarized the status of the ceramic work in December 1995 [23]. Initially he focused the work on a formulation based on the mineral zirconolite, because of its successful use as a durable actinide host in SYNROC. On April 8, 1997, during a video conference with ANSTO, LLNL, and SRTC, Ebbinghaus redirected the effort to focus the work on a pyrochlore-based baseline ceramic formulation.

Beginning in June 1997, data from the development work on both glasses and ceramics were collected and submitted to a Technical Evaluation Panel (TEP) made up of representatives of the laboratories working on the immobilization forms. The panel was also given a report projecting the expected radiation effects in the plutonium immobilization ceramic [24]. The panel evaluated and compared the data for glasses and ceramics using several agreed-upon criteria, and on August 8, 1997 the panel issued its draft report. The final version of this report was published later [25]. Based on the TEP draft report and on weighting factors provided by DOE-MD, LLNL immobilization project management performed an assessment of the alternative forms and attributes against the weighted criteria and generated a decision report that recommended selecting of the ceramic form for the immobilization project [26]. A peer review panel made up of independent experts (Matthew Bunn, Donald Langmuir, Ronald Loehman, David Stahl, and Alan Williams) was convened to examine the available data and to review this recommendation. On August 21, 1997 the peer review panel report concluded that "the LLNL recommendation of the ceramic form is adequately supported by the information presented [27]." On August 27, 1997, LLNL transmitted to DOE-MD a formal recommendation of the ceramic form, including the two evaluation reports and the peer review panel's letter [28]. On September 25, 1997, Howard Canter, then the Acting Director of DOE-MD, announced his approval of the LLNL recommendation to select the ceramic form, and directed LLNL "to focus immobilization efforts on the ceramic form using the preferred can-in-canister approach." Canter particularly highlighted the advantages of the ceramic form in the areas of proliferation resistance, potential worker dose, and cost effectiveness [29].

With the new focus, the roles of the other U.S. laboratories were modified to match their capabilities and experience to the tasks within the expanded ceramic development effort.

### ***3. Form Development Strategy***

---

To complete the development of the ceramic formulation, an extensive testing program was undertaken. This testing covered a range of compositional and processing variables that are discussed later in this report. In order for a testing program to be implemented, certain assumptions were made concerning the characteristics of the plutonium feed streams, the relevant requirements for the HLW repository, and the selection of the formulation and process.

#### **3.1 Plutonium Feed Assumptions**

According to DOE plans, the Materials Disposition Program, which is now identified as NN-60, will receive fissile materials packaged by facilities operated for the Offices of Defense Programs (DP), Environmental Management (EM), and Nuclear Energy (NE). The compositions, forms, and storage packages of surplus plutonium-bearing materials throughout the complex are not well defined. The majority of the separated plutonium that is not in nuclear weapons components is housed in the production plants -- Rocky Flats, Hanford, and Savannah River -- under conditions that are not acceptable for long term storage. These materials will require repackaging, and some will require stabilization or minimal processing to allow safe storage until disposition is complete. Until 1994, complex-wide directives that applied to plutonium storage, including safety and safeguards orders, were general in nature. Therefore, plutonium storage practices varied considerably among the sites. In order to stabilize these materials for long term storage, new standard stabilization, packaging, and surveillance requirements are in the process being implemented at all of the DOE sites [30].

##### **3.1.1 Feed Material Categories**

Chemical data for the plutonium feedstocks targeted for disposition vary in completeness. A summary of the best available data by material type is given in **Table 3.1**. Overall about 13 metric tonnes of Pu are planned to be dispositioned by immobilization. In addition, there are about 7 metric tonnes of other actinides and about 5 metric tonnes of other impurities. The potential feed materials have been organized into six different groups of material. They are defined as follows:

- Group I: Materials with purity far exceeding what is required for immobilization.
- Group IIa: Materials with relatively low impurity levels that can be blended easily into acceptable feed stocks for immobilization.
- Group IIb: Materials with higher levels of impurities that require some treatment before blending to remove or deplete the impurities of concern. These materials will be handled in the Plutonium Conversion Section of the Plutonium Immobilization Plant. They include the "chloride oxides" being stored at Rocky Flats and at Hanford.
- Group IIIa: Materials previously identified by internal DOE studies as requiring processing in the SRS canyon (aqueous dissolution and re-precipitation). These materials include fluoride materials and scrub alloy at Rocky Flats as well as sand, slag and

crucible materials at both Rocky Flats and Hanford. (After processing at Savannah River, these Group IIIa materials would move into Group I.)

- Group IIIb. Salt residues from molten salt processing. These have been previously identified as needing removal of the chloride salts for stabilization purposes. (After removal of about 75% of spent chloride salts, this material would meet the description of Group IIa.)
- Group IIIc. There is also a group of materials that have plutonium contents as low as 5 to 10 wt%. These materials will likely be disposed of as transuranic waste at the Waste Isolation Pilot Plant in Carlsbad, New Mexico.

Currently only group I, IIa, and IIb materials will be dispositioned in the Plutonium Immobilization Facility. The portion of plutonium that is in metallic form will be converted to oxide before feeding to the ceramic immobilization process. The group IIIa, IIIb, and IIIc materials will either be purified so that the Plutonium Immobilization Facility can accept them or they will be disposed of as transuranic waste. A total of about 3 metric tonnes of plutonium are present in groups IIIa, IIIb, and IIIc.

**Table 3.1. Actinide and estimated impurity contents of Pu feed materials [31]**

Category	Sub-Category	Group	Pu (kg)	DU (kg)	NU (kg)	LEU (kg)	EU (kg)	Np (kg)	Am (kg)	Other Impurities (kg)
Plutonium oxide	Short calcine oxide	I	1928							~25
	Long calcine oxide	IIa	2917	3					0.75	~1500
	Chloride wash oxide	IIb	378						0.1	~1000
U/Pu oxide		IIa	859	2859	332		1000			~350
Impure oxide		IIa	1989		1					~1500
Plutonium metal		I	3483					0.5	0.06	~30
Alloys		IIa	269	25	3					~120
Oxide Reactor Fuel		IIa	745	2790						~35
Totals			12566	5677	338	0	1000	0.5	0.9	~4700

DU = Depleted Uranium (~0.2% <sup>235</sup>U), NU = Natural Uranium (~0.7% <sup>235</sup>U), LEU = Low Enriched Uranium (~4% <sup>235</sup>U), EU = Enriched Uranium (~93% <sup>235</sup>U).

### 3.1.2 Impurities and Isotopics

The isotopic composition of the excess plutonium feed stocks varies from 3% <sup>240</sup>Pu to about 40% <sup>240</sup>Pu. The plutonium assay in the candidate materials varies from less than 10 wt% to over 99 wt%. The last date of purification of these materials varies from the mid 1960s to the mid 1980s.

Therefore, the  $^{241}\text{Am}$  content varies from as little as 200 ppm for the recently purified materials to as much as 20 wt % for some of the older reactor grade or americium-enriched materials. The uranium content varies from trace depleted uranium in the plutonium to trace plutonium in fully enriched (93%  $^{235}\text{U}$ ) uranium. The best available data to date on the isotopics of the Pu feed materials are given in **Table 3.2**. Isotopics are valid for the date given in the table.

**Table 3.2. Average isotopics for various Pu feed materials [31]**

Pu Grade	Pu Mass (kg)	$^{238}\text{Pu}$ (wt %)	$^{239}\text{Pu}$ (wt %)	$^{240}\text{Pu}$ (wt %)	$^{241}\text{Pu}$ (wt %)	$^{242}\text{Pu}$ (wt %)	Date
$^{240}\text{Pu} \leq 4\%$	45		97.00	3.00			1980
$4\% \leq ^{240}\text{Pu} \leq 7\%$	8815	0.012	93.76	5.78	0.400	0.05	1985
$7\% \leq ^{240}\text{Pu} \leq 10\%$	236	0.05	89.8	9.0	1.02	0.13	1965
$10\% \leq ^{240}\text{Pu} \leq 13\%$	1584	0.1	86.1	12.0	1.6	0.2	1965
$13\% \leq ^{240}\text{Pu} \leq 16\%$	251	0.4	79.4	15.0	4.3	0.9	1965
$16\% \leq ^{240}\text{Pu} \leq 19\%$	1368	0.7	72.6	18.0	7.0	1.7	1965
$19\% \leq ^{240}\text{Pu}$	262	1.3	60.3	23.5	12.0	3.0	1965
$^{238}\text{Pu}$	5	80	20				1965

Based on the types of feed materials expected, an average and an extreme impurity composition for the  $\text{PuO}_2$  feed has been estimated. These estimated compositions are given in **Table 3.3**. These compositions were calculated from data summaries provided by Riley [32]. These are the best estimates of the impurities that are currently available and they are based on the 17 MT immobilization case and not the 13 MT immobilization case. "Average Feed" is the estimated overall composition if all the feeds were combined into a single batch. The averages given in **Table 3.3** total a little greater than 100% because impurity compositions are only known for a small fraction of the feeds whereas as the actinide content is known for all of the feeds. The fact that the actinide plus impurity content exceeds greater than 100% indicates that the average impurity compositions given in **Table 3.3** are probably greater than the real case. "Max. All Feeds" is the maximum concentration of an impurity in a single container. The maximums given in **Table 3.3** total much greater than 100% because the maximum for each element generally occurs in different feed containers.

In general, the impurities in the existing feed stocks include the following elements: aluminum, carbon, calcium, chlorine, iron, fluorine, gallium, potassium, magnesium, molybdenum, sodium, silicon, tantalum, uranium and tungsten. With the exceptions of some volatile oxides (e.g.  $\text{MoO}_3$ ) and some oxides that form low melting phases (e.g.  $\text{BaO}$  and  $\text{SiO}_2$ ), fairly high levels of all the impurities listed in **Table 3.3** are tolerated by the immobilization form. Feed blending is required for the more extreme cases to decrease impurity concentrations to values closer to the average. Before the feeds are blended and then immobilized, high levels of volatile materials should be removed or depleted, and high halogen contents should also be removed or depleted.

**Table 3.3. Average and extreme impurity contents in the PuO<sub>2</sub> Feed**

	Average Feed	Max. All Feeds		Average Feed	Max. All Feeds
Impurity	(wt %)	(wt %)	Impurity	(wt %)	(wt %)
Al	1.58	7.94	Mo	0.50	2.39
Am	1.74	4.00	Na	0.71	2.36
B	0.13	0.77	Ni	0.28	2.67
Ba	0.53	4.48	Nd	1.03	12.57
Be	0.00	0.00	Np	0.41	3.20
C	1.99	40.68	P	0.01	0.69
Ca	2.14	48.34	Pb	1.98	10.65
Cd	0.00	0.00	Si	1.70	26.38
Ce	0.62	2.16	Sn	0.02	0.23
Cl	1.76	12.37	Ta	0.27	6.07
Cr	0.14	1.37	Th	0.00	0.01
Cu	0.43	2.67	Ti	0.07	2.07
F	2.06	29.94	U	20.92	68.39
Fe	0.60	5.66	V	0.00	0.00
Ga	1.19	9.55	W	0.06	2.16
Gd	0.11	0.59	Zn	0.20	2.25
Hf	0.83	0.63	Zr	0.00	0.02
Hg	0.00	0.00			
K	0.77	7.95	Pu	63.13	134.18
La	0.06	1.71	O	11.74	52.13
Mg	1.08	22.49			
Mn	0.00	0.07	Total	120.79	531.79

### 3.2 Repository Considerations

The immobilization form must provide adequate performance in a geologic repository and be capable of qualification for acceptance by a repository. This implies that the form must:

- Incorporate sufficient neutron absorber(s) to assure long-term criticality safety;
- Be sufficiently durable under disposal conditions;
- Not have a deleterious effect on the repository performance of the surrounding vitrified HLW (assuming the can-in-canister disposition alternative);
- Withstand the thermal cycle associated with the HLW canister cool-down with no adverse effects on performance or the capability to qualify the waste;
- Meet the other applicable requirements for a waste form in a geologic repository as specified by regulations and repository acceptance documents.

### 3.2.1 Criticality Safety and Durability

If arranged in a suitable configuration, the quantity of Pu in a HLW canister of the current can-in-canister design is more than sufficient for nuclear criticality to occur under certain assumed repository conditions. It is therefore necessary to prevent this by the addition of suitable neutron absorbers. Ideally, one would choose a neutron absorber that has chemical characteristics identical to those of Pu so that ceramic degradation and transport processes will not separate the Pu and absorber from one another. Unfortunately, such a material does not exist. We can, however, choose to incorporate neutron absorbers that are known to be relatively insoluble in groundwater, and will therefore remain in the waste package with the Pu, or its principle daughter  $^{235}\text{U}$ , as the ceramic eventually degrades.

In the long term, of course, the Pu will totally decay, primarily to the fissile nuclide  $^{235}\text{U}$ . In the case of uranium, it is possible to add the non-fissile  $^{238}\text{U}$  to isotopically "dilute" the  $^{235}\text{U}$ . The current ceramic formulation does involve addition of depleted or natural U. Although it is not economically feasible to add sufficient  $^{238}\text{U}$  to preclude criticality, the added uranium does assist in making far-field criticality even less likely by increasing the quantity of uranium that must be transported and then reprecipitated in a configuration free from the added neutron absorbers. Should further protection be required for the far-field criticality case, it would be feasible to add additional depleted U in the vicinity of the canister during emplacement.

As fabricated, the proposed ceramic formulation is criticality safe in any configuration, even when fully moderated. As long as the form stays intact, criticality safety is assured. It is only when the form begins to degrade by contact with groundwater in a repository that there might be a question of criticality safety. The rate and mechanism by which the ceramic degrades are thus intimately related to the question of long-term criticality safety. Obviously, the more durable the material, the longer one can be assured of criticality safety. However, there are no simple measures of "sufficiency" for either neutron absorber content or ceramic degradation rate. The envelope of acceptable composition and performance can only be determined by analyses that examine the potential consequence of various credible degradation scenarios of the immobilization form. DOE-RW and its contractors are performing such analyses. Their latest series of criticality analyses were conducted using a ceramic composition and Pu loading consistent with those given in this report. [33] The relative degradation rates of the ceramic, HLW glass, and container were varied independently, within realistic limits. They found no physically realizable scenarios in which a nuclear criticality was found to be possible within the waste packages.

### 3.2.2 Compatibility with High Level Waste

Both the ceramic form and the associated hardware used to contain it in the can-in-canister configuration must be compatible with the vitrified HLW and its canister. Here, compatibility is taken to mean that the can-in-canister materials do not impede the pour of the HLW glass melt into the canister, that they do not react with the melt/glass, and that they do not have a deleterious effect on the performance of the HLW glass under repository conditions. Conversely, the ceramic must be chosen such that the glass does not have a deleterious effect on the performance of the ceramic.

Tests are being conducted within the D&T program [34] to demonstrate that such undesirable interactions do not occur. Testing to date indicates that the ceramic degrades at a rate so much slower than the glass that it can be considered inert from the standpoint of the glass. Similarly, it is not expected that the degradation of the glass will affect the degradation rate of the ceramic. It is possible, however, that colloidal material produced by the alteration of the HLW glass could provide a transport mechanism within the repository for surface-active species such as Pu. Such an interaction, however, would exist for any waste form chosen for Pu disposition in the can-in-canister configuration.

In addition to chemical considerations, the ceramic form must be capable of withstanding the thermal cycle associated with the HLW canister cool-down with no adverse effects on performance or the capability to qualify the waste. Thermal cycling tests conducted with early versions of the current ceramic formulation indicate that no detectable changes occur in mineralogy, chemistry, or grain size of ceramics subjected to simulated cooling histories. Some cracking of the pucks due to thermal shock may occur. The extent to which this occurs may need to be quantified and reported to the repository, as fracturing will change the exposed surface area of the ceramic. Early test results of actual glass pours into canisters containing the ceramic waste form indicate that this cracking does occur as expected, but that it is well within acceptable limits for increasing the surface area.

### 3.2.3 Other Repository Requirements

The current NRC regulation governing the licensing of a high-level nuclear waste repository is 10CFR60<sup>1</sup>. This regulation specifies certain requirements on repository subsystems, including several design requirements that pertain specifically to the contents of the waste packages (including the waste forms). These requirements are that, to the extent that they might compromise the ability of the disposal system to isolate waste, the waste package cannot contain organic materials, free liquids, or explosive, pyrophoric or combustible materials. The ceramic proposed for Pu disposition will easily meet these requirements.

In addition to the regulatory requirements of Part 60, the repository program also requires that any waste form be free of hazardous materials. Specifically, the Producer must determine and report to DOE-EM and DOE-RW the presence or absence of any hazardous waste listed in 40CFR261.31 through 40CFR261.33, in the waste. Any RCRA-listed component in the waste requires the Producer to petition EPA and receive exemption to de-list the waste.

The Producer must also perform the appropriate tests and procedures, as described in 40CFR261.20 through 40CFR261.24, using samples from production runs or prototypical specimens to determine if the immobilized form that will be received by the repository has

---

<sup>1</sup> The NRC is currently in the process of revising Part 60, and is expected to promulgate new regulations (10-CFR-63) that will supersede Part 60 for the case of licensing a repository at Yucca Mountain. The draft of Part 63, which is currently under review, does not include the subsystem specifications and requirements present in Part 60. Requirements are only placed on the system as a whole. Although the regulatory basis for the waste package design requirements may disappear, they are reasonable, and will probably be maintained as requirements imposed by the repository program itself.

hazardous characteristics. Any waste that is shown to have hazardous characteristics must be treated to remove such characteristics.

### 3.3 Selection of the Form and Process

Development of the ceramic formulation is dependent, at least in part, on the fabrication process that is used. For example, an important product property, namely the phase assemblage, is determined primarily by the formulation used. However, the fabrication process (e.g., the sintering temperature and atmosphere) also affects the phase assemblage. For this and other similar reasons, it was therefore necessary to develop the formulation and fabrication process of the ceramic in parallel.

#### 3.3.1 Selection of the Formulation

As noted earlier, the program schedule and the charter assigned to LLNL by DOE-MD (now identified as NN-60) did not permit extensive study of alternative phase assemblages for the plutonium immobilization ceramic. Nevertheless, a few samples of alternative mineral compositions were prepared by mixing oxide precursors with cerium (used as a surrogate for plutonium) and uranium oxides, then cold pressing and sintering. The samples were characterized by x-ray diffraction and scanning electron microscopy with energy dispersive x-ray analysis (SEM-EDS). These included samples of zircon, zirconia, and monazite. Note that these materials are representative of materials under investigation at other research sites on an independent basis for similar applications. As an example, Zircon was being championed by William Weber, Rodney Ewing and Werner Lutze in the U.S. [35], and by Boris Burakov, Evgeny Anderson, and others at the Khlopin Radium Institute (KRI) in St. Petersburg, Russia [36]. Zirconia was also part of the KRI-proposed assemblage, and in addition was proposed as the basis for a once-through, disposable reactor fuel for burning plutonium [37]. Monazite had been studied earlier by Lynn Boatner and others at Oak Ridge National Laboratory (ORNL) as a potential waste form for high level waste [38]. All of these immobilization forms have the capability to incorporate significant amounts of plutonium and offer high durability in geologic environments.

Zircon was of interest because of the large number of natural analogs in nature. Zircons are some of the oldest known minerals on earth, some of which have survived for periods in excess of 1 billion years. In these studies, it was found that zircon was more difficult to fabricate than the titanate minerals of zirconolite and pyrochlore. A higher fabrication temperature was necessary for reactive sintering, and even then, the reaction of the precursor materials was not complete. Seed crystals of zircon were used to facilitate sintering, but little improvement was observed. More elaborate fabrication methods, such as the alkoxide-nitrate fabrication process, were not pursued. This preliminary work found that the straightforward cold pressing and sintering process that is effective for the chosen titanate-based ceramic would not work for zircon. While more exotic processing approaches could be developed, it was not felt that the Pu immobilization mission justified the added development expense and uncertainty coupled with a potentially more expensive production processing requirement which would be required to bring zircon to the same readiness state. Whereas, a very reliable and straightforward production process had already been developed and demonstrated for the titanate-based ceramics.

Preparation of well reacted zirconia was achieved at temperatures as low as 1350°C, but the degree of densification was low compared to the titanate-based ceramics. It was not necessary to charge-balance the 3+ lanthanide with a 5+ element in order to achieve a well reacted product. Zirconia in the cubic structure was expected to be very resistant to radiation damage because it is the same structure as uraninite which does not become metamict, even in a nuclear reactor [39-41]. Zirconia appears to be a good host phase for pure plutonium oxide, but higher sintering temperatures would be required in order to achieve low porosity in the product. For impure plutonium oxide, however, little is known about the relative stability of this phase and the accessory phases that would form. Natural analogs of zirconia do exist in nature, but they are very rare. As a result, the behavior of this mineral over geologic time periods is not well understood.

Preparation of well reacted monazite was also achieved at temperatures as low as 1350°C, but again the densification was not complete. Like zirconia, monazite could be an acceptable host phase for plutonium oxide if higher sintering temperatures were used. A number of impurities can be accommodated into the monazite phase, but much more is known about incorporation of impurities into zirconolites and pyrochlores. Unlike zirconia, there are plenty of monazites in nature which have survived over geologic time periods.

Based upon the small amount of work performed on these alternative host phases, none of them appeared to offer an overall advantage over the titanate-based phases, which had already received considerably more study in connection with high-level nuclear waste programs. This reinforced the idea that titanate-based ceramics were the best form for the immobilization of excess weapons plutonium, although one can always presume that the immobilization form could be improved or optimized with additional research, time, and money.

In the development of the titanate-based mineral form, Ebbinghaus initially selected a formulation consisting primarily of the mineral zirconolite (80 weight percent), with smaller amounts of barium hollandite (15 weight percent) and rutile (5 weight percent) [23]. In choosing this formulation, Ebbinghaus adapted the composition of SYNROC-C to the task of plutonium immobilization. He selected zirconolite as the host mineral for plutonium and gadolinium because of its ability to incorporate them into its crystal structure in large amounts (based on previous work by ANU and ANSTO), and because of its high durability. He selected barium hollandite to serve as the host for cesium, as in SYNROC-C, for the internal radiation barrier concept. For the external barrier case (heterogeneous, or can-in-canister), the cesium could be left out of the formulation. The rutile was present as a chemical buffer, to help prevent the formation of less durable phases. The designed mineralogy was as follows:

80 wt % zirconolite ( $\text{Ca}_{0.75}\text{Gd}_{0.25}\text{Zr}_{0.75}\text{Pu}_{0.25}\text{Ti}_2\text{O}_7$ )  
15 wt % hollandite ( $\text{Ba}_{1.14}\text{Al}_{2.29}\text{Ti}_{5.71}\text{O}_{16}$ )  
5 wt % rutile ( $\text{TiO}_2$ )

The above formulation was then used to calculate the amounts of the precursor components to mix together and process. The precursor is the non-radioactive matrix materials which are generally premixed and then blended with the plutonium and/or uranium oxide to form the

overall desired composition. In this formulation, the fabricated product matched the design mineralogy reasonably well, although traces of pyrochlore were also present. The rutile content appeared to be slightly greater than 5 wt %, and the hollandite content appeared to be slightly less than 15 wt %. Based upon the above formulation, the theoretical maximum density was calculated to be  $4.92 \text{ g/cm}^3$ . The actual geometric density observed was about  $4.5 \text{ g/cm}^3$ . This initial formulation is now referred to as the zirconolite-based form. A secondary electron image (SEI) of the zirconolite-rich Pu ceramic form is shown in **Figure 3.1**.

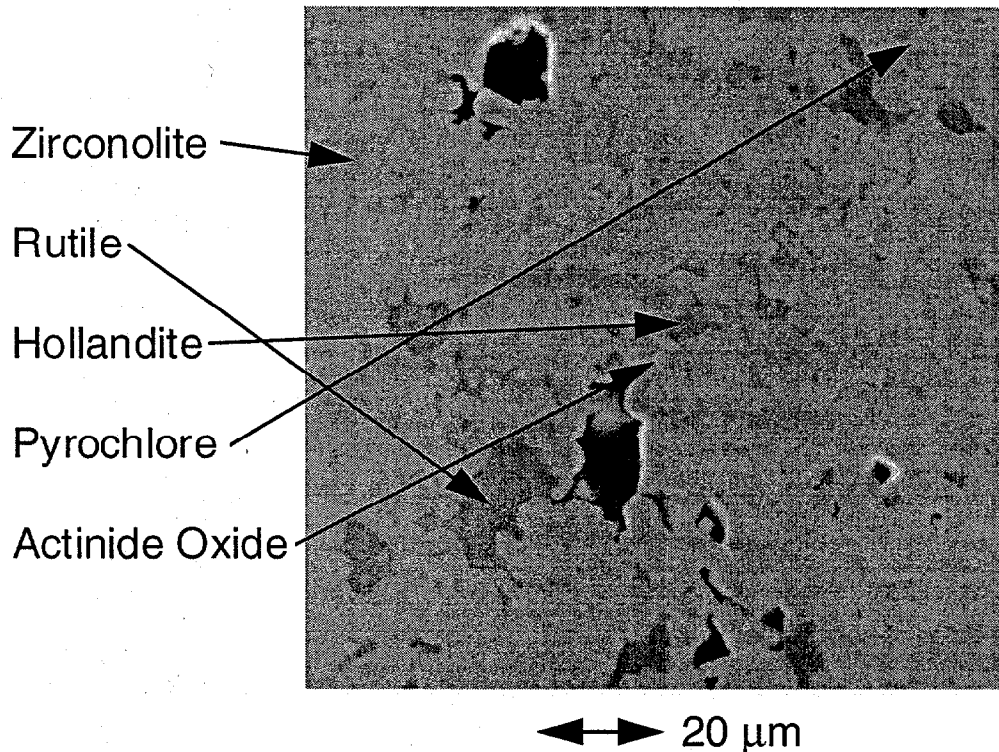


**Figure 3.1. Secondary electron image (SEI) of zirconolite-rich form**

The initial formulation assumed that the feed stream to the Plutonium Immobilization Plant would be relatively pure  $\text{PuO}_2$ . Once the preliminary compositions of the actual feed streams became available, it was apparent that the feed streams targeted for immobilization at that time had on average about equal amounts of uranium (primarily natural and depleted uranium) and plutonium. If the Pu-loading in the form were to remain at about 12 wt %, the excess uranium would stabilize considerable amounts of pyrochlore in the product. The potential for disposing of U-rich HLW had already led to the development of pyrochlore-rich SYNROCs called SYNROC-F [20] and SYNROC-FA [21] (See **Table 2.1**).

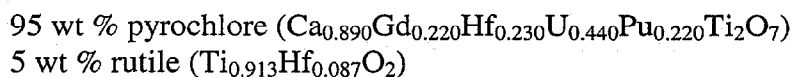
At about the same time as the more realistic feed compositions were being assembled, questions about the radiation damage effects in the ceramic form were raised. An initial conservative long-term degradation analysis performed by OCRWM assumed that after a few thousand years, swelling caused by alpha decay of plutonium in the ceramic would make the zirconolite-rich ceramic fracture into a powder at the grain boundaries [42]. The same analysis by OCRWM indicated that, under worst case assumptions, the gadolinium could become soluble, and that a

small concentration of the insoluble neutron absorber hafnium could prevent criticality. In particular, the small amount of hafnium present as a contaminant in the zirconolite phase (2 to 5 wt % of total zirconium) was found to increase, by 50%, the amount of  $^{239}\text{Pu}$  that could be carried in a waste package without permitting criticality. It was clear that the ceramic form would benefit from a redesign of its formulation.

On April 8, 1997 during a videoconference including researchers from LLNL, SRTC, and ANSTO, Ebbinghaus proposed a new formulation and an initial impurity test matrix later called the Series A matrix [43]. The following criteria were agreed upon:

- Uranium-to-plutonium mole ratio of approximately 2-to-1 (easily accomodates uranium content in most feed streams)
- Gadolinium-to-plutonium mole ratio of 1-to-1 (same as in zirconolite-rich formulation)
- Hafnium-to-plutonium mole ratio of 1-to-1 (replace zirconium with hafnium and select 1-to-1 ratio as was done with gadolinium, to provide additional criticality safety, i.e. "Double Contingency")
- Eliminate BaO and hollandite from the form (removes RCRA-controlled elements from the formulation).
- For purposes of calculating the feed composition, assume a pyrochlore form with a small amount of rutile (95 wt % pyrochlore, 5 wt % rutile).
- Plutonium concentration about the same as in the zirconolite-rich form (reduced to about 10 wt % because of the higher density of pyrochlore)

Given the above criteria, the baseline form was designed as follows:



Note that extra hafnia was added because the rutile in the zirconolite-rich formulation had been found to contain about 6 mol % zirconia. In the absence of specific experimental data for hafnia in rutile, it was expected to behave similarly to zirconia and to substitute into the rutile at about the same mol %. To ensure that enough hafnia would be present, the rutile was assumed to contain about 9 mol % hafnia. Based upon the above formulation, the theoretical maximum density for the new formulation was calculated to be  $5.96 \text{ g/cm}^3$ . The actual geometric (e.g. bulk) density later observed experimentally was about  $5.5 \text{ g/cm}^3$ .

As planned, pyrochlore was to be the primary phase, and rutile was to be present in small amounts. However, the actual form that was produced varied slightly from the design phase assemblage in the respects that brannerite was also formed, and if impurities were present, zirconolite generally formed as well. Although this result was slightly different than expected, zirconolite was known to be a durable phase, and brannerite was expected to be durable as well.

Both have natural mineral analogs that have survived over geologic time periods. Allowing a relatively wide range of pyrochlore, zirconolite, and brannerite abundances in the product made the form much more tolerant to impurities in the  $\text{PuO}_2$  feed than a form based nominally on a single phase.

A backscattered electron image of the product produced from this revised formulation is shown in **Figure 3.2**. The actual product formed was composed of about 80 vol. % pyrochlore, with the balance being about 15 vol. % brannerite and about 5 vol. % rutile. At a form development meeting at LLNL on June 9 – 10, 1998, the results of this formulation were reviewed in detail. While further modification of this form could be made by increasing the rutile content to further increase impurity tolerance, it was not felt to be necessary given the expected impurity levels in the feed.

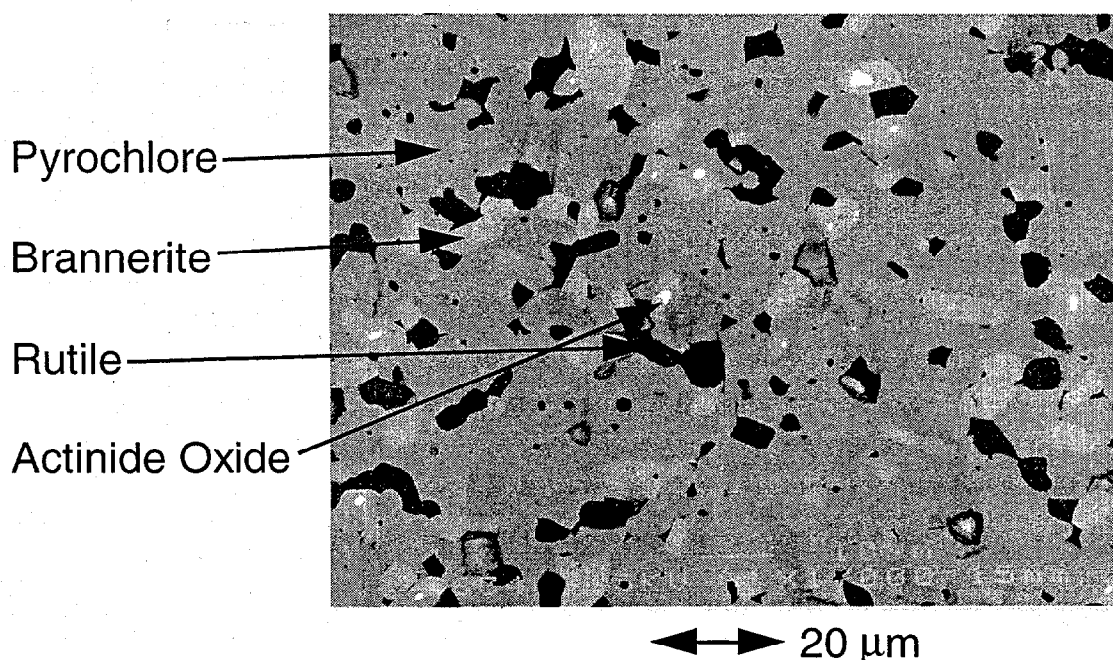
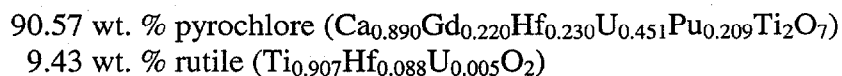


**Figure 3.2. Backscattered electron image (BEI) of pyrochlore-rich form**

Subsequent to this meeting, this form was modified slightly to satisfy safeguards and security requirements at the DWPF by reducing the Pu loading of the ceramic to less than 10%. This reduced Pu loading, which will result in substantial operational savings at DWPF, was done by decreasing the weight fraction of plutonium in the pyrochlore phase and by increasing the abundance of the rutile phase. With this adjustment, the following phase abundances and compositions constitute the formula design for the current baseline formulation:



The theoretical maximum density calculated from these assumed phases is  $5.91 \text{ g/cm}^3$ , which is approximately 1% lower than the density of the original baseline composition. As was observed

in the earlier pyrochlore-rich formulation, a small amount of brannerite is formed along with the pyrochlore and rutile. As expected more rutile is formed in this formulation.

### 3.3.2 Selection of the Fabrication Process

In the past, SYNROC-C had been made primarily by performing hot uniaxial pressing (HUP) of the constituents in a bellows can. This was the scheme used in the ANSTO demonstration plant [16]. Large-scale hot isostatic pressing (HIP) of SYNROC-D in sealed cans had also been demonstrated [44]. Methods such as these, using cans to contain the material in either a hot uniaxial press or a hot isostatic press, are necessary when volatile species such as cesium are to be incorporated into the ceramic. Both HUP and HIP produce a product with a density very near the theoretical maximum value.

In hot pressing, overall throughput favors large product size, because of the long cycle time required in the hot press cycle. Initially, fabrication of the ceramic as uniaxially hot-pressed disks weighing about 30 kg each was considered. These disks would have been about 30 cm (1 foot) in diameter by about 9 cm (3.5 inches) high. However, this large size was not compatible with the can-in-canister process, because it would have obstructed the flow of the molten glass into the canister. Brief consideration was given to using the HIP process to fabricate long and slender ceramic bodies that were compatible with the can-in-canister process [45], but this was not considered feasible due to safety and process complexity for the current application.

One of the standard process operations for commercially fabricating ceramics is cold pressing and sintering. This process is used for making reactor fuel pellets and, in particular, MOX fuel pellets incorporating plutonium oxide. This approach had been demonstrated earlier for SYNROC ceramics by Solomah and coworkers [46]. The initially perceived disadvantages of cold pressing and sintering involved concerns associated with the escape of cesium as a volatile species and possible porosity in the product.

Another approach to fabrication was melting and solidification of the form from the melt. Because of the high melting temperature of the ceramic and the difficulties involved with durability of high temperature crucibles, a cold-crucible approach would have been necessary. Cold crucibles have a significant amount of hold up. As a result, this approach would complicate the materials control and accountability needed for plutonium. If cesium was also to be incorporated, its volatility would be more of a problem at the higher temperatures involved in melting. In addition, melting and solidifying produces a large-grained product that is likely to be less homogeneous and more prone to cracking as a result of differential swelling induced by radiation damage.

As it became clear that the can-in-canister approach offered significant advantages to the program as a whole in terms of simplicity of implementation, cost, and schedule, the problems associated with cesium retention in the ceramic disappeared, thus providing motivation to develop the cold press and sinter approach. The high intrinsic chemical durability of the titanate minerals was expected to prevail in the repository, even if there was a small amount of porosity in the ceramic.

In developing the cold press and sinter process for Pu immobilization, the main differences between the ceramic immobilization product and the mixed (uranium and plutonium) oxide reactor fuel (MOX) are the size and composition of the form. The selection of the size of the ceramic form was based on achieving the largest size possible consistent with ceramic fabrication techniques and the constraints placed on the puck size by the DWPF canister. Early development work in this area indicated that sintered pucks on the order of 2.5 inches in diameter could be made. In considering the canister limitations on form size, care must be taken to minimize interference with the glass stream during pouring which would set an upper limit on the can size containing the form. Even more important was the desire to load the Pu-containing ceramic form into the canister after the DWPF canister had been fully fabricated and qualified. This necessitated loading the ceramic form through the neck of the canister, which was on the order of 4 inches in diameter. Subsequently, a technique for loading the canister was developed which could accommodate a 3 inch outside diameter can containing the ceramic form. Given desired manufacturing tolerances of the form, the size of the sintered form was set at a nominal diameter of  $2.65 + 0.125$  or  $- 0.225$  inches [47]. The selection of the thickness of the form was arbitrary, and was set at nominally 1 inch. Based on discussions with several ceramic engineers and suppliers of automated presses, forms of this size are believed to be about the largest size that could be fabricated reliably by an automated process using cold pressing and sintering. For convenience and because of the similarity in size and shape of these sintered pellets to hockey pucks, they are referred to as pucks.

As noted earlier, cold pressing and reactive sintering had been demonstrated for SYNROC-FA, and it was also under development at LLNL for the Mixed Waste Management Facility project [22], which aimed at developing a ceramic for disposal of mixed wastes. Cold pressing and sintering had been demonstrated to be a very convenient process for making small samples for testing formulations. These samples demonstrated that excellent reactivity could be achieved by integrally mixing milled materials, and the resulting products had the correct phase assemblage and acceptable porosity. Thus, the basic processes used for sample fabrication were modified and adapted to make the larger sizes needed for production scale immobilization operations.

Important steps in the cold press and sinter fabrication process are the milling/mixing step, the granulation and pressing step, and the binder burnout and sintering steps. There were two options considered for the milling/mixing step. In our early laboratory work, the milling/mixing operation was carried out using a wet ball mill process. For plant operations, one option involves the use of a high energy attritor mill, and the other involves the use of a conventional ball mill. In the MOX fuel industry, a processing option using sequential high energy attritor mills was developed by BNFL and is commonly referred to as the "Short Binderless Route" [48,49]. The MOX manufacturing process option using dry ball mills was developed at Belgonucleaire and Cogema and is commonly referred to as the "Mimas" process [50]. Extensive testing with surrogate and uranium based feed materials and ceramic precursors necessary to produce the Pu immobilization form indicated that milling/mixing with attritor mills is far superior to dry ball milling for the immobilization form. Dry ball milling/mixing was found to involve substantial packing and compaction of the product and was not very effective for milling or mixing the disparate types of oxide powders required to make the plutonium immobilization ceramic. If ball milling/mixing had been selected, it is likely that a wet process would have been required similar to the laboratory process initially employed. However, wet processing involves using more

complicated process operations, thus increasing plant complexity. In addition, it is desirable to avoid wet processes for additional safety against nuclear criticality during processing.

For pressing, it is necessary to add a small amount of binder material to the powder prior to feeding the material to the press to assure green puck integrity. For the pressing step, the objective is to obtain sufficient density to assure puck integrity for sintering. Since the sintering process involves substantial chemical changes in the form, densification of the process is driven more by the preparation of the precursors and the milling/mixing process than it is by the density of the pressed green puck. As a result, the pressures required during the pressing cycle are very low compared to those used in MOX and many other ceramic fabrication processes. Pressures as low as 7 MPa (1000 psi) were demonstrated to be adequate for this immobilization form. Additional process operations, such as granulation to reduce dust and improve powder flow to the automatic press, modify the pressing characteristics. Currently, a tumbling granulation process is being used with the addition of water and binder which produces good green pucks with about 14 MPa (2000 psi) pressing pressure. The puck press will be specifically designed for this process, but will probably be very similar to those used in the MOX industry.

For the binder burnout and sintering step, two types of furnaces were considered – a bottom-loading furnace box furnace and a conveyer-type furnace. The conveyer furnace is often preferred in the MOX industry, but a high-temperature bottom-loading furnace is currently believed to be more suitable for the ceramic immobilization plant due to the size of the pucks and the fact that the pucks, particularly ones high in impurities, will stick to each other if they are in contact during the sintering cycle. Experiments on actinide oxide reaction kinetics using the zirconolite-based formulation indicated that a firing temperature of 1350°C for 4 hours was required to achieve good reaction of PuO<sub>2</sub> particles initially less than 20 microns in size with the ceramic precursors. Later experiments on the pyrochlore-based form indicated that lower temperatures could probably be used, but 1350°C for 4 hours has been retained as the baseline sintering temperature and time to assure that thermodynamic equilibrium is approached in the product form. The sintering atmosphere was initially selected to be argon gas. Later experiments on the pyrochlore-based form indicate that air is also a suitable sintering atmosphere [51], e.g. there is little if any difference in the relative abundance of the phases that form. Since air is lower in cost and easier to use than argon, the preferred sintering atmosphere is now air.

## **4. *Development of the Ceramic Form***

---

### **4.1 Overview**

As discussed previously, development of the baseline formulation and baseline process operations are coupled; one cannot be complete without the other. More specifically, the baseline formulation has been designed so that the desired phase assemblage is obtained in the product, while using process operations which are adaptable to production operations.

The Form Development sample test plan [43] described below was designed to develop a detailed understanding of how the selected baseline formulation would be affected by variations in feed composition (including impurities) and processing parameters. At this time, the Form Development activity is essentially complete and the selected baseline formulation has been shown to be sufficiently robust to accommodate expected variations in feed composition and process parameters while producing a product phase assemblage which is sufficiently durable for repository acceptance.

#### **4.1.1 Form Development Tasks**

The Form Development activities were divided into the following four task areas.

##### **Task 1. Planning and Facilities**

- Establish capabilities for small-scale sample fabrications.
- Define the sample test matrix.

##### **Task 2. Baseline Formulation and Process Parameters**

- Define the baseline formulation.
- Provide feed specifications for the PuO<sub>2</sub> feed.
- Provide process data to support scale-up testing and prototype equipment design.

##### **Task 3. Form Qualification Samples**

- Provide samples for durability testing.
- Provide samples for thermodynamic data measurements.
- Determine range and composition of phases in the product.

##### **Task 4. Process Control Model Development**

- Development of a process control model to ensure that the ceramic fabrication process will produce an acceptable product.
- Provide the necessary sample and characterization data to support process control model development.

#### 4.1.2. Participants and Capabilities

The Form Development participants were LLNL, ANSTO, SRTC, and ANL. PNNL has been involved peripherally, and have provided fabrication and testing of the radiation damage test samples. All of these laboratories have capabilities to make small-scale, plutonium-loaded samples. Supporting calorimetric work was performed at UCD and BYU. The types of samples that were prepared at each site were dependent largely upon the characterization equipment available at the site and on the nature of characterization tests (e.g. durability, thermochemical, and non-destructive evaluation (NDE) tests) that would be performed. Some redundancy was built into the test plan, particularly for high priority samples needed for durability testing.

With the exception of the calorimetric work, analytical capabilities for the non-plutonium work were equivalent at all of the sites. As shown in **Table 4.1**, however, there were significant differences in readily available analytical equipment to perform analyses of plutonium-loaded samples. More specifically, ANSTO and SRTC had the capability to perform X-ray diffraction work. LLNL had the only capability for compositional analysis using an electron microprobe. All of the sites had scanning electron microscopy/energy dispersive spectrometry (SEM/EDS) capability, but ANSTO had the most complete selection of standards suitable for quantitative SEM/EDS work on the plutonium-loaded ceramics. ANL and ANSTO were best set up to perform TEM work. ANL was performing a large fraction of the durability tests. Consequently, many of the samples needed for durability testing were fabricated at ANL. SRTC and ANSTO had the capability for performing immersion density testing. However, this capability is relatively easy to install. With some effort, plutonium-containing samples were able to be shipped among the DOE sites. However, shipment of such samples from ANSTO to any of the DOE sites or from any of the DOE sites to ANSTO was essentially precluded by international shipping regulations.

**Table 4.1. Readily available analytical capabilities for Pu-loaded samples**

Analytical Capability	Sites with Readily Available Capabilities for working with Pu-loaded Materials <sup>a</sup>
X-ray Diffraction Analysis	ANSTO, PNNL, and SRTC <sup>b</sup>
Quantitative Microprobe Analysis	LLNL
Quantitative EDS Analysis	ANSTO <sup>c</sup>
TEM Analysis	ANL and ANSTO
Immersion Density	ANSTO, PNNL, and SRTC
Durability Testing	ANL <sup>d</sup>

<sup>a</sup>Note that all sites had additional Pu capabilities that are not listed.

<sup>b</sup>ANL and LLNL also had Pu X-ray diffraction capabilities. At the time, the LLNL equipment needed to be serviced to perform better. The ANL equipment was outside the normal Pu processing area.

<sup>c</sup>ANL, LLNL, PNNL and SRTC all had EDS capabilities that could be made quantitative with a better selection of standards that closely matched the compositions of the minerals in the ceramic product.

<sup>d</sup>LLNL, PNNL and SRS were also involved in a smaller suite of durability tests.

Calorimetric work was limited to non-plutonium work at UCD and BYU. At UCD standard enthalpies of formation of various phases of interest were determined by drop solution calorimetry. Much of the work was performed on uranium- or thorium-bearing samples. Some measurements on plutonium-bearing samples were planned at LANL but were never accomplished. At BYU standard entropies of various phases of interest were determined by integrating low temperature heat capacity measurements. With the exception of one uranium-bearing sample, this work was performed entirely on non-radioactive samples.

## 4.2 Sample Test Matrices

Detailed sample test plans or matrices were first developed in late December 1997 at a review meeting at SRTC. The sample test matrices were reviewed and updated at a project-wide form development planning and review meeting at LLNL in early June of 1998. The test matrices comprised a number of test series; i.e., A, B0, B1, etc. The A series originated in FY'97, and the B series originated in FY'98 [52]. A statistically-derived sample test matrix for impurity studies was later developed by SRTC in FY'00 [53]. The series A and B samples are currently complete. Some of the sample series corresponded to a single composition, while others corresponded to a range of compositions or impurity loading levels. For each composition identified, several to approximately a dozen samples were prepared. Some were sintered at different temperatures or under different atmospheres, some were fabricated by different processes, and so on.

In general, each series supported primarily one task (the solid lines) and peripherally supported at least one of the other tasks (dashed lines). The linkages between the sample test matrices and the tasks are shown in **Figure 4.1**.

The development, testing, and refinement of the baseline formulation was dependent upon all of the sample series. However, the main sample series that supported the selection and development of the baseline formulation were the A Series, B1 Series, B4 Series, and B5 Series.

Although a significant number of validation tests were performed with plutonium, the majority of sample fabrications were performed with various non-radioactive surrogates. Surrogates were selected based on similarity of atomic size, melting point of the constituent oxide, and relative stability of the valence states as a function of oxygen partial pressure. The data for plutonium, americium, and various surrogates are shown in **Table 4.2**. Atomic radii were obtained from Shannon [54]. The melting points of  $\text{CeO}_2$ ,  $\text{ThO}_2$ ,  $\text{PuO}_2$ , and  $\text{Nd}_2\text{O}_3$  were taken from various compilations [55-57]. The melting point of  $\text{Am}_2\text{O}_3$  has not been determined, but it is known to be greater than  $1200^\circ\text{C}$  [57]. Oxygen partial pressures in equilibrium with the oxide phases were calculated using the FACT program [58].

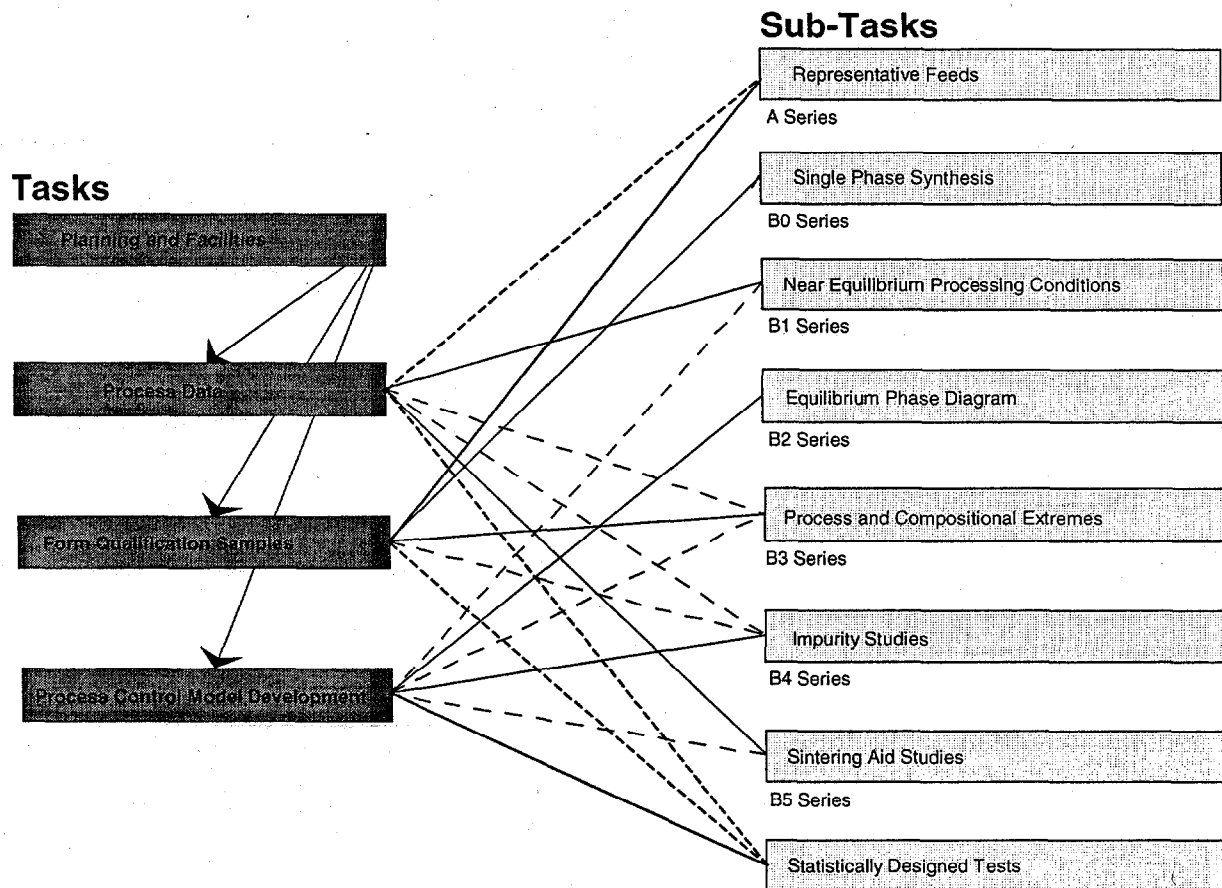


**Figure 4.1 Linkages Between Tasks and Sample Test Matrices**

In the baseline ceramic, the best surrogate for plutonium is generally cerium. Its ionic size is almost identical to the corresponding value for plutonium, and the melting point of its constituent oxide is comparable to that of plutonium oxide, indicating that the strength of the bonding is approximately equivalent. If conditions in the sample preparation are moderately reducing, however, cerium can be a relatively poor surrogate for plutonium, since it will generally convert to the trivalent ion, while plutonium under the same conditions will generally remain as the tetravalent ion. Under reducing conditions, thorium is believed to be a better surrogate for plutonium than is cerium. Thorium is also preferred over cerium as a surrogate for plutonium in the "near equilibrium" tests.  $\text{CeO}_2$  is observed to be much more reactive than  $\text{PuO}_2$  during sintering.  $\text{ThO}_2$  has a considerably lower reactivity than  $\text{CeO}_2$ , much closer to that of  $\text{PuO}_2$ . For tests simulating americium-enriched material, neodymium was selected as the best surrogate. Based on the atomic size, melting points, and relative ionic stability, neodymium is expected to behave very similarly to americium in this ceramic.

**Table 4.2. Surrogates for plutonium and americium**

	<b>CN = 8</b>	<b>AnO<sub>2</sub></b>	<b>An<sub>2</sub>O<sub>3</sub>/AnO<sub>2</sub></b>
Element	r <sup>4+</sup> , (nm)	M.P. (°C)	p(O <sub>2</sub> )*, (atm)
Ce	0.110	2730	2.3x10 <sup>-11</sup>
Th	0.119	3220	N/A
Pu	0.110	2390	2.5x10 <sup>-18</sup>
	<b>CN = 8</b>	<b>An<sub>2</sub>O<sub>3</sub></b>	<b>An<sub>2</sub>O<sub>3</sub>/AnO<sub>2</sub></b>
Element	r <sup>3+</sup> , (nm)	M.P. (°C)	p(O <sub>2</sub> )*, (atm)
Nd	0.125	2315	>6.9x10 <sup>-2</sup>
Am	0.123	>1200	2.1x10 <sup>2</sup>

\*p(O<sub>2</sub>) calculated at a temperature of 1350°C.

To clearly designate which surrogates (if any) are used in a sample, the following nomenclature is used. A sample composed of all baseline elements and no surrogates is referred to as a hafnium-plutonium-uranium sample (i.e., Hf-Pu-U). If cerium is used as a surrogate for plutonium, the sample is referred to as a hafnium-cerium-uranium sample (i.e., Hf-Ce-U). Likewise, if thorium is used as a surrogate for plutonium, the sample is referred to as a hafnium-thorium-uranium sample (i.e., Hf-Th-U). A sample in which cerium is used as a surrogate for both plutonium and uranium is referred to as a hafnium-cerium-cerium sample (i.e., Hf-Ce-Ce). If zirconium is used instead of hafnium, the sample is referred to as a zirconium-cerium-cerium sample (i.e., Zr-Ce-Ce).

#### 4.2.1. The A Series

There were 10 compositions in the A Series [52]. This series included the original pyrochlore-rich composition with nominally 10.5% Pu (A-0), six typical impurity feed compositions (A-1 to A-6) and three compositions with all the impurities: an average case (A-7), an extreme case (A-8), and an intermediate case (A-9). The current baseline pyrochlore-rich composition (A-10) can also be considered part of this series.

#### 4.2.2. The B Series

Whereas the smaller set of A Series samples demonstrated that the ceramic form was suitable for the disposition of excess plutonium, the larger B Series [52] was aimed at assisting in the understanding of key parameters of the ceramic form, providing samples for durability testing, and providing data that will be needed to scale-up and qualify the process. As shown in **Table 4.3**, the B Series is divided into six sub-series, each of which is discussed below.

**Single-Phase Samples (B0 Series).** These samples were used for single-pass, flow-through (SPFT) tests, enthalpy of formation measurements, absolute entropy determinations, radiation damage studies, X-ray standards, and other selected corrosion tests.

**Near-Equilibrium Samples (B1 Series).** These samples were used to demonstrate that the product obtained by various "plant-like" processes is at or near chemical equilibrium.

**Equilibrium Phase Diagrams (B2 Series).** These samples were used to define selected phase equilibria in binary and ternary oxide systems. These phase equilibria are essential in developing the process control model.

**Process and Compositional Extremes (B3 Series).** These are samples prepared at process and compositional extremes. These samples were used for durability and non-destructive evaluation (NDE) testing. Some samples were also used for radiation damage studies.

**Impurity Effects (B4 Series).** These samples, representing the largest group of the B series, were used to determine feed specifications for the form and to develop the preliminary process control model. The B4 series was divided into three sub series as follows:

- *Impurity Saturation (B4-S).* These samples were used to determine which secondary phases form when the primary phases are saturated with impurities. This work was performed primarily at LLNL.
- *Impurity Equivalence (B4-E).* These samples were used to determine which impurities are similar enough in behavior that they can be grouped together. This work was performed primarily at ANSTO.
- *Impurity Volatility (B4-V).* These samples were used to determine the effect of volatile impurities on the product density. This work was performed primarily at SRTC.

**Sintering Aid Studies (B5 Series).** A sintering aid may be needed to increase the product density or to make product densities more uniform from sample to sample. These samples were used to determine which impurities act as sintering aids.

**Table 4.3 Summary of the B series sample test matrices**

Series	I.D.	Sites Involved	Number*
Single Phase Synthesis	B0	ANL, ANSTO, LLNL, PNNL, SRTC, and UCD	33 samples
Near Equilibrium Processing Conditions	B1	ANSTO and LLNL	22 compositions
Equilibrium Phase Diagram	B2	ANSTO and LLNL	16 series
Process and Compositional Extremes	B3	ANL, LLNL, PNNL, and SRTC	22 compositions
Impurity Studies	B4	ANSTO, LLNL, and SRTC	53 series
Impurity Saturation	B4-S	LLNL	35 series
Impurity Equivalence	B4-E	ANSTO	12 series
Impurity Volatility	B4-V	SRTC	6 series
Sintering Aid Studies	B5	LLNL and SRTC	11 series

\*Normally between 2 and 12 samples were made for each composition, and between 2 and 12 compositions were made for each series.

In addition to the above samples, various samples were prepared on an as-needed basis to address various technical issues as they arose.

#### 4.2.3. Statistically Designed Tests

The final phase of testing in the Form Development activity involves statistically designed tests that cover a range of compositional variables and a range of response variables (*i.e.*, product properties). For these tests, a number of assumptions were made to limit the test matrix to a reasonable size. These tests consist of 40 compositions involving 11 compositional variables. These compositional variables occur in 5 different impurity categories. The compositional variables and the impurity categories they belong to are summarized in **Table 4.4**. The experimental plan for these tests has been described by Cozzi [53]. These tests are important in the development of the process control model [34, 59], formerly identified as the product control model.

**Table 4.4. Impurity categories for statistical tests**

Impurity Category	Representative Elements	Elemental Proportions per Valence Group	Maximum Moles Impurity per mole of PuO <sub>2</sub>
Volatile	Cl		1.32
	C		5.48
Pyrochlore Stabilizers	Ta		0.88
	Mo, W	Mo <sub>0.81</sub> W <sub>0.19</sub>	0.66
Zirconolite Stabilizers	Fe, Mg, Ni, Zn	Fe <sub>0.21</sub> Mg <sub>0.68</sub> Ni <sub>0.09</sub> Zn <sub>0.02</sub>	1.39
	Al, Ga	Al <sub>0.80</sub> Ga <sub>0.20</sub>	2.17
Rutile Stabilizers	Cr		1.10
Glass Stabilizers	Si		0.33
	F		0.66
	Na, K	Na <sub>0.61</sub> K <sub>0.39</sub>	0.33

Based on the impurity equivalence testing performed primarily at ANSTO, certain impurities are grouped as a single category or subcategory. These include the groups of Mo/W, Fe/Mg/Ni/Zn, Al/Ga, and Na/K. The elemental proportions chosen for these equivalent impurities is also given in **Table 4.4**. The compositions are based on the average feed composition given in **Table 3.3**. In the statistical design, the abundances of the impurities are allowed to vary up to the limit given in the Feed Specification report [60]. The compositions were selected independently of any predictive model.

Samples of all the compositions have been prepared at full-scale in the Hf-Ce-Ce variety and at small scale in the Hf-Pu-U variety. Some of the compositions have also been prepared full-scale in the Hf-Ce-U variety.

After the samples are prepared, they were inspected visually to determine the extent of cracking, if any, and they will be analyzed to determine density and phase abundance. While these tests are being performed, the methodology for projecting the phase assemblage has been developed and refined. This methodology will be used to project the phase assemblage of each of the 40

compositions that are being prepared. The projected phase assemblage will then be compared with those actually observed in the testing.

## **5. Immobilization Form Specifications**

---

### **5.1. Baseline Formulation**

The baseline formulation consists of the composition of the ceramic immobilization form, specifications on the precursors and actinide oxide feeds, impurity tolerances, and projected phase abundance in the product.

#### **5.1.1 Composition**

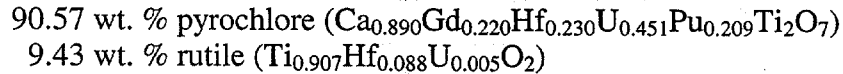
In the original version of this report, dated February 1999 [52], the former baseline composition and two alternative compositions (low-plutonium and high-plutonium) were presented. The former baseline contained 10.488 wt. % plutonium on an elemental basis. The low-plutonium alternative contained 10.000 wt. % plutonium, and the high-plutonium alternative contained 15.000 wt. % plutonium.

The low-plutonium alternative was formulated to be available in the event that safeguards and security guidelines at the DWPF required that there be no more than 10 wt. % plutonium in the ceramic. In this alternative, the abundance of rutile was increased by roughly 5 wt. % compared to the original baseline. The increase in rutile content lowered the plutonium content of the ceramic as a whole, without changing the mineralogy (phases present). The extra rutile also gives this formulation more flexibility to accommodate impurities in the plutonium feed streams.

The high-plutonium alternative was formulated to be available in case a policy decision was made that all 50 metric tonnes of declared excess U.S. weapons-usable plutonium were to be immobilized in ceramic. In this case, the higher plutonium loading would have been cost-effective, because it would have significantly decreased the total amount of ceramic that would have to be produced.

As requirements at DWPF became more firmly established, it became clear that safeguards and security guidelines favored a composition that incorporated less than 10 wt. % plutonium. Furthermore, DOE decided that the U.S. would produce MOX fuel from a large portion of the plutonium designated as excess to the needs of national security. As a consequence, In January, 2000, program management requested a new baseline formulation containing 9.5 wt % Pu rather than 10.488 wt % Pu. The formulation was redesigned using the approach described above for the Low-Plutonium Alternative, together with a slight increase in the ratio of uranium to hafnium in the pyrochlore phase. These changes preserve the phase assemblage (mineralogy) of the former baseline formulation, and thus do not affect the process for making the ceramic or the expected durability of the ceramic in the repository. These changes were made with a high degree of confidence without performing an extensive retesting program because of the foundation established in the earlier work on phase equilibria and leach testing for this ceramic system. Based on this work, the most important feature of the ceramic formulation that governs chemical durability is the identity of the mineral phases present. It has also been determined which elemental substitutions can be made without affecting the phases present.

As mentioned in Section 3.3, the new baseline formulation is based upon the designed mineralogy and phase composition shown below:



The production of this product mineralogy composition requires the input composition as given in **Table 5.1** below. Note that up to about 3 wt % total of sintering aids may still be added to the baseline formulation. The sintering aids, if needed, will be specified after the fabrication process is finalized.

**Table 5.1 Feed composition to produce baseline ceramic form**

Oxide	Weight Percent
CaO	9.488
HfO <sub>2</sub>	11.100
UO <sub>2</sub>	23.286
PuO <sub>2</sub>	10.771
Gd <sub>2</sub> O <sub>3</sub>	7.580
TiO <sub>2</sub>	37.774
Pu	9.500

Although the new baseline formulation has a 9.5 wt % plutonium loading, there are a range of other formulations that can be used without departing from the designed phase assemblage (*i.e.* by adding rutile or by exchanging uranium for plutonium or plutonium for uranium in the formulation provided the maximum actinide loading in the form is 31.4 wt %) if there is a further need to increase or decrease the plutonium loading in the immobilization form.

### 5.1.2 Precursor and Actinide Feed Specifications

The input compositions for the ceramic precursors (*e.g.*, starting materials exclusive of the actinide feed) are given in **Table 5.2**. Also shown are the allowable uncertainties in the chemical composition. A vendor would likely prepare these precursors, and these compositions would be part of the specification used in procuring the precursor material from the vendor. Precursor 1 is the primary precursor, which contains CaO. Precursor 2 is a make-up precursor to offset excess Ca (present as CaO, CaCl<sub>2</sub>, or CaF<sub>2</sub>) which may be present in the PuO<sub>2</sub> feed streams. Precursor 2 does not contain any CaO.

**Table 5.2 Precursor feed compositions for the baseline formulation**

	Precursor 1	Precursor 2
Oxide	(wt. %)	(wt. %)
CaO	14.39 ± 0.1	-----
HfO <sub>2</sub>	16.83 ± 0.5	19.66 ± 0.5
Gd <sub>2</sub> O <sub>3</sub>	11.50 ± 0.5	13.43 ± 0.5
TiO <sub>2</sub>	57.28 ± 0.5	66.91 ± 0.5

All materials added to the immobilization process must meet specifications on chemical form, particle size, and purity. The recommended specifications for the oxides used to prepare the ceramic precursors are given in **Table 5.3**. If the feed materials meet the specifications given, and the precursors are prepared by the process described in Section 5.2.1 and are stored in isolated containers so that carbon dioxide and moisture are not absorbed, the precursors produced will be suitable for use in the plutonium immobilization plant.

**Table 5.3 Feed specifications for precursor preparation**

Oxide	Form	Particle Size	Purity
CaO	Ca(OH) <sub>2</sub> (or CaO)	-325 mesh	> 99 % < 5 % CaCO <sub>3</sub>
HfO <sub>2</sub>	HfO <sub>2</sub>	-600 mesh	Hf+Zr > 99.99 % Hf > 95 % U < 1000 ppm
Gd <sub>2</sub> O <sub>3</sub>	Gd <sub>2</sub> O <sub>3</sub>	-325 mesh	REE* > 99.99 % Gd > 95%
TiO <sub>2</sub>	TiO <sub>2</sub> (anatase)	-600 mesh	> 99.95% < 0.05 % P

\*REE = Rare earth element

The specifications for the actinide oxides are given in **Table 5.4**. If the actinide oxides meet the specifications given, an acceptable ceramic product can be obtained. For plutonium oxide, the specifications referenced in **Table 5.6** are the specifications that the oxide must meet after blending and do not specify what will be accepted by the plant. Such plant specifications depend on the degree of processing in the Pu conversion operations and the degree of blending prior to the formation of the ceramic, and a separate set of specifications will be prepared for the plant which will likely be different from those in **Table 5.6**.

**Table 5.4 Uranium and plutonium oxides feed specifications**

Oxide	Form	Particle Size	Purity
UO <sub>2</sub>	UO <sub>2</sub> (or U <sub>3</sub> O <sub>8</sub> )	-100 mesh	> 99.99 %
PuO <sub>2</sub>	PuO <sub>2</sub> with UO <sub>2</sub> or U <sub>3</sub> O <sub>8</sub>	-150 mesh	See <b>Table 5.6</b>

The previous version of this report [52] presented a table showing preliminary impurity

specifications for the PuO<sub>2</sub> feed. At a project meeting held on June 21-22, 1999 [60] these specifications were revised, taking advantage of the results of the experimental work that had become available since the preliminary specifications were generated. **Table 5.5** shows the nominally expected ranges for various parameters for the ceramic forms which are being fabricated based on experimental work to date, and establishes the maximum limit criteria which, if satisfied, will result in an acceptable ceramic form for repository acceptance.

On the basis of the tentative product acceptability criteria shown in **Table 5.5** and the combined results of all the impurity studies performed to date, a set of maximum impurity limits was established. The maximum impurity limits for uncompensated impurities are shown in **Table 5.6**. Uncompensated impurities are those which can be added to the mix without adjusting the composition of the precursors.

**Table 5.5. Product acceptability criteria used to define feed impurity specifications**

	Nominal Expected Values
<b>Density</b>	<ul style="list-style-type: none"> <li>• Puck density &gt; 90% of theoretical</li> </ul>
<b>Mineralogy</b>	<ul style="list-style-type: none"> <li>• &gt;50 vol% of pyrochlore,</li> <li>• &lt;50 vol% of brannerite,</li> <li>• &lt;50 vol% of zirconolite (any polytype),</li> <li>• &lt;20 vol% of rutile plus hafnium titanate,</li> <li>• &lt;1 vol% of actinide oxide, and</li> <li>• &lt; 10 vol% of other phases</li> </ul>
<b>Composition</b>	<ul style="list-style-type: none"> <li>• Overall composition of each puck is within the range analyzed by RW</li> <li>• Mole fraction of Pu &lt; mole fraction of Hf plus Gd in all mineral phases within each puck</li> </ul>
<b>Grain Size</b>	<ul style="list-style-type: none"> <li>• Generally less than 20 microns</li> </ul>
<b>Processability</b>	<ul style="list-style-type: none"> <li>• For each puck, little or no melting is observed</li> </ul>
<b>Integrity</b>	<ul style="list-style-type: none"> <li>• For each puck, little or no cracking is observed</li> </ul>

In addition to the impurity specifications shown in **Table 5.6**, more detailed impurity specifications are given in the Feed Specification Tables [60]. The impurity specifications given in this report and in the Feed Specification Tables [60] supercede those given in previous reports [52,61] and will form the bases for the acceptability of both feed receipt for the plant and the batched feeds from blending prior to acceptance for the ceramification process.

The PuO<sub>2</sub> feed impurity specifications in **Table 5.6** were prepared based on experimental work performed with an earlier formulation which was designed for 10.5 wt % Pu loading as discussed earlier, and are conservative specifications for the new baseline formulation specified in this report. For other formulations which may be considered in the future, particularly those where it is desired to increase Pu loading to greater than 10.5 wt %, the specifications must be modified by the following relationship:

$$(\text{Modified Specification}) = (\text{Table 5.6 Specification}) \times 10.5/(\text{Pu wt \% in Other Formulation})$$

If the plutonium loading is raised, the impurity specifications are lowered. For the new baseline formulation the specifications given in **Table 5.6** are conservative by about 10 % and could, if desired, be raised by a factor of 1.10 (e.g. 10.5/9.5)

**Table 5.6 Limits on uncompensated impurities**

Impurity Category	Elements in Category	Maximum Limit	
		Moles Impurity per mole of Pu <sub>2</sub>	Allowed Uncertainty
<i>Volatiles</i>	<i>Halides/2 + Carbon/5 + Metals</i>	0.80	----
<i>Pyrochlore Stabilizers</i>	+3/+4, +5, +6 Elements	1.50	----
<i>Zirconolite Stabilizers</i>	+2, +3, +4 Elements	3.25	----
<i>Rutile Stabilizers</i>	Titanium, Other +4 Elements	Not Limited	----
<i>Glass Stabilizers (Si with +1, +2, +3 Elements)</i>	Silica, Fluoride, +1, +2, +3 Elements	1.90	----
<i>Silica Stabilizers (No +1, +2, +3 Elements)</i>	Si (Ge)	0.85	0.15
<i>Whitlockite/Vanadate Stabilizers</i>	P, V	1.00	0.10
<i>BaTi<sub>4</sub>O<sub>9</sub> Stabilizers</i>	Ba, (Sr)	0.35	0.05
<i>Bromellite Stabilizers</i>	(Be)	(Not Limited)	0.50
<i>Alloy Stabilizers</i>	(Rh, Pd, Ag, Ir, Pt, Au)	(Not Limited)	0.50

**5.1.3. Product Phase Assemblage**

The approximate phase abundances in the baseline product are given in **Table 5.7**. When impurities are present in the PuO<sub>2</sub> feed, the relative abundances of the minerals can vary substantially from those of the baseline. Within the original A Series samples, the ranges of observed phase abundances varied approximately as given in **Table 5.7**. The expected ranges, which should also be acceptable as currently proposed, are also given in the table. Based on the durability and process data currently available, it is not likely that the expected ranges will be narrowed from those given here.

**Table 5.7 Phase abundances in baseline and product extremes**

Phase	Nominal Baseline (vol %)	Observed Range (vol %)	Expected Range (vol %)
Pyrochlore	80	40 – 95	> 50
Brannerite	15	0 – 50	0 – 50
Zirconolite	0	0 – 40	0 – 50
Rutile	5	0 – 15	0 – 20
Actinide Oxide	0.5	0 – 1	0 – 1
Other Minor Phases	0	0 – 10	0 – 10

**Baseline:** The observed mineral abundances in the baseline product without impurities.

**Observed Range:** The approximate observed range of phase abundances in the product with the addition of various impurities.

**Expected Range:** The expected range, which will be the targeted range of control for the Process Control Model.

As indicated in **Table 5.7**, the ceramic product contains a mixture of three actinide-bearing phases (pyrochlore, zirconolite, and brannerite), some rutile, and a trace amount of partially or unreacted actinide oxide. The primary actinide-bearing phases all have natural mineral analogs that have survived for geologic time periods, which suggests that they are suitable actinide host phases for geologic disposal. The experimental work in this program has developed single phase samples or samples dominated by a given phase of these principle phases for durability testing. Testing to date on these single phase materials indicates that all of the principle phases (pyrochlore, zirconolite, brannerite, and rutile) are sufficiently durable to meet the repository acceptability requirements. Note that, depending upon the impurity loadings in the PuO<sub>2</sub> feed, a variety of other phases could be present in small amounts.

The properties of these principle phases are discussed in more detail below.

### **Pyrochlore**

Pyrochlore has a cubic structure which is similar to the fluorite structure. The empirical formula unit is given as A<sub>2</sub>B<sub>2</sub>O<sub>6</sub>X. The space group symmetry is Fd3m, and each unit cell contains 8 formula units. The coordination numbers of the A and B sites are 8 and 6, respectively [62]. For the plutonium immobilization ceramic, the A site can be occupied by Ca<sup>2+</sup>, Gd<sup>3+</sup>, U<sup>4+</sup>, Pu<sup>4+</sup>, and Hf<sup>4+</sup>. The B site is occupied primarily by Ti<sup>4+</sup>, and the X site is occupied by O<sup>2-</sup>.

Pyrochlore is a relatively common mineral in nature. Natural pyrochlores are grouped into three varieties, pyrochlore (niobium-rich), microlite (tantalum-rich), and betafite (titanium- and uranium-rich) [63]. Of the three varieties, betafite most closely matches the composition of the pyrochlore phase in the plutonium immobilization ceramic.

Some alteration in natural betafites has been observed, resulting from the loss of relatively soluble matrix species such as NaF, KF, and CaO, but actinides are effectively retained by most betafites for geologic time periods up to 1.4 billion years [64]. If sufficient alteration has occurred by depletion of the soluble matrix species, a second stage of alteration can begin in which up to 30% of the original amount of uranium is lost. A large fraction of this uranium is retained in nearby phases. The nominal compositions of betafite [64-66] and the plutonium pyrochlore phases are shown in **Table 5.8**. Although the compositions are similar, there are some significant differences between the compositions of the natural pyrochlores and the pyrochlores in the plutonium immobilization ceramic. Most notably the natural pyrochlores have substantial amounts of niobium and/or tantalum while the pyrochlores in the plutonium immobilization ceramic do not contain any of these elements unless they are present as impurities in the PuO<sub>2</sub> feed stream. Natural pyrochlores also contain small but significant amounts of sodium, potassium, and fluoride ions. These ions are generally the first to be depleted in natural pyrochlores that have undergone geochemical alteration.

### Zirconolite

Zirconolite has many polytypes (*i.e.* structural variants) [67,68]. The most common polytype is zirconolite-2M, which is also the polytype that is generally found in the plutonium immobilization ceramic. Zirconolite-2M has a monoclinic structure. Zirconolite-4M, which is also monoclinic, and zirconolite-3O, which is orthorhombic, can also be found in the ceramic. However, the other known polytypes (*i.e.* zirconolite-3T and zirconolite-6T) have not yet been observed in the plutonium immobilization ceramic. All the zirconolite polytypes and the pyrochlore structure are closely related to each other by the stacking of a common fundamental unit of  $\text{TiO}_6$  octahedra that form a linked plane of hexagonal and triangular rings [66,68]. The hexagonal rings are joined to form planar layers. The polytypes differ in the way the layers are stacked. The most symmetric stacking of layers forms pyrochlore. All of the other stacking arrangements produce various zirconolite polytypes.

The empirical formula unit is given as  $\text{ABC}_2\text{O}_7$ . The space group symmetry for zirconolite-2M is  $C2/c$  and each unit cell contains 8 formula units. The coordination numbers of the A and B sites are 8 and 7, respectively. There are three different C sites. Two of the C sites have a coordination number of 6. One of the C sites has a coordination number of 5 [68]. For the plutonium immobilization ceramic, the A site can be occupied by  $\text{Ca}^{2+}$ ,  $\text{Gd}^{3+}$ , and  $\text{Pu}^{3+}$ . The B site can be occupied by  $\text{Hf}^{4+}$ ,  $\text{Gd}^{3+}$ ,  $\text{U}^{4+}$ , and  $\text{Pu}^{4+}$ , and the C sites are occupied primarily by  $\text{Ti}^{4+}$ .

Zirconolite minerals are also found in nature. Natural zirconolites up to 650 million years in age have been found. With the exception of metamictization, no alteration has been observed, and the actinides and decay products have been retained in the mineral, *e.g.* they are concordant [69]. The nominal compositions of natural zirconolite [69-71] and the zirconolite phases in the plutonium immobilization ceramic are shown in **Table 5.8**. For the most part, the compositions of the natural zirconolites and the zirconolites in the plutonium immobilization ceramic are comparable.

### Brannerite

The empirical formula unit of brannerite is given as  $\text{AB}_2\text{O}_6$ . Brannerite has a monoclinic structure, and its space group symmetry is  $C2/m$ . There are 2 formula units per unit cell. Coordination numbers of the A and B sites are both 6 [72]. In the Pu ceramic, the A site can be occupied by  $\text{U}^{4+}$ ,  $\text{Pu}^{4+}$ , and lesser amounts of  $\text{Hf}^{4+}$  and  $\text{Gd}^{3+}$ . The B site is occupied primarily by  $\text{Ti}^{4+}$ .

Brannerites are also found in nature. Lumpkin, et al. [73] has studied natural brannerites with ages ranging from approximately 20 million to 1.6 billion years old. Samples up to about 190 millions years old show no loss of the actinide or decay products, *e.g.* they are concordant. Older samples are significantly altered with up to 80 % loss of the lead decay product. In general, natural brannerites are equal to or less durable than natural pyrochlores, and natural pyrochlores are equal to or less durable than natural zirconolites [73]. The nominal compositions of natural brannerites [72-75] and the brannerite phases in the plutonium immobilization ceramic are shown in **Table 5.8**. For the most part, the compositions of the natural brannerites and the brannerites in the plutonium immobilization ceramic are comparable.

**Table 5.8 Nominal composition of Pu ceramic and natural analog phases**

	Pyrochlore Pu Ceramic	Pyrochlore Natural	Zirconolite Pu Ceramic	Zirconolite Natural	Brannerite Pu Ceramic	Brannerite Natural
Element	(mole)	(mole)	(mole)	(mole)	(mole)	(mole)
Na,K	----	0.06 ± 0.09	----	0.01 ± 0.04	----	----
Ca	0.97 ± 0.04	0.41 ± 0.38	0.73 ± 0.06	0.74 ± 0.11	0.07 ± 0.02	0.24 ± 0.09
Y,REE <sup>a</sup>	0.24 ± 0.06	0.04 ± 0.03	0.19 ± 0.02	0.08 ± 0.10	0.15 ± 0.04	0.07 ± 0.10
Th	----	0.02 ± 0.02	----	0.10 ± 0.12	----	0.04 ± 0.05
U	0.39 ± 0.03	0.50 ± 0.18	0.16 ± 0.02	0.02 ± 0.02	0.45 ± 0.04	0.56 ± 0.14
Pu	0.22 ± 0.03	----	0.09 ± 0.02	----	0.20 ± 0.03	----
Zr,Hf <sup>b</sup>	0.17 ± 0.04	0.002 ± 0.003	0.62 ± 0.06	1.01 ± 0.08	0.09 ± 0.02	0.000 ± 0.002
Mg,Mn,Fe	----	0.23 ± 0.27	----	0.36 ± 0.24	----	0.18 ± 0.08
Al, Ga	0.01 ± 0.01	0.05 ± 0.07	0.31 ± 0.12	0.04 ± 0.03	0.05 ± 0.04	0.02 ± 0.03
Ti	2.00 ± 0.05	1.33 ± 0.34	1.91 ± 0.06	1.38 ± 0.29	2.00 ± 0.03	1.69 ± 0.11
Nb,Ta	----	1.29 ± 0.34	----	0.25 ± 0.23	----	----
Pb	----	0.04 ± 0.02	----	0.003 ± 0.007	----	0.03 ± 0.02
Si	----	0.02 ± 0.08	----	0.001 ± 0.002	----	0.15 ± 0.13
F	----	0.12 ± 0.15	----	0.01 ± 0.03	----	----
O (calc)	7.10 ± 0.04	7.41 ± 0.59	7.11 ± 0.07	6.83 ± 0.12	6.06 ± 0.02	5.79 ± 0.13

<sup>a</sup>For the Pu ceramic Y, REE is Gd only.

<sup>b</sup>For the Pu ceramic Zr,Hf is Hf and for the natural minerals Zr,Hf is Zr with a trace of Hf.

Uncertainties are given as one standard deviation.

### Rutile

The empirical formula unit of rutile is given as  $AO_2$ . Rutile has a tetragonal structure and a space group symmetry of  $P4_2/mnm$ . Each unit cell contains 2 formula units. In the plutonium immobilization ceramic, the A site can be occupied by  $Ti^{4+}$  and lesser amounts of  $Hf^{4+}$ . Rutile does not accommodate any plutonium or any significant amount of uranium in its structure.

### Actinide Oxide

The actinide oxides have a cubic fluorite structure. The empirical formula unit of actinide oxide is  $AO_2$ . The space group symmetry is  $Fm-3m$ , and each unit cell contains 4 formula units. The coordination number of the A site is 8. In the plutonium immobilization ceramic, the A site can be occupied by  $U^{4+}$  and  $Pu^{4+}$  and lesser amounts of  $Hf^{4+}$  and  $Gd^{3+}$ .

### Other Minor Phases

Depending upon the impurities present in the  $PuO_2$  feed, any of the following phases could be present in small amounts in the ceramic product:

Silicate Glasses (Calcium-Aluminum-Titanium-Silicates)

Hafnium Titanate ( $HfTiO_4$ )

Loveringite ( $CaTi_{21}O_{38}$ )

Magnetoplumbite ( $CaAl_{12}O_{19}$ )

Perovskite ( $CaTiO_3$ )

Pseudobrookite ( $Al_2TiO_5$ ) - Armalcolite ( $Mg_2TiO_5$ )

Scheelite ( $CaWO_4$ ) - Powellite ( $CaMoO_4$ )

Ulvospinel( $\text{TiFe}_2\text{O}_4$ ) - Spinel( $\text{MgAl}_2\text{O}_4$ )  
Whitlockite ( $\text{Ca}_3(\text{PO}_4)_2$ ) – Monazite ( $\text{GdPO}_4$ )

Example end-member compositions of these minerals are given in parentheses. Of these phases, the most common in the plutonium immobilization ceramic are glasses, perovskites, and pseudobrookite-armalcolites.

### Phase Relationships

The acceptable processing range is a potentially important boundary yet to be finalized for the plutonium immobilization ceramic. The boundary given in **Table 5.7** is depicted in the simplified ternary diagram in **Figure 5.1**. Note that the baseline ceramic has six oxide components. To reduce the six-variable system to three variables, the following assumptions are made:

- $\text{UO}_2$  and  $\text{PuO}_2$  behave similarly enough that they can be treated as one oxide,  $\text{AnO}_2$
- $\text{TiO}_2$  is always in excess, so the  $\text{TiO}_2$  activity is fixed at unity
- $\text{Gd}_2\text{O}_3$  is distributed relatively evenly among the actinide bearing phases, so it is neglected in the phase equilibria

Each of these assumptions reduces the variables by one, thus resulting in a three-variable system (e.g.,  $\text{CaO}$ ,  $\text{HfO}_2$ , and  $\text{UO}_2+\text{PuO}_2$ ) which can be plotted on the ternary diagram shown in **Figure 5.1**. The Baseline Precursor 1 composition is at 23.8 mole %  $\text{HfO}_2$ , 76.2 mole %  $\text{CaO}$ , and 0 mole %  $\text{AnO}_2$  in the figure. Addition of  $\text{UO}_2/\text{PuO}_2$  moves the composition in a straight line toward  $\text{AnO}_2$ . The intersection across the green region is the acceptable compositional regime as it is currently defined. Thus, amounts between about 30 and 50 mole %  $\text{AnO}_2$  can be added to the baseline product, and an acceptable product will be produced. These boundaries are modified slightly by the addition of impurities.

To help ensure that the immobilized plutonium is not separated from the neutron absorbers over time in the repository, it is important that the most abundant plutonium-bearing phases also incorporate significant quantities of the neutron absorbers. Although not as important, it will be more defensible in the repository license application if the less abundant plutonium-bearing phases also accommodate significant quantities of neutron absorbers. For each mineral phase that has been observed in the plutonium immobilization ceramic, its ability to accommodate Gd, Hf, U, and Pu is summarized in **Table 5.9**. Data are given in weight percent of oxide in each phase. Except for the residual actinide oxide, all of the primary phases accommodate more neutron absorber atoms (Gd + Hf) than plutonium atoms. The other minor phases also accommodate more neutron absorber atoms (Gd + Hf) than plutonium atoms. The only possible exceptions are the whitlockite, magnetoplumbite, and perovskite phases. These phases can accommodate significant amounts of Pu if present in the +3 valence state. When sintered in air, Pu is in the +4 valence, so under oxidizing conditions Pu is not observed in the whitlockite, magnetoplumbite, or perovskite phases. These are also the only phases that can accommodate significant amounts of plutonium without accommodating uranium. These phases prefer trivalent actinides because the substitution occurs on the Ca site, and trivalent actinide ions are much closer in size to the

$\text{Ca}^{2+}$  ions than the tetravalent actinides and the trivalent cations are more easily charge balanced.

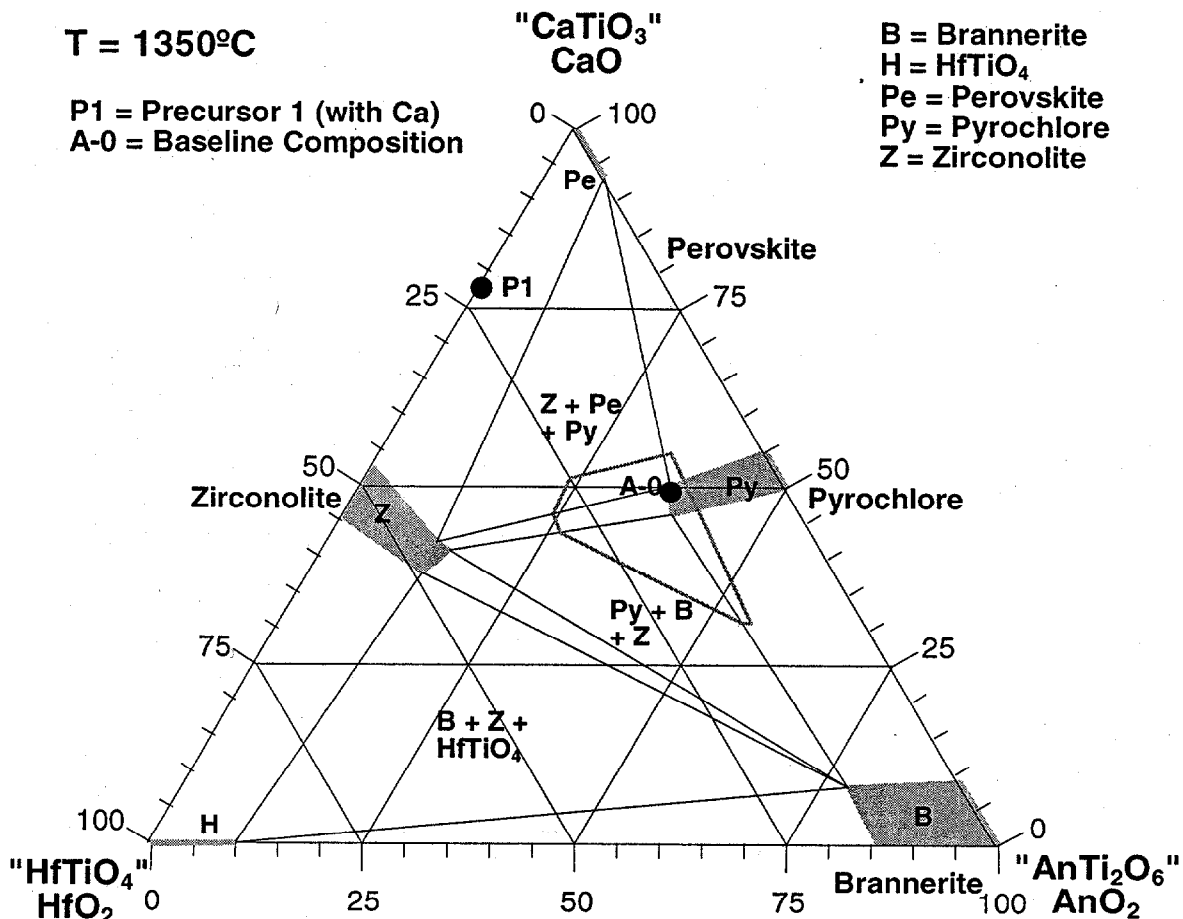


Figure 5.1 Depiction of the processing regime

## 5.2 Baseline Fabrication Process

As noted earlier, the baseline formulation could not be finalized without some definition of how the material is to be processed. As a result, the baseline fabrication process is an integral part of this report. The fabrication process has been the subject of intense development, and is now well developed and currently being adapted to plant production operations at the present time. The baseline formulation given in Section 5.1 is valid provided that the following four criteria are met in the baseline fabrication process:

- No significant processing changes are introduced at a later date which depart from the process described here.
- The fabricated ceramic product is at or near thermodynamic equilibrium at the end of the sintering step. In the process, this is largely controlled by controlling the degree of actinide milling and mixing prior to pressing and sintering.

- The redox conditions during sintering are not altered significantly from those described herein.
- The sintering temperature and time are not altered significantly from those described herein.

**Table 5.9 Composition of phases in the ceramic**

	CaO	Gd <sub>2</sub> O <sub>3</sub>	HfO <sub>2</sub>	UO <sub>2</sub>	PuO <sub>2</sub>	TiO <sub>2</sub>
<b>Primary Phases</b>	(wt %)	(wt %)	(wt %)	(wt %)	(wt %)	(wt %)
Pyrochlore	11.8 ± 0.7	9.4 ± 2.6	7.9 ± 1.9	22.6 ± 1.9	12.6 ± 1.6	34.6 ± 1.1
Brannerite	1.0 ± 0.4	7.0 ± 1.7	5.0 ± 1.2	31.1 ± 2.9	13.7 ± 1.8	40.9 ± 1.1
Zirconolite-2M	9.1 ± 0.9	7.6 ± 0.5	29.0 ± 1.8	9.6 ± 1.2	5.5 ± 0.9	33.9 ± 1.3
Rutile	0.1 ± 0.1	0.1 ± 0.1	14.2 ± 4.8	4.4 ± 4.9	0.1 ± 0.05	79.1 ± 8.4
Actinide Oxide	0.1 ± 0.3	1.0 ± 1.6	0.8 ± 0.7	0.6 ± 25	98.4 ± 25	0.3 ± 0.3
<b>Other Minor Phases</b>						
Glass-Silica	14.1 ± 5.9	1.1 ± 1.2	1.1 ± 0.7	3.3 ± 2.4	0.9 ± 1.3	8.5 ± 6.0
Hafnium Titanate	0.0	0.0	53.5 ± 4.2	7.1 ± 1.3	1.0 ± 1.3	38.4 ± 2.5
Lovingite	3.1 ± 0.5	0.0	5.0 ± 0.7	5.6 ± 1.7	1.0 ± 0.9	52.3 ± 13.3
Magnetoplumbite	5.7 ± 1.0	0.8 ± 0.7	1.8 ± 1.8	0.8 ± 1.2	0.4 ± 0.6	13.9 ± 3.7
Perovskite	31.9 ± 1.9	9.4 ± 2.9	1.8 ± 0.2	0.6 ± 0.1	1.2 ± 0.4	54.3 ± 1.1
Pseudobrookite/Armalcolite	0.8 ± 1.0	0.5 ± 0.9	2.3 ± 1.5	0.9 ± 1.0	0.7 ± 1.0	50.9 ± 12.1
Scheelite/Powellite	24.5 ± 4.3	0.8 ± 0.1	0.2 ± 0.2	0.1 ± 0.1	0.1 ± 0.4	0.2 ± 0.1
Ulvospinel/Spinel	0.0	0.0	0.8 ± 0.2	0.0	0.0	28.8 ± 0.3
Whitlockite/Monazite	42.6 ± 1.4	9.7 ± 2.2	0.2 ± 0.2	0.4 ± 0.3	0.6 ± 0.4	0.4 ± 0.2

Uncertainties are given as one standard deviation.

Significant changes in the fabrication process could also affect the tolerance of the form to impurities which in turn would alter the allowable PuO<sub>2</sub> feed specifications. The greater the deviation from thermodynamic equilibrium in the as-fabricated ceramic product, the greater the product properties are dependent on how the product was made. This trend would create a greater dependence on the control of processing variables that affect product properties. If the as-fabricated ceramic product is at or near thermodynamic equilibrium, however, only changes in feed composition, redox conditions during sintering, or sintering temperature could significantly alter the product phase assemblage.

The term “baseline fabrication process” as used here applies not only to the immobilization process, but also to the preparation of the precursor materials. The compositions of the precursors were given in Section 5.1.2. The mixing recipes and conditions for precursor preparation, uranium oxide, and plutonium oxide are given in Sections 5.3.1 and 5.3.2.

### 5.2.1. Ceramic Precursor Preparation

A commercial vendor will likely supply the oxide precursors to the Plutonium Immobilization Facility. The recommended precursor preparation process is shown in **Figure 5.2**. The recommended process consists of wet mixing/milling of the precursors, drying of the precursor

slurry, and pulverization (i.e. size reduction) of the dried clumps as necessary. A final calcination step is performed to partially react the precursor materials and to remove residual materials that would be volatile during the sintering process. Some flexibility in the preparation process may be desirable to allow the vendor to arrive at an optimally cost-effective process. Alternative preparation processes are acceptable, so long as an acceptable ceramic product can be made from the precursors that are supplied. The process recommended here has been used successfully numerous times on full-scale fabrications of Hf-Ce-Ce and Hf-Ce-U formulations (*i.e.*, ceramics in which cerium is used as an analog for plutonium or for both plutonium and uranium) and on several full-scale Hf-Pu-U fabrications. More details on the precursor requirements can be found in the report prepared by Herman [76].

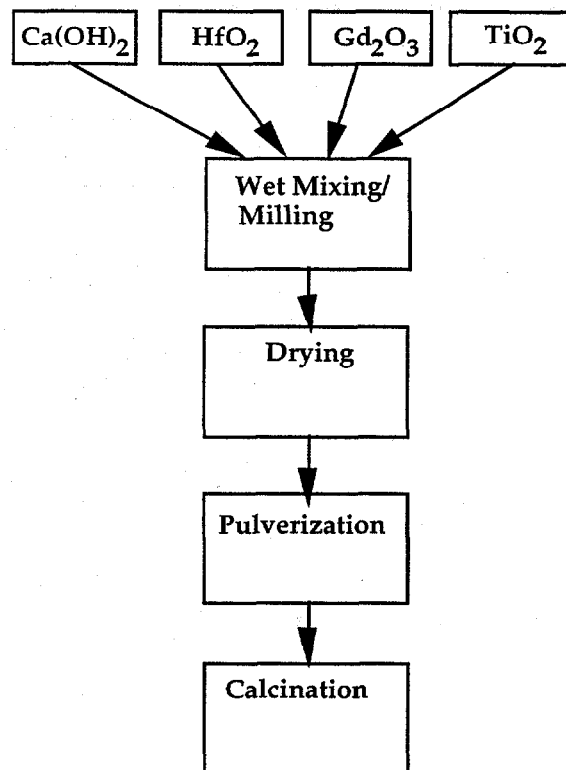


**Figure 5.2 Recommended process for preparing ceramic precursors**

**Wet Mixing/Milling**

In this step, the precursor feeds are weighed, mixed together, and ball milled wet for a minimum of 1 hour or until uniformly blended. To minimize contamination potentially incompatible with the ceramic form, the preference is to use a zirconia milling jar and zirconia grinding media. However, other milling jars (*e.g.*, alumina, porcelain, Teflon, and high density polyethylene) are routinely used and have been shown to produce an acceptable product.

**Drying**

In this step the wet slurry is transferred to a tray and dried in an oven at about 110°C overnight (approximately 16 hours). Convection drying is preferred over vacuum drying.

### **Pulverization**

After the drying step, a friable cake is formed. This cake must be size-reduced to a granular and flowable powder. This pulverization step can be accomplished using a flake breaker followed by a disk pulverizer.

### **Calcination**

Calcination is used to decompose compounds and impurities that would release gas during the sintering process and to partially react the precursor material. Volatile impurities include, but are not limited to, nitrates and volatile salts. Partially reacting the precursor and removing excess volatile materials reduces the likelihood of crack formation during sintering. The key to calcination is to heat-treat the powdered material at a temperature high enough such that volatile substances are released as gases, but low enough that most of the reactivity of the powder is retained. For this precursor composition, calcination between 700 and 800°C for 1 hour in air is recommended. If performed in a tray rather than a rotary calciner, the layer of powder should not be more than about 5 cm (2 inches) thick during calcinations to allow water and other volatile species to escape.

Processing of the precursors will be performed under appropriate quality assurance controls with limits placed on the acceptable impurities (See **Table 5.3**). After completion of all processing steps, the precursor materials will be packaged for shipment to the Plutonium Immobilization Facility. Appropriate packaging will be required so that no excess moisture or impurities can enter the containers.

### **5.2.2. Baseline Immobilization Process**

The envisioned Process Flow Diagram for the Plutonium Immobilization Facility is shown in **Figure 5.3**. In summary, the process consists of milling/mixing the actinide oxide powders with commercially fabricated precursors, granulating (if needed) the milled/mixed powders, pressing the conditioned powders, and sintering the pressed pellets/pucks.

When the commercially supplied precursor is received at the Plutonium Immobilization Plant, it is anticipated that each lot of the vendor-supplied materials will be analyzed to ensure that the precursors are within acceptance specifications (See section 5.1.2.). Preliminary specifications have been written to cover the targeted chemical composition, phase assemblage, impurity limits, flowability constraints, moisture limits, and particle size of the precursor materials [76]. Acceptance specifications for the precursor materials will be similar to those currently in place for the glass frit used in the Defense Waste Processing Facility (DWPF). It is anticipated that no batch of precursor material will be processed in the Plutonium Immobilization Facility without first undergoing acceptance testing to ensure that an acceptable product can be made.

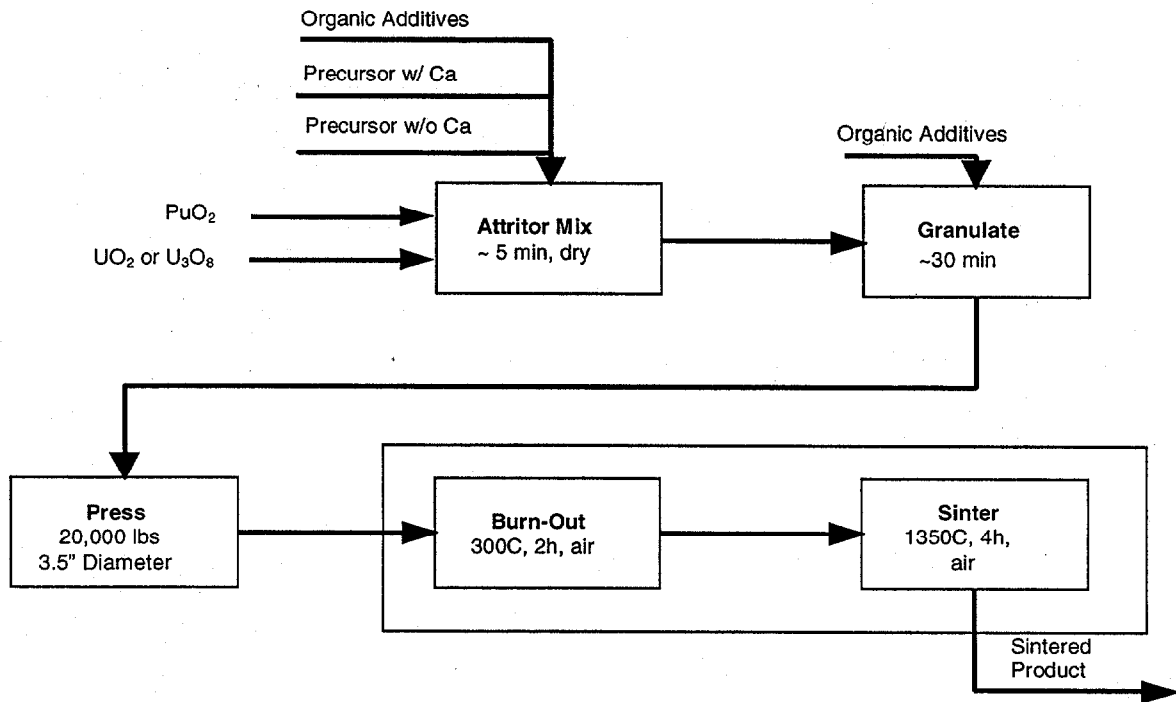


**Figure 5.3 The ceramic immobilization process flow diagram**

The current process flow diagram is based on receiving blended  $\text{PuO}_2$  which has an impurity content which meets established limits. The  $\text{PuO}_2$  powder will be less than 100 mesh since all feeds will be milled to less than 100 microns. The impurity content is controlled by operations in the Pu conversion operation and calcining feed materials at high temperatures in air. Batches of feed material will be prepared in a large batch blender, and samples will be taken to characterize the batch for impurities which can impact the process operations or repository acceptance of the ceramic product. In addition, the blending of the feed streams minimizes compositional variations and the effects of impurities on the plutonium immobilization ceramic associated with the incoming  $\text{PuO}_2$  feed stream. The blended  $\text{PuO}_2$  must meet the specifications in **Table 5.6** before it can be immobilized. Out-of-specification material will be rebled.

In addition to the  $\text{PuO}_2$  feed and precursor, Uranium oxide (depleted or natural) will also be added in the process to fabricate the plutonium immobilization ceramic. The uranium oxide that is to be immobilized will most likely be from commercial fuel fabricators or from well-characterized excess DOE stock. The preferred form is  $\text{UO}_2$ , but  $\text{U}_3\text{O}_8$  is also acceptable.

### **Attritor Milling/Mixing**

The attritor milling and mixing operation is critical for the preparation of the materials into a powder form in which the mixing of actinides and precursors on the sub-micron scale. This sub-micron mixing assures that the product ceramic will approach thermodynamic equilibrium (due to minimized reaction distances) provided the feed specifications are met for actinide feed and precursors and the product is sintered according to specifications. Note that, while milling and mixing occurs on a sub-micron scale, the actual particle size distribution of the powder that exits

the mill is much larger, being on the order of 5 microns due to clumping of the finely milled powder as it exits the mill.

The amounts of precursors and actinide oxides to be blended and milled will be determined by the equations given in Section 5.3. If the correct amounts of the specified precursors are blended with actinide oxide which also meets the feed specifications given in Section 5.1.2, acceptable phases will be produced. The range of acceptable phases are given in Section 5.1.3.

Studies to date have shown that blending of precursors and actinide oxides on a micro-scale is necessary to produce dense, fully reacted (approaching thermodynamic equilibrium), and high-integrity pellets. Of the options tested (V-blender, wet ball mill, dry ball mill, and attritor), the attritor has been shown to be the most favorable milling option to achieve micro-scale blending. The high energy of the attritor provides excellent mixing with minimal time required resulting in high product throughput and a high degree of product consistency.

The current equipment undergoing development and testing for the milling/mixing operation is an attritor mill manufactured by Union Process. The attritor mill is best described as a high-energy stirred ball mill. A rotating ribbed shaft stirs the media at high-speed, causing shearing and impact forces on the material, resulting in size reduction and dispersion. The high speed of the attritor mill imparts a large amount of energy to the feed powder. This high energy dramatically reduces the time required to mill--from hours down to minutes. Another advantage of the attritor mill is that milling/blending can be accomplished with a completely dry process which greatly simplifies follow-on process operations. The attritor mill is manufactured in various sizes to accommodate different feed batch sizes, and scale-up of the attritor mill has proven to be easily accomplished.

Due to the high efficiency of the mixing in the attritor, the two precursor feeds and the two actinide oxide feeds can be fed to the blending attritor as four separate feed streams. Additional macro-scale blending equipment will not be necessary. The attritor mill has also been shown to be highly effective at co-milling and mixing. Therefore, two process steps (*i.e.*, milling of the actinide oxides and mixing of the actinide oxides with the ceramic precursors) have been combined into one processing step using a single piece of equipment. In testing with uranium oxide, the use of only one attritor has been shown to be effective in achieving the desired actinide milling while simultaneously creating a micron-scale blended product with the precursors.

In operation, a discharge additive is necessary during the milling/mixing operations to assist with feed discharge from the mill. Currently, the baseline additive for this step is 8 wt. % Airvol 21-205 solution added to the precursor. The Airvol 21-205 additive is an approximately 21 wt % solution of polyvinyl alcohol in a balance of water. The precursor is dried before milling/mixing in the attritor mill. This results in about 1.6 wt % polyvinyl alcohol in the precursors, and the total amount of organic present is about 1.2 wt % after the actinide oxides have been added to the precursors.

### **Granulation**

The milled and blended powder must be fed to a press to produce the ceramic pucks for subsequent sintering. To condition the powders for pressing, a granulation step is currently

being used on the blended powder. The purposes of the granulation step are to improve the powder flowability into the die set, to minimize dusting of the powder, and to assist with even filling of the die set. Granulation is currently being accomplished using a Gemco double cone blender or equivalent operating in a tumbling mode. While the blender is tumbling the milled powder, an organic additive (roughly 50 vol% Airvol 21-205/50 vol% water, equivalent to about 10 wt% polyvinyl alcohol/90 wt% water), is sprayed onto the fine powder. The amount of binder/water solution that is added to the powders is about 10 wt %. This additive causes the powder to agglomerate into larger particles. The combination of agglomeration coupled with the tumbling action of the blender produces an acceptable granular product with reduced dustiness and improved flow characteristics.

### **Pressing**

The prepared powder must be pressed into the green ceramic puck shape prior to sintering. The baseline pressing process utilizes a nominal 8.89-cm (3.5-inch) diameter die for pressing the feed powders, which has been shown to produce the nominal sintered puck target diameter of 2.625" (+0.125, -0.225). The die size is subject to change, depending on feed impurities, amount of recycle, if any, and any variations in the powder treatment prior to pressing

The press configuration is double-action pressing. This double-action pressing provides more even density distribution in the green pellet than a single-action press. This press configuration is expected to minimize cracking that can occur during the sintering operation.

The milled, blended, and granulated powder is pressed to form a green puck for sintering. The minimum pressure required will be that necessary to maintain green puck integrity and which also results in high-density pucks with the appropriate mineral phases and minimal porosity. With the current granulated powders being produced, the nominal force used is 62 kN (14,000 pounds force) or 13.8 MPa (2,000 psi) pressing pressure to produce an 8.89-cm (3.5-inch) diameter green puck. A dwell time of 10 seconds is currently used.

From the press, the green pucks will be transferred to the sintering furnaces using remote handling equipment. The transfer operation also includes a measurement step which verifies puck dimensions, weight, and green density for process control.

### **Binder Burn-out and Sintering**

The baseline sintering schedule and temperature are defined as shown in **Figure 5.4**. This sintering cycle has been found to produce pucks of sufficiently high density such that the internal porosity is closed. However, 100% of theoretical density is also not desired since radiation damage will cause some swelling of the crystalline structure, and some residual porosity will be needed to help reduce swelling and micro cracking resulting from alpha-decay damage of the ceramic over time. The theoretical maximum density of the pucks has been calculated to be 5.91 g/cm<sup>3</sup>. Densities in excess of 90% of theoretical are normally achieved in prototype production operations.

The baseline sintering specification is 1350°C for four hours in air. Heating rate is currently about 5°C/minute, with a slower initial rate and hold at 300°C during heat-up to burn out the binder. Cooling rate is currently 5°C/minute or slower. The sintering time and temperature will

not change, but the ramp rates and binder burn-out schedule are still subject to change pending investigations with the full-scale furnace. The sintering atmosphere is air.

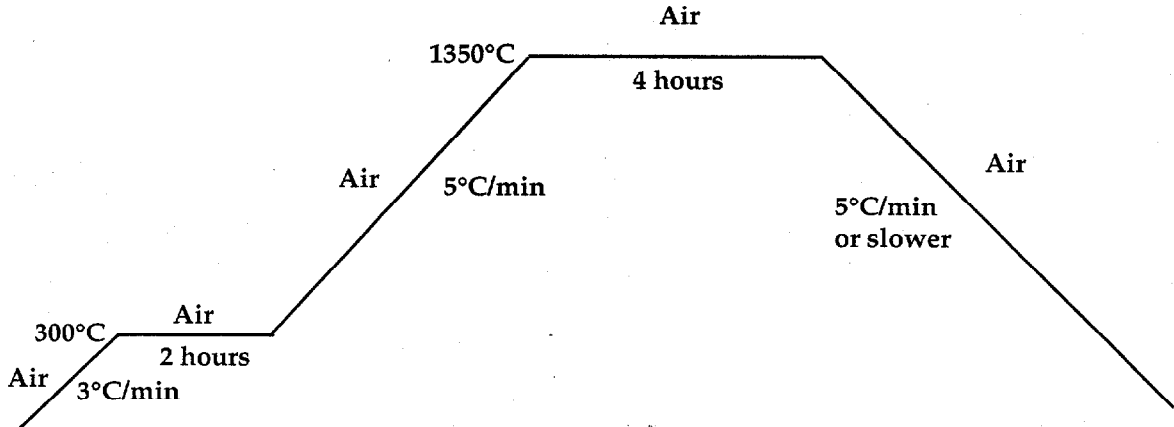


**Figure 5.4** The overall baseline firing schedule

The parameters for the baseline burn-out schedule are given in **Table 5.10** and those for the baseline sintering schedule are given in **Table 5.11**. These processes are assumed to be performed sequentially to give the overall firing schedule shown in **Figure 5.4**. To reduce the cycle time in the Plutonium Immobilization Plant, it is currently assumed that the sintered samples will be removed before they cool completely to room temperature. The maximum temperature at which the sintered pucks can be removed will depend on the heat removal design of the processing equipment, but should be in the range of 100 to 200°C.

**Table 5.10** Baseline burn-out schedule

	Start Temp.	End Temp.	Duration	Atmosphere
Segment	(°C)	(°C)	(min)	
1	30	300	90	Air
2	300	300	120	Air

**Table 5.11** Baseline sintering schedule

	Start Temp.	End Temp.	Duration	Atmosphere
Segment	(°C)	(°C)	(min)	
1	300	1350	210	Air
2	1350	1350	240	Air
3	1350	300	210 or longer	Air

Further description of the fabrication process can be found in the draft System Design Description for Ceramic Immobilization [77].

### 5.3 Mixing Recipes

In the attritor mill, a relatively pure depleted or natural  $\text{UO}_2$  feed will be blended with the relatively impure  $\text{PuO}_2$  feed and the two precursor feed streams. The amount of  $\text{UO}_2$  added to the  $\text{PuO}_2$  will depend upon how much  $^{238}\text{U}$  is already present in the  $\text{PuO}_2$  feed. Depleted or natural  $\text{UO}_2$  will be added to maintain a 2.17-to-1 molar ratio of U-to-Pu.  $\text{ThO}_2$  impurity in the  $\text{PuO}_2$  will be counted as  $^{238}\text{UO}_2$  on a 1-to-1 molar basis.  $\text{NpO}_2$ ,  $^{233}\text{UO}_2$ ,  $^{235}\text{UO}_2$ , and  $\text{AmO}_{1.5}$  will be counted as  $\text{PuO}_2$  on a 1-to-1 molar basis.

In the attritor, the actinide oxides will be blended with the two precursor feed streams. The relative amount of Precursor 2 is dependent upon the amount of calcium in the  $\text{PuO}_2$  feed. The amount of Precursor 1 is dependent upon the amounts of plutonium and calcium in the blended  $\text{PuO}_2$  feed. The three parameters needed are defined as follows:

$X_{\text{Ca}}$ : Total mass of Ca in the  $\text{PuO}_2$  feed

$X_{\text{NF}}$ : Total mass of  $^{238}\text{U}$  in the  $\text{PuO}_2$  feed

$X_{\text{F}}$ : Total mass of Pu in the  $\text{PuO}_2$  feed  
(Atomic mass of Pu is assumed to be 239.10 g/mol)

It is expected that the  $^{235}\text{U}$ , Np, Pu, and Am masses will be determined by material control and accountability (MC&A) equipment after blending. The Th and  $^{238}\text{U}$  contents will be determined either by MC&A or analytical sampling of the blended  $\text{PuO}_2$  feed material. The Ca content will also need to be determined quantitatively. Note also that the amounts of all the other impurities do not affect the amounts of  $\text{UO}_2$ , Precursor 1, or Precursor 2 that will be added to the processes. The result is that the impurities will be added over and above all the other components and will not be compensated for by varying the feed composition of any of the primary precursor constituents.

#### 5.3.1 Attritor Mill/Mixer Recipe

The amount of depleted or natural  $\text{UO}_2$  that will be added to the attritor mill/mixer is given by the Eqn. (5.1).

$$(5.1) \quad W_{\text{UO}_2} = 2.4514X_{\text{F}} - 1.1344X_{\text{NF}}$$

Where:  $X_{\text{F}}$  and  $X_{\text{NF}}$  are defined above

$W_{\text{UO}_2}$ : Mass of  $\text{UO}_2$  (depleted or natural) added to the attritor mill.

(If  $\text{U}_3\text{O}_8$  is used instead of  $\text{UO}_2$ , multiply  $W_{\text{UO}_2}$  by 1.0395 to get  $W_{\text{U}_3\text{O}_8}$ ).

The amount of Precursor 1 and Precursor 2 that will be added to the attritor mill/mixer is given by the Eqns. (5.2) and (5.3), respectively.

$$(5.2) \quad W_{\text{Precursor 1}} = 6.9415X_{\text{F}} - 9.7244X_{\text{Ca}}$$

Where:  $X_F$  and  $X_{Ca}$  are defined above

$$(5.3) \quad W_{\text{Precursor 2}} = 8.3252X_{Ca}$$

Where:  $X_F$  and  $X_{NF}$  are defined above.

$W_{\text{Precursor 1}}$  : Mass of Precursor 1 (Ca-containing) to add to the attritor mill/mixer.

$W_{\text{Precursor 2}}$  : Mass of Precursor 2 (Ca-free) to add to the attritor mill/mixer.

Precursor 1 is the primary component added to the attritor mixer/blender. Precursor 2 does not contain any calcium and is used to offset calcium that is present in the  $\text{PuO}_2$  feed stream. All of the calculations given in Eqns (5.1), (5.2), and (5.3) will be performed automatically by the process control model.

For other actinides the above relationships are adjusted on a mole per mole bases using the appropriate molecular weights which are given in **Table 5.12**.

**Table 5.12. Table of molecular weights**

Element/ Isotope	Molecular Weight (g/mol)
Th	232.0380
Nat-U	238.0290
<sup>233</sup> U	233.0396
<sup>235</sup> U	235.0439
<sup>238</sup> U	238.0508
Np	237.0480
Pu	239.1000
Am	241.0567

### 5.3.2 Calculated Ceramic Compositions

As an illustration of how Eqns (5.1), (5.2), and (5.3) are used, they are applied here to yield product compositions for the baseline formulation with three different  $\text{PuO}_2$  feed streams as shown below.

- Clean  $\text{PuO}_2$  with no impurities
- An overall average feed stream
- An extreme case of all the impurities

The compositions of the average and extreme feed streams which are expected to be received by the plant have been given in **Table 3.3**. The  $\text{UO}_2$  that is added is assumed in this case to be from natural uranium. These impurity combinations are given in **Table 5.13** below. For simplicity, all the impurities have been grouped together. They are in the same ratio as given in **Table 3.3**. The

compositions given are those present before sintering. Some of the impurities (e.g., chlorine, fluorine, and zinc) are volatilized at the sintering temperature and will be partially or completely lost, thus reducing slightly the total quantity of impurities in the sintered product. As expected, the composition calculated for clean PuO<sub>2</sub> corresponds approximately to the baseline composition shown in **Table 5.1**. The slight deviation arises because the <sup>235</sup>U in the natural uranium is counted as plutonium. The calculated isotopic composition for the uranium and plutonium elements are given in **Table 5.14**. The isotopic composition for uranium is calculated from the data in **Table 3.1** and by the amount of natural uranium that is added. The isotopic composition for plutonium is calculated just by the data in **Table 3.1**.

**Table 5.13 Calculated product compositions**

	<b>Clean PuO<sub>2</sub></b>	<b>Average Feed</b>	<b>Maximum All Feeds</b>
<b>Oxide</b>	(wt %)	(wt %)	(wt %)
<i>Nonradioactive</i>			
CaO	9.502	9.107	7.652
TiO <sub>2</sub>	37.830	36.273	30.637
Gd <sub>2</sub> O <sub>3</sub>	7.591	7.293	6.147
HfO <sub>2</sub>	11.117	10.784	8.989
<i>Actinide</i>			
ThO <sub>2</sub>	0.000	0.000	0.001
UO <sub>2</sub>	23.321	22.779	19.310
NpO <sub>2</sub>	0.000	0.061	0.182
PuO <sub>2</sub>	10.639	9.459	7.640
Am <sub>2</sub> O <sub>3</sub>	0.000	0.253	0.221
<i>Impurity</i>			
Total *	0.000	3.990	19.222

\*Assumes that impurities are not lost by volatilization

**Table 5.13 Calculated isotopic compositions**

	<b>Clean PuO<sub>2</sub></b>	<b>Average Feed</b>	<b>Maximum All Feeds</b>
<b>Element/Isotope</b>	(wt %)	(wt %)	(wt %)
<i>Uranium</i>			
<sup>235</sup> U	0.700	2.478	3.306
<sup>238</sup> U	99.300	97.522	96.694
<i>Plutonium</i>			
<sup>238</sup> Pu	0.165	0.165	0.165
<sup>239</sup> Pu	89.411	89.411	89.411
<sup>240</sup> Pu	8.496	8.496	8.496
<sup>241</sup> Pu	1.600	1.600	1.600
<sup>242</sup> Pu	0.328	0.328	0.328

## 6. *References*

---

1. Committee on International Security and Arms Control, National Academy of Sciences, Management and Disposition of Excess Weapons Plutonium, National Academy Press, Washington, D.C. (1994).
2. Office of the Press Secretary, The White House, "Fact Sheet: Nonproliferation and Export Control Policy," (September 27, 1993).
3. G. Rudy, "Overview of Surplus Weapons Plutonium Disposition," p. 21-23 in "Final Proceedings, Plutonium Stabilization & Immobilization Workshop," CONF-951259, U. S. Department of Energy, Washington, D.C. (May 30, 1996).
4. A.M. Wijesinghe et al., "Fissile Materials Disposition Program, Alternative Technical Summary Report for Immobilized Disposition in Deep Boreholes, Immobilized Disposal of Plutonium in Coated Ceramic Pellets in Grout Without Canisters," UCRL-LR-121736, Lawrence Livermore National Laboratory, Livermore, CA (August 23, 1996).
5. A.M. Wijesinghe et al., "Fissile Materials Disposition Program, Alternative Technical Summary Report for Direct Disposition in Deep Boreholes, Direct Disposal of Plutonium Metal/Plutonium Dioxide in Compound Canisters," UCRL-LR-121737, Lawrence Livermore National Laboratory, Livermore, CA (August 23, 1996).
6. U.S. Dept. of Energy, "Record of Decision for the Storage and Disposition of Weapons-Usable Fissile Materials Programmatic Environmental Impact Statement," 62 FR 3014-30 (January 14, 1997).
7. U.S. Dept. of Energy, "Storage and Disposition of Weapons-Usable Fissile Materials Final Programmatic Environmental Impact Statement," DOE/EIS-0229 (December, 1996).
8. L. W. Gray, et al. "Screening of Alternate Immobilization Candidates for Disposition of Surplus Fissile Materials," UCRL-ID-118819, Lawrence Livermore National Laboratory, Livermore, CA (February 1996).
9. A. Jostsons, "Status of SYNROC Development," *Australian Nuclear Association 9<sup>th</sup> Pacific Basin Nuclear Conference*, 94/6, May (1994).
10. J. Campbell, C. Hoenig, F. Bazan, F. Ryerson, M. Guinan, R. Van Konynenburg, and R. Rozsa, "Properties of SYNROC-D Nuclear Waste Form: A State-of-the-Art Review," UCRL-53240, Lawrence Livermore National Laboratory, Livermore, CA (January 1982).
11. R.A. Van Konynenburg, R.W. Hopper, J.A. Rard, F.J. Ryerson, D.L. Phinney, I.D. Hutcheon, and P.G. Curtis, "Ceramic Waste Form for Residues from Molten Salt Oxidation of Mixed Wastes," *Materials Research Society Symposium Proceedings*, Vol. 412, Scientific Basis for Nuclear Waste Management XIX, W.M. Murphy and D.A. Knecht, eds., Materials Research Society, Pittsburgh, PA (1996).
12. R. Van Konynenburg, memo to Bill Halsey, "A Titanate Mineral Waste Form for Dismantled Weapons Plutonium," Lawrence Livermore National Laboratory, Livermore, CA (February 10, 1994).
13. Personal communication, V.M. Oversby to R.A. Van Konynenburg, Lawrence Livermore National Laboratory (1994).
14. A. E. Ringwood, Safe Disposal of High Level Nuclear Reactor Wastes: A New Strategy, Australian Nuclear University Press, Canberra, Australia and Norwalk., Conn, USA (1978).
15. A.E. Ringwood, S.E. Kesson, K.D. Reeve, D.M. Levins and E.J. Ramm, "Synroc," Chapter 4 in W. Lutze and R. C. Ewing, eds., Radioactive Waste Forms for the Future, North-Holland, New York (1988), pp. 233-334.

16. A. Jostsons, A. Ridal, D. J. Mercer, and E. R. "Lou" Vance, "Experience Gained with the Synroc Demonstration Plant at ANSTO and its Relevance to Plutonium Immobilization," pp. 347-358 in "Final Proceedings, Plutonium Stabilization & Immobilization Workshop," CONF-951259, U. S. Department of Energy, Washington, D.C. (May 30, 1996).
17. A. E. Ringwood, S. E. Kesson, N. G. Ware, W. Hibberson, and A. Major, "Immobilization of High Level Nuclear Reactor Wastes in SYNROC," *Nature*, **278**, 219-223 (1979).
18. A. E. Ringwood, "Disposal of High-level Nuclear Wastes: A Geological Perspective," *Mineralogical Magazine*, **49**, 159-176 (1985).
19. S. E. Kesson and A. E. Ringwood, "Immobilization of HLW in SYNROC-E," *Materials Research Society Symposium Proceedings*, **26**, 507-512 (1984).
20. S. E. Kesson and A. E. Ringwood, "Safe Disposal of Spent Nuclear Fuel," *Radioactive Waste Management and the Nuclear Fuel Cycle*, **4**, 159-174 (1983).
21. A. G. Solomah, P. G. Richardson, and A. K. McIlwain, "Phase Identification, Microstructural Characterization, Phase Microanalysis and Leaching Performance Evaluation of SYNROC-FA Crystalline Ceramic Waste Form," *Journal of Nuclear Materials*, **148**, 157-165 (1987).
22. V. M. Oversby, R. A. VanKonynenburg, W. E. Glassley, and P. G. Curtis, "Immobilization in Ceramic Waste Forms of the Residues from Treatment of Mixed Wastes," *Materials Research Society Symposium Proceedings*, **333**, 285-292 (1994).
23. B. Ebbinghaus, R. Van Konynenburg, E. Vance, A. Jostsons, R. Anthony, C. Philip, and D. Wronkiewicz, pp. 253-261 in "Final Proceedings, Plutonium Stabilization & Immobilization Workshop," CONF-951259, U. S. Department of Energy, Washington, D.C. (May 30, 1996).
24. R.A. Van Konynenburg, "Expected Radiation Effects in Plutonium Immobilization Ceramic," UCRL-ID-128580, Lawrence Livermore National Laboratory, Livermore, CA (September 1997).
25. B. R. Myers, G. A. Armantrout, C. M. Jantzen, A. Jostsons, J. M. McKibben, H. F. Shaw, D. M. Strachan, and J. D. Vienna, "Technical Evaluation Panel Summary Report: Ceramic and Glass Immobilization Options," UCRL-ID-129315, Lawrence Livermore National Laboratory, Livermore, CA (1998).
26. S. G. Cochran, W. H. Dunlop, T. A. Edmunds, T. H. Gould and L. M. MacLean, "Fissile Materials Disposition Program Final Immobilization Form Assessment and Recommendation," UCRL-10-128705, Oct. 1997
27. Peer Review Panel, letter to Dr. Stephen Cochran, Lawrence Livermore National Laboratory (August 21, 1997).
28. Letter, S. G. Cochran to H. R. Cantor, August 27, 1997.
29. H.R. Canter, U.S. Dept. of Energy, letter to Dr. Steven G. Cochran, Lawrence Livermore National Laboratory (September 25, 1997).
30. D. Horrell, K. Dodson, R. Mason, J. McClard, J. Stakebake, R. Szempruch, and G. Thompson, "Integrated Surveillance Program in Support of Stabilization, Packaging, and Storage of Plutonium-bearing Materials," LA-UR-00-3246, Los Alamos National Laboratory Report (August 2000).
31. L. Gray, memo to Henry Shaw, "Best Guess of Materials Coming into Immobilization," PIP00-100, Plutonium Immobilization Program, Lawrence Livermore National Laboratory, Livermore (August 30, 2000).
32. Personal communication from David C. Riley (April 1998).

33. CRWMS/M&O, Waste Package Related Impacts of Plutonium Disposition Waste Forms in a Geologic Repository. January 2000, TDR-EBS-MD-000003 REV 01.
34. "Integrated Development and Testing Plan for the Plutonium Immobilization Project," UCRL-ID-131608, PIP-98-064, Plutonium Immobilization Program, Lawrence Livermore National Laboratory, Livermore (July 1998).
35. W.J. Weber, R.C. Ewing, and W. Lutze, "Performance Assessment of Zircon as a Waste Form for Excess Weapons Plutonium Under Deep Borehole Burial Conditions," *Materials Research Society Symposium Proceedings*, **412**, pp. 25-32, Materials Research Society, Pittsburgh, PA (1996).
36. B. E. Burakov, E. B. Anderson, V. S. Rovsha, S. V. Ushakov, R. C. Ewing, W. Lutze, and W. J. Weber, "Synthesis of Zircon for Immobilization of Actinides," *Materials Research Society Symposium Proceedings*, **412**, pp. 33-39, Materials Research Society, Pittsburgh, PA (1996).
37. C. Degueudre, U. Kasemeyer, F. Botta, and G. Ledergerber, "Plutonium Incineration in LWRs by a Once-through Cycle with a Rock-like Fuel," *Materials Research Society Symposium Proceedings*, **412**, pp. 15-23, Materials Research Society, Pittsburgh, PA (1996).
38. L. A. Boatner and B. C. Sales, "Monazite," pp. 495-564 in Radioactive Waste Forms for the Future, W. Lutze and R.C. Ewing, eds., North-Holland, New York (1988).
39. R. C. Ewing, B. C. Chakoumakos, and G. R. Lumpkin, and T. Murakami, "The Metamict State," *Material Research Society Bulletin*, May 16/June 15, 58-66 (1987).
40. L. D. Loch and J. F. Quirk, "Ceramics," in *Reactor Handbook*, Second Edition, Volume I, Materials, C. R. Tipton, Jr., ed., Interscience Publishers, New York, p. 291 (1960).
41. W. J. Weber, "Ingrowth of Lattice Defects in Alpha Irradiated UO<sub>2</sub> Single Crystals," *J. Nucl. Mater.*, **98**, 206-215 (1981).
42. Civilian Radioactive Waste Management System, Report on Evaluation of Plutonium Waste Forms for Repository Disposal, Rev 01, DI:A000000000-01717-5705-00009 REV 01 (March 29, 1996).
43. J. S. Allender, "Program Plan for Feed Impurity Tolerance Tests: Ceramic Immobilization Form for Plutonium," SPM-SPI-97-0049, Westinghouse Savannah River Company, (April 28, 1997).
44. C.L. Hoenig and H.T. Larker, "Large Scale Densification of a Nuclear Waste Ceramic by Hot Isostatic Pressing," *Ceramic Bulletin*, **62**, 1389-90 (1983).
45. S. Moricca, A. J. Brownscombe, N. Webb, M. W. A. Stewart, R. A. Day, M. Hambley, E. R. Vance, and A. Jostsons, "Demonstration of Pu Immobilization in Synroc at the 50 g of PuO<sub>2</sub> Scale," ANSTO Report/C511 (June 1997).
46. A.G. Solomah, T.M. Hare and H. Palmour III, "Demonstration of the Feasibility of Subsolidus Sintering of Radwaste-Containing SYNROC-B Composition," *Nuclear Technology*, **49**, 183-5 (July 1980).
47. Guy Armantrout, "Immobilization Dimensional Tolerances Guidance," CCN-000062 (September 1998).
48. H. M. MacLeod and G. Yates, "Development of Mixed-Oxide Fuel Manufacture in the United Kingdom and the Influence of Fuel Characteristics on Irradiation Performance," *Nuclear Technology*, **102**, 3-17 (1993).
49. J. Edwards, J. M. Brennan, H. M. MacLeod, and C. Brown, "MOX Fuel at BNFL," *The Nuclear Engineer*, **37**, 178-181 (1996).

50. D. Haas, A. Vandergheynst, J. VanVliet, R. Lorenzelli, and J.-L. Nigon, "Mixed-Oxide Fuel Fabrication Technology and Experience at the Belgonucleaire and CFCa Plants and Further Developments for the Melox Plant," *Nuclear Technology*, **106**, 60-81 (1994).
51. G. Chandler, A. Cozzi, C. Herman, J. Marra, M. Mitchell, and R. Pierce, "Binder Burnout and Sintering Studies (Milestone 6.6a)," Savannah River Technology Center report, Plutonium Immobilization Program, WSRC-TR-99-00321, PIP-99-118 (October 1999).
52. B.B. Ebbinghaus, C. Cicero-Herman, L. Gray, and H. Shaw, "Plutonium Immobilization Project Baseline Formulation," UCRL-ID-133089, PIP-99-012, Plutonium Immobilization Project, Lawrence Livermore National Laboratory, Livermore, CA (February 1999).
53. A. D. Cozzi, "Experimental Plan for Investigating Impurity Additions to the Ceramic Form for the Immobilization of Plutonium," Interoffice Memorandum SRT-GFM-2000-004, Westinghouse Savannah River Company, Aiken, South Carolina (February 2, 2000).
54. R. D. Shannon, "Revised Effective Ionic Radii and Systematic Studies of Interatomic Distances in Halides and Chalcogenides," *Acta Crystallographica*, **A32**, 751-67 (1976).
55. L. Brewer, "The Thermodynamic Properties of the Oxides and Their Vaporization Processes," *Chemical Reviews*, **52**, 1-75 (1953).
56. V. P. Glushko, L. V. Gurvich, G. A. Bergman, I. V. Veyts, V. A. Medvedev, G. A. Khachkuruzov, V. S. Yungman, Thermodinamicheskie Svoistva Individual'nykh Veshchestv. Tom IV, Nauka, Moskava (1982).
57. E. H. P. Cordfunke and R. J. M. Konings, Thermochemical Data for Reactor Materials and Fission Products, North-Holland, Elsevier Science Publishers B.V., Amsterdam Netherlands (1990).
58. C. W. Bale, A. D. Pelton, FACT, Version 3.0, Thermfact/CRCT, Center for Research in Computational Chemistry, Montreal, Canada (January 1999).
59. B. Ebbinghaus, A. Cozzi, T. Edwards, C. Herman, O. Krikorian, J. Marra, F. Ryerson, R. VanKonynenburg, "The Product Control Methodology," PIP-00-036, Plutonium Immobilization Project, Lawrence Livermore National Laboratory, Livermore, CA (January 2000).
60. B. Ebbinghaus, C. Banochie, M. Hash, C. Herman, A. Jurgenson, O. Krikorian, J. Marra, F. Ryerson, E. Vance, and R. Van Konynenburg, "Provide Feed Specifications Summary Tables (Milestone 3.2.a)," PIP-99-153, Plutonium Immobilization Project, Lawrence Livermore National Laboratory, Livermore, CA (July 1999).
61. L. W. Gray, B. B. Ebbinghaus, T. A. Edmunds, R. A. VanKonynenburg, D. C. Riley, "Materials Disposition Acceptance Specification for the Plutonium Immobilization Project," PIP-98-047 (August 1998).
62. M. A. Subramanian, G. Aravamudan, and G. V. Subba Rao, "Oxide Pyrochlores – A Review," *Progress in Solid State Chemistry*, **15**, 55-143 (1983).
63. D. D. Hogarth, "Classification and Nomenclature of the Pyrochlore Group," *American Mineralogist*, **62**, 403-410 (1977).
64. G. R. Lumpkin and R. C. Ewing, "Geochemical Alteration of Pyrochlore Group Minerals: Betafite Group," *American Mineralogist*, **81**, 1237-1248 (1996).
65. D. D. Hogarth, "A Study of Pyrochlore and Betafite," *Canadian Mineralogist*, 610-633.
66. G. R. Lumpkin, K. P. Hart, P. J. McGlenn, and T. E. Payne, "Retention of Actinides in Natural Pyrochlores and Zirconolites," *Radiochimica Acta*, **66/67**, 469-474 (1994).
67. P. Bayliss, F. Mazzi, R. Munno, and T. J. White, "Mineral Nomenclature: Zirconolite," *Mineralogical Magazine*, **53**, 565-569 (1989).

68. T. J. White, R. L. Segall, J. L. Hutchison, and J. C. Barry, "Polytypic Behavior of Zirconolite," *Proceedings of the Royal Society of London, A* **392**, 343-358 (1984).
69. V. M. Oversby and A. E. Ringwood, "Lead Isotopic Studies of Zirconolite and Perovskite and Their Implications for Long Range Synroc Stability," *Radioactive Waste Management*, **1**, 289-307 (1981).
70. R. C. Ewing and R. F. Haaker, "Zirconolites from Sri Lanka, South Africa, and Brazil," *Scientific Basis for Nuclear Waste Management*, S. V. Topp, Ed., 249-256 (1982).
71. F. Purtscheller and R. Tessadri, "Zirconolite and Baddeleyite from Metacarbonates of the Oetztal-Stubai Complex," *Mineralogical Magazine*, **49**, 523-529 (1985).
72. J. T. Szymanski and J. D. Scott, "A Crystal-Structure Refinement of Synthetic Brannerite,  $UTi_2O_6$ , and its Bearing on Rate of Alkaline-Carbonate Leaching of Brannerite Ore," *Canadian Mineralogist*, **20**, 271-279 (1982).
73. Lumpkin, Colella, Leung, Task 2: Performance Testing – Task 2.4: Natural Mineral Analog Studies: Physical and Chemical Characteristics of Brannerite in Natural Systems," R00m023, Australian Nuclear Science and Technology Organization (April 2000).
74. D. F. Hewett, J. Stone, and H. Levine, "Brannerite from San Bernardino County, California," *U.S. Geological Survey*, 30-38 (1956).
75. A. Pabst, "Brannerite from California," *American Mineralogist*, **39**, 109-117 (1954).
76. C. C. Herman, "Preliminary Precursor Preparation Baseline Report – Process Description and Specifications," PIP-99-036, Plutonium Immobilization Project, Lawrence Livermore National Laboratory, Livermore, CA (February 1999).
77. "System Design Description for Ceramification Module 2.2," PIP-99-167, Plutonium Immobilization Project, Lawrence Livermore National Laboratory, Livermore, CA (December 1999).

## ***Appendix A***

### ***List of Acronyms***

---

ANL	Argonne National Laboratory
ANSTO	Australian Nuclear Science and Technology Organization
ANU	Australian National University
BEI	backscatter electron image
BNFL	British Nuclear Fuels Limited
BYU	Brigham Young University
CISAC	Committee on International Security and Arms Control
D&T	development and testing
DHLW	defense high-level waste
DOE	Department of Energy
DOE-DP	Department of Energy Office of Defense Programs
DOE-EM	Department of Energy Office of Environmental Management
DOE-MD	Department of Energy Office of Material Disposition
DOE-NE	Department of Energy Office of Nuclear Energy
DOE-NN	Department of Energy Office of Nuclear Nonproliferation
DOE-RW	Department of Energy Office of Radioactive Waste Management
DWPF	Defense Waste Processing Facility
EDS	energy dispersive spectroscopy
EPA	Environmental Protection Agency
FY	Fiscal Year
HIP	hot isostatic pressing
HLW	high-level waste
HUP	hot uniaxial pressing
KRI	Khlopin Radium Institute
LANL	Los Alamos National Laboratory
LLNL	Lawrence Livermore National Laboratory
MC&A	material control and accountability
MOX	mixed oxide (fuel)
MT	metric tonnes
NDE	nondestructive evaluation
NRC	Nuclear Regulatory Commission
OCRWM	Office of Civilian Radioactive Waste Management
ORNL	Oak Ridge National Laboratory
PIP	Plutonium Immobilization Program
PNNL	Pacific Northwest National Laboratory
RCRA	Resource Conservation and Recovery Act
REE	rare earth element
SEI	secondary electron image
SEM	scanning electron microscopy
SPFT	single-pass flow-through (test)
SRS	Savannah River Site
SRTC	Savannah River Technology Center
SYNROC	synthetic rock
TEM	transmission electron microscopy
TEP	technical evaluation panel
TRU	transuranic (waste)
UCD	University of California at Davis
WIPP	Waste Isolation Pilot Plant

Thermodynamics of formation for Hf-zirconolite,  $\text{CaHfTi}_2\text{O}_7(\text{cr})$  and  $\text{HfO}_2(\text{cr})$  from  $T=0\text{ K}$  to  $T=1500\text{ K}$ ; Revised values of  $\Delta_f^T G_m^o$  for  $\text{CaZrTi}_2\text{O}_7(\text{cr})$  over the same temperature.

Robert L. Putnam,<sup>a,b</sup> Jose Gutierrez, Alexandra Navrotsky Thermochemistry Facility; Department of Chemical Engineering and Materials Science; University of California at Davis; Davis, CA 95616

Rebecca Stevens, Benjamin K. Hom, Juliana Boerio-Goates, and Brian F. Woodfield Department of Chemistry and Biochemistry; Brigham Young University; Provo, UT 84602.

<sup>a</sup> Author to whom correspondence should be addressed.  
Email: [rputnam@LANL.gov](mailto:rputnam@LANL.gov)

<sup>b</sup> Present Address. Los Alamos National Laboratory; Nuclear Materials Technology; Mail Stop G721; Los Alamos, NM 87545

Short Title: Thermodynamics of Hf-zirconolite

To be submitted to: J. Chem. Thermodynamics.

## Abstract

Hf-zirconolite,  $\text{CaHfTi}_2\text{O}_7(\text{cr})$ , and a solid solution between Hf-zirconolite and zirconolite,  $\text{CaZrTi}_2\text{O}_7(\text{cr})$ , have been prepared. The enthalpies of drop solution,  $\Delta_{298.15\text{K}}^{973\text{K}} H_m(\text{sol})$  in a lead borate melt,  $2\text{PbO} \cdot \text{B}_2\text{O}_3$ , at  $T = 973\text{ K}$  have been measured for  $\text{HfO}_2(\text{cr})$ ,  $\text{CaHfTi}_2\text{O}_7(\text{cr})$ , and  $\text{CaZr}_{0.26}\text{Hf}_{0.74}\text{Ti}_2\text{O}_7(\text{cr})$  and are  $(56.43 \pm 1.96)\text{ kJ} \cdot \text{mol}^{-1}$ ,  $(261.44 \pm 3.45)\text{ kJ} \cdot \text{mol}^{-1}$ , and  $(267.87 \pm 11.9)\text{ kJ} \cdot \text{mol}^{-1}$ , respectively. The standard molar enthalpies of formation,  $\Delta_f H_m^\circ$ , are  $-(3752.27 \pm 4.99)\text{ kJ} \cdot \text{mol}^{-1}$  and  $-(3754.5 \pm 12.3)\text{ kJ} \cdot \text{mol}^{-1}$  for  $\text{CaHfTi}_2\text{O}_7(\text{cr})$  and  $\text{CaZr}_{0.26}\text{Hf}_{0.74}\text{Ti}_2\text{O}_7(\text{cr})$ , respectively. The standard molar Gibbs free energies of formation,  $\Delta_f G_m^\circ$ , for  $\text{CaHfTi}_2\text{O}_7(\text{cr})$  and  $\text{CaZr}_{0.26}\text{Hf}_{0.74}\text{Ti}_2\text{O}_7(\text{cr})$  are  $-(3552.81 \pm 4.99)\text{ kJ} \cdot \text{mol}^{-1}$  and  $-(3556.6 \pm 12.3)\text{ kJ} \cdot \text{mol}^{-1}$ , respectively. Recent crystallographic data on zirconolite established the existence of disorder at the Ti(2) site which results in a zero-point entropy contribution of  $\frac{1}{2}R \ln 2$  not previously included in the thermodynamic tabulation for zirconolite. Corrections to our previously published  $\Delta_f^T G_m^\circ$  for  $\text{CaZrTi}_2\text{O}_7(\text{cr})$  are presented. The molar heat capacity,  $C_{p,m}$ , third law entropy  $\Delta_0^T S_m^\circ$ , standard molar enthalpy of formation  $\Delta_f^T H_m^\circ$  and standard molar Gibbs free energies of formation  $\Delta_f^T G_m^\circ$  for  $\text{CaZrTi}_2\text{O}_7(\text{cr})$  and  $\text{CaHfTi}_2\text{O}_7(\text{cr})$  are tabulated from  $T = 0\text{ K}$  to  $T = 1500\text{ K}$  and from  $T = 298.15\text{ K}$  to  $T = 1800\text{ K}$  for  $\text{HfO}_2(\text{cr})$ .

**KEYWORDS:** Enthalpy of formation, nuclear waste, Gibbs Free energy of formation, calorimetry,  $\text{CaHfTi}_2\text{O}_7$ ,  $\text{CaZrTi}_2\text{O}_7$ ,  $\text{HfO}_2$ , Solid Solution

## Introduction

The United States Department of Energy has decided that at least 17 tonne of an estimated 50 tonne of surplus weapons plutonium belonging to the United States will be incorporated into a ceramic waste material and then disposed in a geological repository.<sup>(1)</sup> The remaining plutonium is expected to be used in nuclear reactors capable of burning mixed oxide (U + Pu oxides) or MOx fuels.<sup>(2)</sup> The form the plutonium waste ceramic will take is a solid solution in the system {CaHfTi<sub>2</sub>O<sub>7</sub>(cr) + CaUTi<sub>2</sub>O<sub>7</sub>(cr) + CaPuTi<sub>2</sub>O<sub>7</sub>(cr) + Gd<sub>2</sub>Ti<sub>2</sub>O<sub>7</sub>(cr)}. The latter three phases crystallize in the pyrochlore<sup>(3)</sup> structure and CaHfTi<sub>2</sub>O<sub>7</sub>(cr) in the related structure of zirconolite, CaZrTi<sub>2</sub>O<sub>7</sub>(cr).<sup>(4, 5)</sup>

An understanding of the thermodynamics of the various phases to be incorporated into a ceramic waste form is vital for optimizing the proposed waste form in terms of composition, waste loading, environmental and geologic stability, and for manufacturing purposes. We have previously reported the formation energetics on other phases<sup>(5-10)</sup> related to these nuclear waste materials. In this paper and in its companion paper<sup>(11)</sup>, we have applied two different calorimetric techniques, low-temperature adiabatic calorimetry<sup>(6,12-13)</sup> and high-temperature oxide-melt solution calorimetry<sup>(5,14-15)</sup> to obtain the heat capacity, third law entropies, standard molar enthalpies of formation, and Gibbs free energies of formation for CaHfTi<sub>2</sub>O<sub>7</sub>(cr) and CaZr<sub>0.26</sub>Hf<sub>0.74</sub>Ti<sub>2</sub>O<sub>7</sub>(cr), a solid solution between CaHfTi<sub>2</sub>O<sub>7</sub>(cr) and CaZrTi<sub>2</sub>O<sub>7</sub>(cr).

## Experimental

Two samples of  $\text{CaHfTi}_2\text{O}_7(\text{cr})$  were synthesized from  $\text{CaCO}_3(\text{cr})$  (Alpha Aesar),  $\text{TiO}_2$  (cr, anatase) (Alpha Aesar, mass fraction  $> 0.9999$ ), and  $\text{HfO}_2(\text{cr})$  (Alpha Aesar, mass fraction  $> 0.999$ ). Each sample was synthesized in the same manner. Reactants were ground in a high density alumina mortar under ethanol, dried, and then sintered three times for 24, 48, and 96 h at  $T = 1573$  K in platinum crucibles. Between sinterings the samples were ground under ethanol in an alumina mortar.

The resulting material in both samples was confirmed to be  $\text{CaHfTi}_2\text{O}_7(\text{cr})$  using powder X-ray diffraction. The two samples of  $\text{CaHfTi}_2\text{O}_7(\text{cr})$  were identified as Sample A (~ 1 g) and Sample B (~30 g). Sample A was used in the high-temperature oxide-melt solution calorimetry experiments reported here and Sample B was used in the heat capacity determination reported elsewhere.<sup>(11)</sup>

The solid solution,  $\text{CaZr}_{0.24}\text{Hf}_{0.76}\text{Ti}_2\text{O}_7(\text{cr})$  was synthesized using the same procedure but with the addition of  $\text{ZrO}_2(\text{cr}, \text{baddeleyite})$  (Alpha Aesar, mass fraction  $> 0.999$ ) as a reactant. The zirconolite structure was confirmed through powder X-ray diffraction. This solid solution,  $\text{CaZr}_{0.26}\text{Hf}_{0.74}\text{Ti}_2\text{O}_7(\text{cr})$ , was used in both the heat capacity determination<sup>(15)</sup> and in the high-temperature oxide-melt solution calorimetry reported here.

The compositions of the two Hf-zirconolite samples and the solid solution were verified using a Cameca SX-50 electron micro probe. Sample A was found to be single phase and stoichiometric  $\text{CaHfTi}_2\text{O}_7(\text{cr})$ , while sample B and the solid solution contained small amounts of perovskite,  $\text{CaTiO}_3(\text{cr})$ . The presence

of perovskite in our samples was treated as though it was present as a mechanical mixture<sup>(5, 16)</sup> with the phase of interest. The composition of sample B was determined to be  $(0.0684 \text{ CaTiO}_3 + 0.9315 \text{ CaHfTi}_2\text{O}_7)(\text{cr})$  and that of the solid solution to be  $(0.0637 \text{ CaTiO}_3 + 0.9363 \text{ CaZr}_{0.26}\text{Hf}_{0.74}\text{Ti}_2\text{O}_7)(\text{cr})$  using energy dispersive spectroscopy (EDS) on the Cameca SX-50 and analyzing for the presence of Ca, Zr, Hf, Ti, and Al (from the grinding media). No aluminum was found to be present above the instrument background. Compositions were derived from the values of metals measured (Ca, Zr, Hf, Ti, and Al) as a function of total metal concentration and represent the mean stoichiometry of the materials studied.

Our application of high-temperature oxide melt solution calorimetry to refractory materials such as those reported here has been discussed previously.<sup>(5,7,8)</sup> Two types of high-temperature calorimetric experiments have been performed on our samples.

Transposed temperature drop (TTD) experiments are used to measure the molar enthalpy increment,  $\Delta_T^{298.15K} H_m$ , and the energetics of any phase transformation, decomposition, or oxidation-reduction of a sample pellet dropped from room temperature into a calorimeter maintained at high temperature with no solvent. In drop solution calorimetry (DS), a sample at room temperature is dropped into a calorimeter that contains the solvent. The sample then dissolves in the solvent. Contributions to this DS enthalpy include the molar enthalpy increment,  $\Delta_T^{298.15K} H_m$ , the enthalpy of solution, and the enthalpy of any other process (e.g., gas evolution or oxidation reduction) occurring during dissolution.

The solvent used for all DS experiments reported here was a lead borate glass having the composition  $2\text{PbO}\cdot\text{B}_2\text{O}_3(\text{vit})$ . As in our previous papers,<sup>(5,7,8)</sup> we have used the symbols  $\Delta_{298.15\text{K}}^{973\text{K}}H_m$  and  $\Delta_{298.15\text{K}}^{973\text{K}}H_m(\text{sol})$  to represent the enthalpy associated with TTD and DS experiments, respectively, for a calorimeter operating temperature of  $T=973\text{K}$ .

We have previously<sup>(5,8)</sup> described and used a DS technique which bubbles a gas through the lead borate melt as the sample reacts. The bubbling gas assists in the dissolution of samples that are slow to dissolve by acting as a stirring agent. In this work we have also applied this technique to our samples. Oxygen with a flow rate of  $(3.3 \times 10^{-2} \text{ to } 5 \times 10^{-2}) \text{ cm}^3 \cdot \text{s}^{-1}$  was used as a bubbling gas. At this flow rate and in our lead borate melt maintained at  $T=973\text{K}$ , bubble formation and release occurs approximately every 2 s.

For all experiments, calibration of the calorimeter was performed against the molar enthalpy increment,  $\Delta_T^{298.15\text{K}}H_m$ , of 0.005 g or 0.025 g pellets of powdered  $\alpha\text{-Al}_2\text{O}_3(\text{cr})$  (Mass fraction  $> 0.99997$ ) that had previously been sintered at  $T=1773\text{K}$  for at least 8 h to guarantee the  $\alpha$ - or corundum phase of  $\text{Al}_2\text{O}_3(\text{cr})$ .

## Results

Three samples,  $\{\text{HfO}_2(\text{cr}), \text{CaHfTi}_2\text{O}_7(\text{cr}), \text{ and } (0.0637 \text{ CaTiO}_3 + 0.9363 \text{ CaZr}_{0.26}\text{Hf}_{0.74}\text{Ti}_2\text{O}_7)(\text{cr})\}$ , were measured using bubbling DS and/or TTD experiments and the results are found in Table 1 and Table 2. Nine DS experiments on  $\text{HfO}_2(\text{cr})$  and 2 test DS experiments on the solid solution (0.0637

$\text{CaTiO}_3 + 0.9363 \text{ CaZr}_{0.26}\text{Hf}_{0.74}\text{Ti}_2\text{O}_7(\text{cr})$  may be found in Table 1. Five DS experiments, 9 TTD experiments at  $T = 973 \text{ K}$ , and 9 TTD experiments at  $T = 1073 \text{ K}$  on  $\text{CaHfTi}_2\text{O}_7(\text{cr})$  are found in Table 2.

Table 3 shows the thermodynamic cycle required to yield the standard molar enthalpy of formation from the elements,  $\Delta_f H_m^\circ$ , for  $\text{CaHfTi}_2\text{O}_7(\text{cr})$  from high-temperature oxide melt solution calorimetric experiments. As may be seen from reaction (2) in Table 3,  $\Delta_{298.15\text{K}}^{973\text{K}} H_m(\text{sol})$  for  $\text{HfO}_2(\text{cr})$  must be measured to complete the cycle. Table 1 shows the experimental results of our drop solution experiments on  $\text{HfO}_2(\text{cr})$  yielding the enthalpy of DS,  $\Delta_{298.15\text{K}}^{973\text{K}} H_m(\text{sol})(\text{HfO}_2) = 56.43 \pm 1.96 \text{ kJ}\cdot\text{mol}^{-1}$ . The calorimetric sample of  $\text{HfO}_2(\text{cr})$  was a high purity (Strem Chemicals, Inc., mass fraction  $>0.99998$ ) sample.

Early bubbling DS experiments on pellets of pure  $\text{HfO}_2(\text{cr})$  were problematic. The pellets did not fully dissolve and results yielded inconsistent values for  $\Delta_{298.15\text{K}}^{973\text{K}} H_m(\text{sol})(\text{HfO}_2)$ . The determination that the samples were not dissolving completely was made based on optical microscopy where small chunks recognizable as portions of the undissolved  $\text{HfO}_2(\text{cr})$  pellets were observed in the quenched glass. This observation was also supported by the inconsistent results as Putnam et al.<sup>(7)</sup> has previously discussed.

In an effort to facilitate the dissolution of  $\text{HfO}_2(\text{cr})$  in our lead borate melt, a mechanical mixture of the  $\text{HfO}_2(\text{cr})$  sample and the lead borate solvent was prepared. When pelletized and dropped into the calorimeter, the mixed sample pellets fell apart rapidly as the lead borate in the pellet melted and the powdered  $\text{HfO}_2(\text{cr})$  was then disbursed throughout the melt by the bubbling gas where it

dissolved. Corrections were then made for the presence of lead borate in the measured sample.

Complete dissolution of  $\text{HfO}_2(\text{cr})$  was verified using optical microscopy by the absence of any undissolved or recrystallized materials in the quenched glass. Once the mixture was used in the bubbling DS experiments, the resulting measurements yielded consistent values of  $\Delta_{298.15\text{K}}^{973\text{K}} H_m(\text{sol})(\text{HfO}_2)$  as may be seen in Table 1.

After six unsuccessful attempts at dissolving pellets of pure  $\text{CaHfTi}_2\text{O}_7$  (cr, sample A) in lead borate we once again utilized a mechanical mixture of  $\text{CaHfTi}_2\text{O}_7(\text{cr})$  and lead borate solvent. After using the mixture,

$\Delta_{298.15\text{K}}^{973\text{K}} H_m(\text{sol})(\text{CaHfTi}_2\text{O}_7)$  was found to be  $(261.44 \pm 3.45) \text{ kJ}\cdot\text{mol}^{-1}$ . Table 4 shows the thermodynamic cycle used to obtain the standard molar enthalpy of formation for  $\text{CaHfTi}_2\text{O}_7(\text{cr})$ ,  $\Delta_f H_m^\circ = -(3752.27 \pm 4.99) \text{ kJ}\cdot\text{mol}^{-1}$ .

Using our previously published<sup>(11)</sup> molar entropy for  $\text{CaHfTi}_2\text{O}_7(\text{cr})$ ,  $\Delta_{298.15\text{K}}^{298.15\text{K}} S_m^\circ = 197.0 \text{ J}\cdot\text{K}^{-1}\cdot\text{mol}^{-1}$ , in the Gibbs free energy relationship,  $\Delta G = \Delta H - T\Delta S$ , along with  $\Delta_{298.15\text{K}}^{298.15\text{K}} S_m^\circ$  values for the standard state elements from references (17) and (19) we have determined that the standard molar Gibbs free energy of formation is,  $\Delta_f G_m^\circ(\text{CaHfTi}_2\text{O}_7) = -(3552.81 \pm 4.99) \text{ kJ}\cdot\text{mol}^{-1}$ .

The heat capacities and entropies are known for the standard state elements<sup>(17, 19)</sup> and for  $\text{CaHfTi}_2\text{O}_7(\text{cr})$ <sup>(11)</sup> from  $T=0$  to  $T=1500 \text{ K}$ . With these values and our  $\Delta_f H_m^\circ$  for  $\text{CaHfTi}_2\text{O}_7(\text{cr})$  we have tabulated the formation

enthalpies, entropies, and Gibbs free energies of formation for  $\text{CaHfTi}_2\text{O}_7(\text{cr})$  from  $T=0\text{ K}$  to  $T=1500\text{ K}$  which are found in Table 4 part A.

In obtaining the values for  $\Delta_f^T H_m^o$ ,  $\Delta_0^T S_m^o$ , and  $\Delta_f^T G_m^o$  for  $\text{CaHfTi}_2\text{O}_7(\text{cr})$  found in Table 4 part A it was noted that the previously tabulated<sup>(20)</sup> values of  $\Delta_f^T H_m^o$ ,  $\Delta_0^T S_m^o$ , and  $\Delta_f^T G_m^o$  for  $\text{HfO}_2(\text{cr})$  were based on an incorrect<sup>(21,22)</sup> value -  $(1144.74 \pm 1.25)\text{ kJ}\cdot\text{mol}^{-1}$  of  $\Delta_f H_m^o$  for  $\text{HfO}_2(\text{cr})$ . We have corrected these quantities using the corrected<sup>(17,22)</sup> value of  $\Delta_f H_m^o(\text{HfO}_2) = -(1117.6 \pm 1.3)\text{ kJ}\cdot\text{mol}^{-1}$  and assuming that the heat capacity results on  $\text{HfO}_2(\text{cr})$  reported previously<sup>(20,23)</sup> were correct. We present these new values of  $\Delta_f^T H_m^o$ ,  $\Delta_0^T S_m^o$ , and  $\Delta_f^T G_m^o$  for  $\text{HfO}_2(\text{cr})$  from  $T=298.15\text{ K}$  to  $T=1800\text{ K}$  in Table 4 part B.

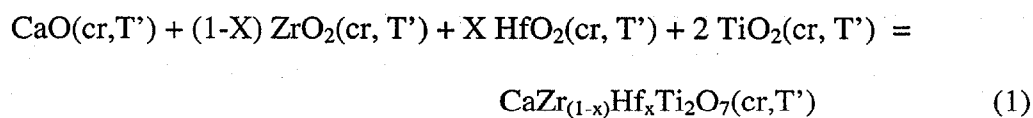
Two crystallographic studies on zirconolite,  $\text{CaZrTi}_2\text{O}_7(\text{cr})$ <sup>(24,25)</sup> have established the existence of disorder at the Ti(2) site in the zirconolite structure. Our previous report<sup>(5)</sup> of  $\Delta_f^T H_m^o$ ,  $\Delta_0^T S_m^o$ , and  $\Delta_f^T G_m^o$  for  $\text{CaZrTi}_2\text{O}_7(\text{cr})$  did not incorporate a zero-point entropy arising from this disorder. We report corrected values for these quantities in Table 4 part C which includes this zero-point entropy.<sup>(11)</sup>

## Discussion

Table 1 contains the results of two test DS experiments on our  $(0.0637\text{ CaTiO}_3 + 0.9363\text{ CaZr}_{0.26}\text{Hf}_{0.74}\text{Ti}_2\text{O}_7)(\text{cr})$  solid solution sample,  $\Delta_{298.15\text{K}}^T H_m(\text{sol}) = (261.6 \pm 11.9)\text{ kJ}\cdot\text{mol}^{-1}$ . When corrected for the presence of perovskite and then

normalized to one mole of  $\text{CaZr}_{0.26}\text{Hf}_{0.74}\text{Ti}_2\text{O}_7(\text{cr})$ ,  $\Delta_{298.15\text{K}}^T H_m(\text{sol}) = (267.87 \pm 11.9) \text{ kJ}\cdot\text{mol}^{-1}$ . These test experiments were performed in an effort to determine if  $\text{CaHfTi}_2\text{O}_7(\text{cr})$  and  $\text{CaZrTi}_2\text{O}_7(\text{cr})$  might form an ideal solid solution or, if not, what type of deviation from ideality (negative or positive) might be observed. Table 5 shows the thermodynamic cycle used to determine that  $\Delta_f H_m^\circ$  for  $\text{CaZr}_{0.26}\text{Hf}_{0.74}\text{Ti}_2\text{O}_7(\text{cr})$  is  $-(3754.5 \pm 12.3) \text{ kJ}\cdot\text{mol}^{-1}$ . We have previously published<sup>(11)</sup> the molar heat capacity and third law entropy for  $\text{CaZr}_{0.26}\text{Hf}_{0.74}\text{Ti}_2\text{O}_7(\text{cr})$  which allows us to then determine that  $\Delta_f G_m^\circ$  for  $\text{CaZr}_{0.26}\text{Hf}_{0.74}\text{Ti}_2\text{O}_7(\text{cr})$  is  $-(3556.6 \pm 12.3) \text{ kJ}\cdot\text{mol}^{-1}$ .

Our results confirm that there is significant solid solubility between  $\text{CaZrTi}_2\text{O}_7(\text{cr})$  and  $\text{CaHfTi}_2\text{O}_7(\text{cr})$ . Figure 1 shows the measured enthalpies of the reaction,  $\Delta_r H_m^\circ$  (1):



as a function of the mole fraction of  $\text{CaHfTi}_2\text{O}_7(\text{cr})$ ,  $X_{\text{Hf}}$  (filled symbols and solid line). These values of  $\Delta_r H_m^\circ$  (1) are found in Tables 3 and 5 as reactions (10) and (13), respectively. For  $\text{CaZrTi}_2\text{O}_7(\text{cr})$  we have previously reported<sup>(5)</sup> a value of  $-(88.79 \pm 4.00) \text{ kJ}\cdot\text{mol}^{-1}$ . If  $\text{CaHfTi}_2\text{O}_7(\text{cr})$  and  $\text{CaZrTi}_2\text{O}_7(\text{cr})$  formed ideal solid solutions then there would be no enthalpy associated with their mixing and  $\Delta_r H_m^\circ$  (1) would plot as indicated by the dashed line and open symbols in

Figure 1. Clearly, with the application of our test measurements, this may not be the case indicating that a deviation from ideality possibly exists.

Our examination of the solid solution,  $\text{CaZr}_{.26}\text{Hf}_{.74}\text{Ti}_2\text{O}_7(\text{cr})$ , between these end member compositions indicate that they most likely form a regular solution as may be seen in Figure 2 where we plot the measured enthalpy of mixing,  $\Delta_{\text{mix}}H_m$ , as a function of mol fraction of  $\text{CaHfTi}_2\text{O}_7(\text{cr})$ ,  $X_{\text{Hf}}$ ,

$\Delta_{\text{mix}}H_m$  may be obtained by subtracting the measured enthalpy of formation from the binary oxides ( $\text{CaO}$ ,  $\text{TiO}_2$ ,  $\text{HfO}_2$ , and  $\text{ZrO}_2$ ),  $\Delta_f H_m^\circ(1)$ , from what would be predicted if  $\text{CaZrTi}_2\text{O}_7(\text{cr})$  and  $\text{CaHfTi}_2\text{O}_7(\text{cr})$  mixed ideally,  $\Delta_{\text{mix}}H_m = 0 \text{ kJ}\cdot\text{mol}^{-1}$  (see the dashed line in Figure 1).

Our earlier report<sup>(11)</sup> of the heat capacities,  $C_{p,m}$ , on  $\text{CaZr}_{.26}\text{Hf}_{.74}\text{Ti}_2\text{O}_7(\text{cr})$  noted a difference between the measured heat capacity ( $C_{\text{meas}}$ ) and one calculated, ( $C_{\text{calc}}$ ) as a weighted sum of the pure components of the solid solution,  $\text{CaZrTi}_2\text{O}_7(\text{cr})$  and  $\text{CaHfTi}_2\text{O}_7(\text{cr})$ . Over the entire temperature range of our reported measurements<sup>(11)</sup>  $C_{\text{meas}}$  was systematically lower than ( $C_{\text{calc}}$ ) and indicates a mixture lattice that is more tightly bound than an ideal solution would suggest. Solid solutions exhibiting such behavior in their heat capacities would also be expected to exhibit a negative deviation from ideality in their enthalpies of mixing as suggested by our test experiments with  $\text{CaZr}_{.26}\text{Hf}_{.74}\text{Ti}_2\text{O}_7(\text{cr})$  as noted in Figure 2. More definitive studies of  $\Delta_{\text{mix}}H_m$  are planned to better characterize any deviation from ideality in the solid-solution series formed between  $\text{CaZrTi}_2\text{O}_7(\text{cr})$  and  $\text{CaHfTi}_2\text{O}_7(\text{cr})$  and the results will be reported at a later date.

In conclusion we have synthesized Hf-zirconolite,  $\text{CaHfTi}_2\text{O}_7(\text{cr})$  and one of its solid solution compounds with  $\text{CaZrTi}_2\text{O}_7(\text{cr})$  and have determined that Hf-zirconolite and Zr-zirconolite appear to form a regular solid solution with possibly a negative deviation from ideality. We have determined and reported the standard molar enthalpies of formation for  $\text{CaHfTi}_2\text{O}_7(\text{cr})$  and a solid solution of the composition  $\text{CaZr}_{.26}\text{Hf}_{.74}\text{Ti}_2\text{O}_7(\text{cr})$  and we have corrected the previously tabulated values of  $\Delta_f^T H_m^\circ$ ,  $\Delta_0^T S_m^\circ$ , and  $\Delta_f^T G_m^\circ$  for  $\text{HfO}_2(\text{cr})$  and  $\text{CaZrTi}_2\text{O}_7(\text{cr})$  from  $T=0\text{ K}$  to  $T=1500\text{ K}$  (from  $T=298.15\text{ K}$  to  $T=1800\text{ K}$  for  $\text{HfO}_2$ ). We have also reported  $\Delta_f^T H_m^\circ$ ,  $\Delta_0^T S_m^\circ$ , and  $\Delta_f^T G_m^\circ$  for  $\text{CaHfTi}_2\text{O}_7(\text{cr})$  from  $T=0\text{ K}$  to  $T=1500\text{ K}$ .

This work was supported in part by a grant from Lawrence Livermore National Laboratory and by Department of Energy grant number DE-FG07-97ER45673.

## References

1. Record of Decision for the Surplus Plutonium Disposition. Final Environmental Impact Statement. January 4, 2000. US Department of Energy.
2. Record of Decision for the storage and disposition of weapons usable fissile materials. Final programmatic environmental impact statement. January 14, 1997. US Department of Energy.
3. Lutze, W.; Ewing, R.C. *Radioactive Waste Forms for the Future*; North Holland: New York, 1988.
4. Ewing, R. C.; Lutze, W.; Weber, W. J. *J. Mater. Res.*; **1995**, 10, 2, 243-246.
5. Putnam, R. L.; Navrotsky, A.; Woodfield, B. F.; Boerio-Goates, J.; Shapiro, J.L. *J. Chem. Thermodynamics* **1999**, 31, 229-243.
6. Woodfield, B.F.; Boerio-Goates, J.; Shapiro, J.; Putnam, R. L.; Navrotsky, A. *J. Chem. Thermodynamics* **1999**, 31, 245-253.
7. Putnam, R.L.; Navrotsky, A.; Cordfunke, E.H.P.; Huntelaar, M.E. J.; *J. Chem. Thermodynamics* **2000**, 32, 911-921.
8. Hom, B.K.; Stevens, R.; Shapiro, J. L.; Woodfield, B. F.; Boerio-Goates, J.; Putnam, R. L.; Helean, K.B.; Navrotsky, A. *J. Chem. Thermodynamics* **2000**, in press.
9. Putnam, R. L. Ph.D. dissertation, Princeton University, November 1999.
10. Woodfield, B. F.; Shapiro, J. L.; Stevens, R.; Boerio-Goates, J.; Putnam, R. L.; Helean, K. B.; Navrotsky, A. *J. Chem. Thermodynamics* **1999**, 31, 1573-1583.
11. Stevens, R.; Hom, B. K.; Boerio-Goates, J.; Woodfield, B. F.; Putnam, R.L.; Gutierrez, J.; Navrotsky, A. *J. Chem. Thermodynamics* Submitted.
12. Boerio-Goates, J.; Woodfield, B.F. *Can. J. Chem.* **1988**, 66, 645-650.
13. Battley, E. H.; Putnam, R. L.; Boerio-Goates, J. *Thermochim. Acta* **1997**, 298, 37-46.
14. Navrotsky, A. *Phys. Chem. Min.* **1977**, 2, 89-104.

15. Navrotsky, A. *Phys. Chem. Min.* **1997**, 24, 222-241.
16. Putnam, R.L.; Navrotsky, A.; Woodfield, B.F.; Shapiro, J.L.; Stevens, R.; Boerio-Goates, J. *Mat. Res. Soc. Symp. Proc.* 1999, 556, 11-18.
17. Robie, R.A.; Hemingway, B. S. *Thermodynamics Properties of Minerals and Related Substances at 298.15 K and 1 Bar ( $10^5$  Pascals) Pressure and at Higher Temperatures* Geological Survey Bulletin #2131. United States Government Printing Office: Washington D. C. **1995**.
18. Kiseleva, I.; Navrotsky, A.; Belitsky, I. A.; Fursenko, B. A., *am. Mineral.* **1996**, 81, 668-675.
19. Chase, M. W. Jr. *J. Phys. Chem. Ref. Data* **1998**, 9.
20. Robie, R. A.; Hemingway, B.S.; Fisher, J. R. *Thermodynamics Properties of Minerals and Related Substances at 298.15 K and 1 Bar ( $10^5$  Pascals) Pressure and at Higher Temperatures* Geological Survey Bulletin #1452. United States Government Printing Office: Washington D. C. **1979**, page 174.
21. Huber, E.J.Jr.; Holley, C. E. Jr. *J Chem. Eng. Data* **1968**, 13, 252.
22. Kornilov, A. N.; Uchakova, I.M.; Huber, E. J. Jr.; Holley, C. E. Jr. *J. Chem. Thermodynamics* **1975**, 7, 21-26.
23. Orr, R. L. *J. Am. Chem. Soc.* **1953**, 75, 1231-1232.
24. Cheary, R.W.; Coelho, A. A. *Phys. Chem. Minerals* **1997**, 24, 447-454.
25. Gatehouse, G.M.; Grey, I.E.; Roderick, J.H.; Rossell, J.H. *Acta Cryst.* **1981**, B37, 306-312.
26. Molodetsky, I.; Navrotsky, A.; Lajavardi, M.; Brune, A. *Z. Phys. Chem.* **1998**, 207, 59-65.

## 27. Figure Legends:

FIGURE 1. The standard molar enthalpy of reaction from the binary oxides  $\Delta_r H_m^o(1)$  as a function of  $\text{CaHfTi}_2\text{O}_7(\text{cr})$  content,  $X_{\text{Hf}}$ , in the solid solution series:  $\text{CaZr}_x\text{Hf}_{(1-x)}\text{Ti}_2\text{O}_7(\text{cr})$  ( $X=0, 0.74,$  and  $1$ ). The solid line and filled symbols are the measured values of  $\Delta_r H_m^o(1) / \text{kJ}\cdot\text{mol}^{-1}$  and the dashed line and open symbols are calculated based on an ideal mixing model where  $\Delta_{\text{mix}} H_m = 0 \text{ kJ}\cdot\text{mol}^{-1}$ .

FIGURE 2. The enthalpy of mixing,  $\Delta_{\text{mix}} H_m$ , as a function of  $\text{CaHfTi}_2\text{O}_7(\text{cr})$  content,  $X_{\text{Hf}}$ , in the solid solution series:  $\text{CaZr}_x\text{Hf}_{(1-x)}\text{Ti}_2\text{O}_7(\text{cr})$  ( $X=0, 0.74,$  and  $1$ ). The solid line and filled symbols are the measured values of  $\Delta_{\text{mix}} H_m$  and the dashed line and open symbols are calculated based on an ideal solution model. At  $X=1$  and  $0$  the filled and open symbols overlap.

TABLE 1. Measured enthalpy of drop solution,  $\Delta_{298.15K}^T H_m(sol)$ , experiments on  $HfO_2(cr)$  ( $M=210.45 \text{ g}\cdot\text{mol}^{-1}$ ) and  $(0.0637 \text{ CaTiO}_3 + 0.9363 \text{ CaZr}_{0.24}\text{Hf}_{0.26}\text{Ti}_2\text{O}_7)(cr)$  ( $M= 403.4726 \text{ g}\cdot\text{mol}^{-1}$ ). Calorimeter temperature was  $T = 973 \text{ K}$  and the solvent is lead borate ( $2\text{PbO}\cdot\text{B}_2\text{O}_3$ ) (vit). Errors reported are twice the standard deviation of the mean;  $m$  denotes the mass of the sample.

\*  $HfO_2$  sample pellets were a mechanical mixture of  $HfO_2(cr)$  (75.83 mg) and lead borate solvent (155.91 mg). Results have been corrected for the presence of lead borate.

\*\*  $(0.0637 \text{ CaTiO}_3 + 0.9363 \text{ CaZr}_{0.24}\text{Hf}_{0.26}\text{Ti}_2\text{O}_7)$  sample pellets were a mechanical mixture of  $(0.0637 \text{ CaTiO}_3 + 0.9363 \text{ CaZr}_{0.26}\text{Hf}_{0.74}\text{Ti}_2\text{O}_7)(cr)$  (202.55 mg) and lead borate solvent (563.37 mg). Results have been corrected for the presence of lead borate.

$HfO_2$ *		$(0.0637 \text{ CaTiO}_3 + 0.9363 \text{ CaZr}_{0.26}\text{Hf}_{0.74}\text{Ti}_2\text{O}_7)$ **	
$m / \text{mg}$	$\Delta_{298.15K}^T H_m(sol) / \text{kJ}\cdot\text{mol}^{-1}$	$m / \text{mg}$	$\Delta_{298.15K}^T H_m(sol) / \text{kJ}\cdot\text{mol}^{-1}$
5.87	58.70	8.50	267.6
6.31	54.22	9.05	255.7
6.79	60.23		
6.80	53.78		
7.27	53.99		
7.32	56.02		
7.43	53.90		
7.72	61.40		
7.72	55.67		

$$\begin{aligned} <\Delta_{298.15K}^T H_m(sol)> / \text{kJ}\cdot\text{mol}^{-1} \\ = 56.43 \pm 1.96 \end{aligned}$$

$$\begin{aligned} <\Delta_{298.15K}^T H_m(sol)> / \text{kJ}\cdot\text{mol}^{-1} \\ = 261.6 \pm 11.9 \end{aligned}$$

$$\begin{aligned} <\Delta_{298.15K}^T H_m(sol)> / \text{kJ}\cdot\text{mol}^{-1} \\ = 267.87 \pm 11.9^a \end{aligned}$$

<sup>a</sup> Corrected for the presence of perovskite,  $\text{CaTiO}_3(cr)$ . Value represents the thermodynamic quantity for  $\text{CaZr}_{0.26}\text{Hf}_{0.74}\text{Ti}_2\text{O}_7(cr)$ .

TABLE 2. Measured enthalpy of drop solution (DS),  $\Delta_{298.15K}^T H_m(sol)$ , and transposed temperature drop (TTD),  $\Delta_{298.15K}^T H_m$ , experiments on  $\text{CaHfTi}_2\text{O}_7(\text{cr})$  (Sample A) ( $M=426.3658 \text{ g}\cdot\text{mol}^{-1}$ ). Calorimeter temperatures were  $T=973 \text{ K}$  and  $T=1073 \text{ K}$  as noted. The solvent is lead borate ( $2\text{PbO}\cdot\text{B}_2\text{O}_3$ ) (vit). Errors reported are twice the standard deviation of the mean;  $m$  denotes the mass of the sample.

\*  $\text{CaHfTi}_2\text{O}_7$  sample pellets for DS experiments were a mechanical mixture of  $\text{CaHfTi}_2\text{O}_7(\text{cr})$  (556.05 mg) and lead borate solvent (1106.91 mg). Results have been corrected for the presence of lead borate.

$\text{CaHfTi}_2\text{O}_7$ *		$\text{CaHfTi}_2\text{O}_7(\text{cr})$		$\text{CaHfTi}_2\text{O}_7(\text{cr})$	
$T=973 \text{ K}$		$T=973 \text{ K}$		$T=1073 \text{ K}$	
$m / \text{mg}$	$\Delta_{298.15K}^T H_m(sol) / \text{kJ}\cdot\text{mol}^{-1}$	$m / \text{mg}$	$\Delta_{298.15K}^T H_m / \text{kJ}\cdot\text{mol}^{-1}$	$m / \text{mg}$	$\Delta_{298.15K}^T H_m / \text{kJ}\cdot\text{mol}^{-1}$
13.40	262.00	17.23	161.63	21.45	190.47
15.27	256.47	17.57	168.30	22.00	196.48
15.53	262.22	17.91	170.01	26.30	195.03
15.56	266.96	18.89	168.49	29.03	197.47
16.18	259.58	19.58	163.12	29.09	201.15
		20.86	167.17	33.37	199.77
		24.20	167.91	42.30	196.62
		29.06	167.99	45.50	203.78
		42.73	167.34	47.57	205.72
$\langle \Delta_{298.15K}^T H_m(sol) \rangle / \text{kJ}\cdot\text{mol}^{-1}$		$\langle \Delta_{298.15K}^T H_m \rangle / \text{kJ}\cdot\text{mol}^{-1}$		$\langle \Delta_{298.15K}^T H_m \rangle / \text{kJ}\cdot\text{mol}^{-1}$	
$= 261.44 \pm 3.45$		$= 166.88 \pm 1.80$		$= 198.49 \pm 3.10$	

TABLE 3. Calculation of  $\Delta_f H_m^\circ$  and  $\Delta_r H_m^\circ$  of  $\text{CaHfTi}_2\text{O}_7(\text{cr})$  ( $M=426.3658 \text{ g}\cdot\text{mol}^{-1}$ ),  $T'=298.15 \text{ K}$  and  $T=973 \text{ K}$ . Reaction (10) is the sum of reactions (1) through (6) and reaction (11) is the sum of reactions (1) through (9). Solvent was lead borate,  $2\text{PbO}\cdot\text{B}_2\text{O}_3$  (vit).

Reaction	$\Delta_r H_m^\circ / \text{kJ}\cdot\text{mol}^{-1}$
1. $\text{CaO}(\text{sol}, T) + \text{HfO}_2(\text{sol}, T) + 2 \text{TiO}_2(\text{sol}, T) = \text{CaHfTi}_2\text{O}_7(\text{cr}, T')$	- 261.44 $\pm$ 3.45
2. $\text{HfO}_2(\text{cr}, T') = \text{HfO}_2(\text{sol}, T)$	56.43 $\pm$ 1.96
3. $2 \{ \text{TiO}_2(\text{cr}, T') = \text{TiO}_2(\text{sol}, T) \}$	2 (55.4 $\pm$ 0.82) <sup>a</sup>
4. $\text{CaO}(\text{cr}, T') + \text{CO}_2(\text{g}, T') = \text{CaCO}_3(\text{cr}, T')$	- 178.8 $\pm$ 1.0 <sup>b</sup>
5. $\text{CO}_2(\text{g}, T) = \text{CO}_2(\text{g}, T')$	-31.96 <sup>b</sup>
6. $\text{CaCO}_3(\text{cr}, T') = \text{CaO}(\text{sol}, T) + \text{CO}_2(\text{g}, T)$	193.4 $\pm$ 0.70 <sup>c</sup>
7. $\text{Ca}(\text{cr}, T') + \frac{1}{2} \text{O}_2(\text{g}, T') = \text{CaO}(\text{cr}, T')$	-635.1 $\pm$ 0.9 <sup>b</sup>
8. $\text{Hf}(\text{cr}, T') + \text{O}_2(\text{g}, T') = \text{HfO}_2(\text{cr}, T')$	-1117.6 $\pm$ 1.3 <sup>b</sup>
9. $2 \{ \text{Ti}(\text{cr}, T') + \text{O}_2(\text{g}, T') = \text{TiO}_2(\text{cr}, T') \}$	2 ( - 944.0 $\pm$ 0.8) <sup>b</sup>
10. $\text{CaO}(\text{cr}, T') + \text{HfO}_2(\text{cr}, T') + 2 \text{TiO}_2(\text{cr}, T') = \text{CaHfTi}_2\text{O}_7(\text{cr}, T')$	$\Delta_r H_m^\circ = - ( 111.57 \pm 4.46 ) / \text{kJ}\cdot\text{mol}^{-1}$
11. $\text{Ca}(\text{cr}, T') + \text{Hf}(\text{cr}, T') + \text{Ti}(\text{cr}, T') + 7/2 \text{O}_2(\text{g}, T') = \text{CaHfTi}_2\text{O}_7(\text{cr}, T')$	$\Delta_f H_m^\circ = - ( 3752.27 \pm 4.99 ) / \text{kJ}\cdot\text{mol}^{-1}$

<sup>a</sup> Taken from reference 5.

<sup>b</sup> Taken from reference 17.

<sup>c</sup> Taken from reference 18.

TABLE 4. The molar heat capacity  $C_{p,m}$ , third law entropy  $\Delta_0^T S_m^o$ , standard molar enthalpy of formation from the elements  $\Delta_f^T H_m^o$  and standard molar Gibbs free energies of formation  $\Delta_f^T G_m^o$  for CaHfTi<sub>2</sub>O<sub>7</sub> (cr) (Part A), HfO<sub>2</sub> (cr) (Part B), and corrected values for CaZrTi<sub>2</sub>O<sub>7</sub> (cr) (Part C). Part C replaces Table 7 in reference 5. Heat capacities and entropies for HfO<sub>2</sub> (cr) have previously been tabulated incorrectly in reference 20 using  $C_{p,m}$  data from reference 23 and an incorrect  $\Delta_f H_m^o$  as noted in the text of this report. Heat capacities and entropies for CaHfTi<sub>2</sub>O<sub>7</sub> (cr) and Zr<sub>0.24</sub>Hf<sub>0.26</sub>Ti<sub>2</sub>O<sub>7</sub> (cr) are taken from reference 15.

Part A

CaHfTi<sub>2</sub>O<sub>7</sub> (cr)

T / K	$C_{p,m} / \text{J}\cdot\text{K}^{-1}\cdot\text{mol}^{-1}$	$\Delta_0^T S_m^o / \text{J}\cdot\text{K}^{-1}\cdot\text{mol}^{-1}$	$\Delta_f^T H_m^o / \text{kJ}\cdot\text{mol}^{-1}$	$\Delta_f^T G_m^o / \text{kJ}\cdot\text{mol}^{-1}$
0	0.0	2.882	- 3733.74	- 3733.74
100	74.5	42.9	- 3744.36	- 3682.97
200	160.4	123.4	- 3750.84	- 3618.58
298.15	207.0	197.0	- 3752.27	- 3552.81
300	207.7	198.3	- 3752.25	- 3551.57
400	233.7	261.8	- 3750.92	- 3484.80
500	251.5	316.0	- 3748.33	- 3418.63
600	265.3	363.1	- 3745.09	- 3353.19
700	277.1	404.9	- 3741.23	- 3288.51
800	287.7	442.6	- 3737.87	- 3224.01
900	297.6	477.1	- 3733.29	- 3160.36
1000	307.1	508.9	- 3728.58	- 3097.22
1100	316.3	538.7	- 3723.71	- 3034.56
1200	325.3	566.6	- 3734.49	- 2971.32
1300	334.2	593.0	- 3726.77	- 2907.99
1400	343.0	618.0	- 3718.44	- 2845.06
1500	351.7	642.0	- 3709.43	- 2782.78

Table 4 (cont.)

Part B

HfO<sub>2</sub>(cr)

T / K	$C_{p,m} / \text{J}\cdot\text{K}^{-1}\cdot\text{mol}^{-1}$	$\Delta_0^T S_m^\circ / \text{J}\cdot\text{K}^{-1}\cdot\text{mol}^{-1}$	$\Delta_f^T H_m^\circ / \text{kJ}\cdot\text{mol}^{-1}$	$\Delta_f^T G_m^\circ / \text{kJ}\cdot\text{mol}^{-1}$
298.15	60.25	59.33	- 1117.6	- 1060.8
400	66.91	78.06	- 1116.8	- 1042.0
500	70.94	93.45	- 1115.6	- 1023.3
600	73.77	106.65	- 1114.4	- 1005.0
700	75.93	118.19	- 1113.1	- 986.9
800	77.65	128.45	- 1111.7	- 969.0
900	79.09	137.68	- 1110.3	- 951.2
1000	80.32	146.08	- 1109.0	- 933.6
1100	81.39	153.78	- 1107.6	- 916.2
1200	82.35	160.91	- 1106.3	- 898.8
1300	83.21	167.53	- 1105.0	- 881.6
1400	83.99	173.73	- 1103.7	- 864.4
1500	84.72	179.55	- 1102.5	- 847.4
1600	85.39	185.04	- 1101.3	- 830.4
1700	86.02	190.23	- 1100.1	- 813.5
1800	86.61	195.17	- 1096.9	- 794.7

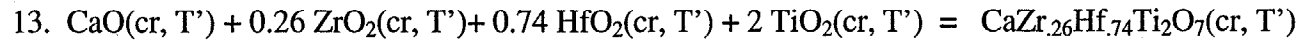
## Part C

CaZrTi<sub>2</sub>O<sub>7</sub> (cr)

T / K	$C_{p,m} / \text{J}\cdot\text{K}^{-1}\cdot\text{mol}^{-1}$	$\Delta_0^T S_m^\circ / \text{J}\cdot\text{K}^{-1}\cdot\text{mol}^{-1}$	$\Delta_f^T H_m^\circ / \text{kJ}\cdot\text{mol}^{-1}$	$\Delta_f^T G_m^\circ / \text{kJ}\cdot\text{mol}^{-1}$
0	0.0	2.882	-3695.9	-3695.9
100	73.7	39.5	-3706.5	-3645.1
200	163.8	120.7	-3712.8	-3580.9
298.15	211.9	196.2	-3713.7	-3515.6
300	212.6	197.5	-3713.7	-3514.4
400	238.9	262.6	-3711.8	-3447.5
500	255.5	317.8	-3708.6	-3381.4
600	267.7	365.5	-3704.8	-3315.9
700	278.0	407.5	-3700.5	-3251.3
800	287.4	445.3	-3696.8	-3187.2
900	296.4	479.6	-3692.0	-3124.0
1000	305.5	511.3	-3687.2	-3061.2
1100	314.7	540.9	-3682.4	-2999.2
1200	324.3	568.7	-3696.9	-2936.2
1300	334.2	595.0	-3688.9	-2873.2
1400	344.6	620.2	-3680.1	-2810.6
1500	355.4	644.3	-3670.7	-2748.6

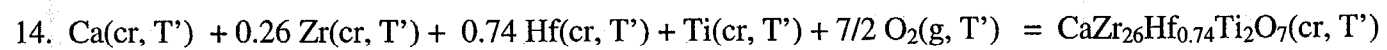
TABLE 5: Calculation of  $\Delta_f H_m^\circ$  and  $\Delta_r H_m^\circ$  for zirconolite solid solution of the composition  $\text{CaZr}_{.26}\text{Hf}_{.74}\text{Ti}_2\text{O}_7(\text{cr})$ ,  $T' = 298.15 \text{ K}$  and  $T = 973 \text{ K}$ . Reaction (13) is the sum of reactions (1) through (8) and reaction (14) is the sum of reactions (1) through (12). Solvent was lead borate,  $2\text{PbO} \cdot \text{B}_2\text{O}_3$  (vit).

Reaction	$\Delta_r H_m^\circ / \text{kJ} \cdot \text{mol}^{-1}$
1. $\text{CaO}(\text{sol}, T) + 0.26 \text{ZrO}_2(\text{sol}, T) + 0.74 \text{HfO}_2(\text{sol}, T) + 2 \text{TiO}_2(\text{sol}, T) = \text{CaZr}_{.26}\text{Hf}_{.74}\text{Ti}_2\text{O}_7(\text{cr}, T')$	$-\Delta_{298.15\text{K}}^T H_m^\circ(\text{sol})(\text{CaZr}_{.26}\text{Hf}_{.74}\text{Ti}_2\text{O}_7)$
2. $(1-X)\{\text{HfO}_2(\text{cr}, T') = \text{HfO}_2(\text{sol}, T)\}$	0.74 (56.43 $\pm$ 1.96)
3. $0.26 \{\text{ZrO}_2(\text{cr}, T) = \text{ZrO}_2(\text{sol}, T)\}$	0.26 (24.25 $\pm$ 0.71) <sup>a</sup>
4. $0.26 \{\text{ZrO}_2(\text{cr}, T') = \text{ZrO}_2(\text{cr}, T)\}$	0.26 (45.29 $\pm$ 0.73) <sup>a</sup>
5. $2 \{\text{TiO}_2(\text{cr}, T') = \text{TiO}_2(\text{sol}, T)\}$	2 (55.4 $\pm$ 0.82) <sup>b</sup>
6. $\text{CaO}(\text{cr}, T') + \text{CO}_2(\text{g}, T') = \text{CaCO}_3(\text{cr}, T')$	-178.8 $\pm$ 1.0 <sup>c</sup>
7. $\text{CO}_2(\text{g}, T) = \text{CO}_2(\text{g}, T')$	-31.96 <sup>c</sup>
8. $\text{CaCO}_3(\text{cr}, T') = \text{CaO}(\text{sol}, T) + \text{CO}_2(\text{g}, T)$	193.4 $\pm$ 0.70 <sup>d</sup>
9. $\text{Ca}(\text{cr}, T') + \frac{1}{2} \text{O}_2(\text{g}, T') = \text{CaO}(\text{cr}, T')$	-635.1 $\pm$ 0.9 <sup>c</sup>
10. $0.74 \{\text{Hf}(\text{cr}, T') + \text{O}_2(\text{g}, T') = \text{HfO}_2(\text{cr}, T')\}$	0.74 (-1117.6 $\pm$ 1.3) <sup>c</sup>
11. $0.26 \{\text{Zr}(\text{cr}, T') + \text{O}_2(\text{g}, T') = \text{ZrO}_2(\text{cr}, T')\}$	0.26 (-1100.3 $\pm$ 0.7) <sup>c</sup>
12. $2\{\text{Ti}(\text{cr}, T') + \text{O}_2(\text{g}, T') = \text{TiO}_2(\text{cr}, T')\}$	2 (-944.0 $\pm$ 0.8) <sup>c</sup>



$$\Delta_r H_m^\circ (\text{CaZr}_{.26}\text{Hf}_{.74}\text{Ti}_2\text{O}_7) = - (118.3 \pm 12.1) / \text{kJ} \cdot \text{mol}^{-1}$$

TABLE 5 continued.



$$\Delta_f H_m^\circ (\text{CaZr}_{26}\text{Hf}_{0.74}\text{Ti}_2\text{O}_7) = - (3754.5 \pm 12.3) / \text{kJ}\cdot\text{mol}^{-1}$$

<sup>a</sup> Taken from reference 26.

<sup>b</sup> Taken from reference 5.

<sup>c</sup> Taken from reference 17.

<sup>d</sup> Taken from reference 18.

Figure 1

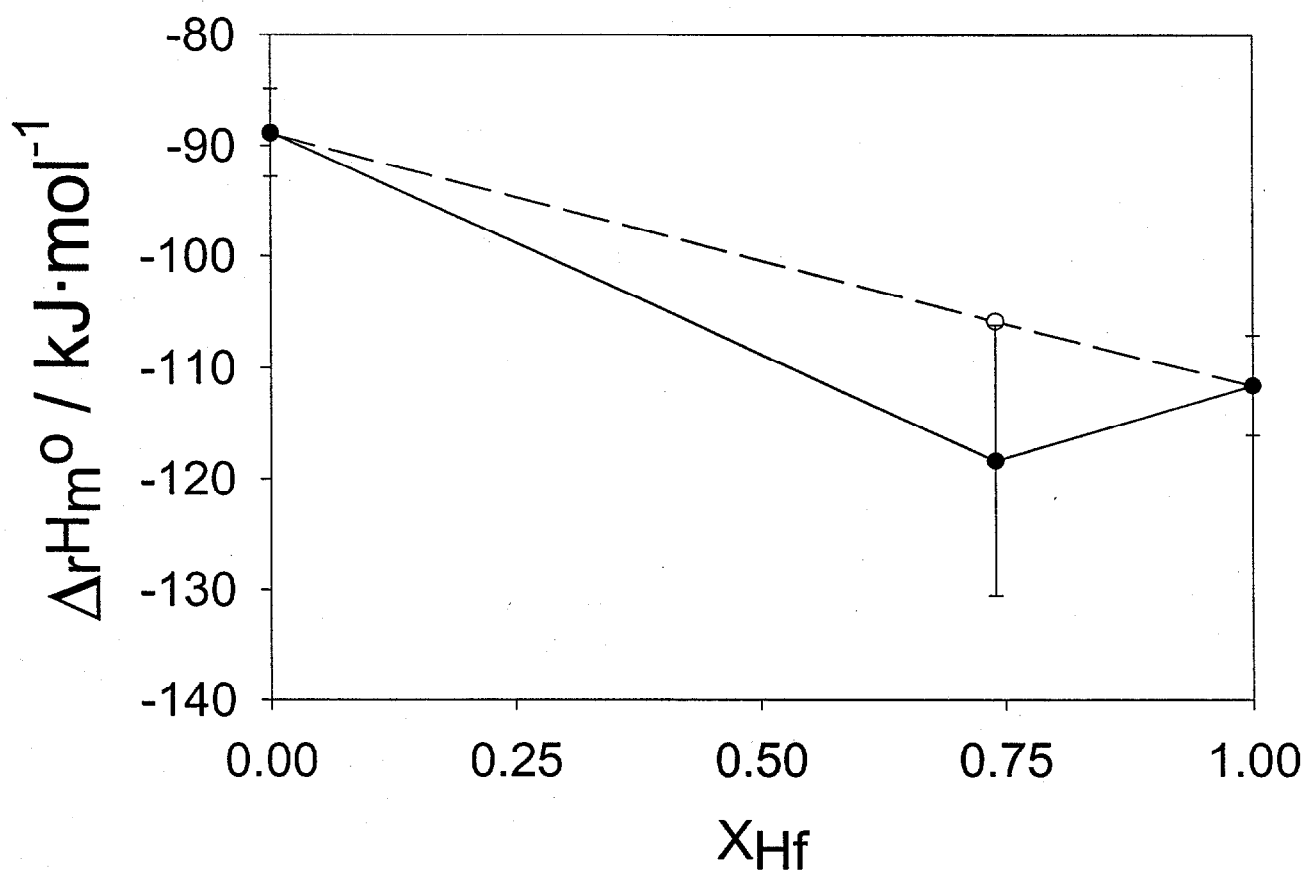
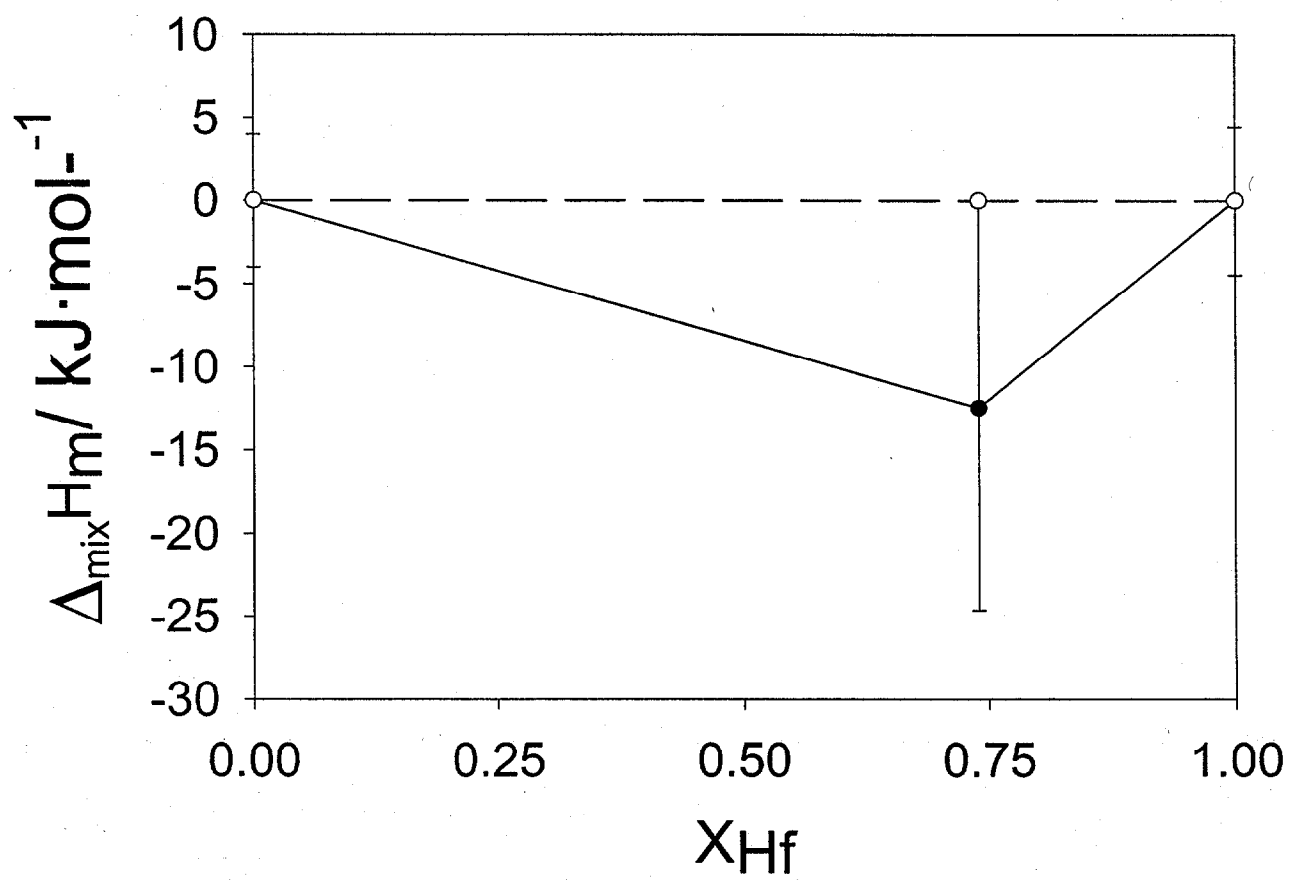


Figure 2



**The Molar Heat Capacity and Thermodynamic Functions of  $\text{CaHfTi}_2\text{O}_7(\text{cr})$  and the Solid Solution  $\text{CaZr}_{0.26}\text{Hf}_{0.74}\text{Ti}_2\text{O}_7(\text{cr})$ ; New Values for the Entropy of  $\text{CaZrTi}_2\text{O}_7(\text{cr})$ .**

Rebecca Stevens, Benjamin K. Hom, Juliana Boerio-Goates, and Brian F. Woodfield<sup>1</sup>  
Brigham Young University, Department of Chemistry and Biochemistry, Provo, UT 84602  
U.S.A.

Robert L. Putnam,<sup>2</sup> Jose Gutierrez, and Alexandra Navrotsky  
University of California, Davis; Thermochemistry Facility, Department of Chemical Engineering  
and Materials Science, 4440 Chemistry Annex, Davis, CA 95616 U.S.A.

---

<sup>1</sup> To whom correspondence should be addressed  
E-mail: Brian\_Woodfield@byu.edu

<sup>2</sup> Current Address: Los Alamos National Laboratory, NMT-16; MS – G721; Los Alamos, NM  
87545

## Abstract

As part of an ongoing study of titanate-based ceramic materials for the disposal of surplus weapons plutonium, we report the molar heat capacities and thermodynamic functions for the zirconolite ( $\text{CaZrTi}_2\text{O}_7$ ) analogue Hf-zirconolite ( $\text{CaHfTi}_2\text{O}_7$ ) and a solid solution of the two,  $\text{CaZr}_{0.26}\text{Hf}_{0.74}\text{Ti}_2\text{O}_7$ . Measurements have been made on the solid solution to probe the extent zirconolite/Hf-zirconolite mixtures form ideal solutions. The molar heat capacity for both samples was measured from  $T = 13$  K to  $T = 400$  K in an adiabatic calorimeter and extrapolated to  $T = 1500$  K using an equation fitted to the low-temperature results. The results at  $T = 298.15$  K are  $\Delta_0^{298.15\text{K}} S_m^\circ = (196.98 \pm 0.39) \text{ J} \cdot \text{K}^{-1} \cdot \text{mol}^{-1}$  for  $\text{CaHfTi}_2\text{O}_7$  and  $\Delta_0^{298.15\text{K}} S_m^\circ = (199.76 \pm 0.39) \text{ J} \cdot \text{K}^{-1} \cdot \text{mol}^{-1}$  for the mixture  $\text{CaZr}_{0.26}\text{Hf}_{0.74}\text{Ti}_2\text{O}_7$ . Recent crystallographic data on zirconolite established the existence of disorder at the Ti(2) site which results in a zero-point entropy contribution of  $\frac{1}{2}R \ln 2$  not previously included in the thermodynamic tabulation for zirconolite. The molar entropies of  $\text{CaHfTi}_2\text{O}_7$  and  $\text{CaZr}_{0.26}\text{Hf}_{0.74}\text{Ti}_2\text{O}_7$  reported here include this zero-point entropy of  $\frac{1}{2}R \ln 2$ , and the solid solution includes an additional zero-point entropy contribution of  $4.765 \text{ J} \cdot \text{K}^{-1} \cdot \text{mol}^{-1}$  to account for the random mixing of  $\text{Zr}^{4+}$  and  $\text{Hf}^{4+}$  on the zirconium crystallographic site. The large zero-point entropy associated with the solid solution implies a substantial entropy stabilization contribution for other nuclear waste disposition mixtures.

KEYWORDS:  $\text{CaHfTi}_2\text{O}_7$ ,  $\text{CaZrTi}_2\text{O}_7$ , zirconolite, solid solution, heat capacity, entropy, thermodynamics, enthalpy

## 1. Introduction

Titanate-based compounds are being considered as a ceramic host matrix for the disposal of surplus nuclear weapons material.<sup>(1,2)</sup> Among the phases found in these ceramics is zirconolite ( $\text{CaZrTi}_2\text{O}_7$ ).<sup>(3-5)</sup> Important to the development, performance modeling, and optimization of a nuclear waste host is an understanding of the formation energetics of the phases that comprise the waste material.<sup>(5,6)</sup> Hf-zirconolite,  $\text{CaHfTi}_2\text{O}_7$ , is another important end-member of the proposed host material for excess plutonium and uranium but for which no thermodynamic data have been reported.

An ability to accurately predict the thermodynamic properties of various mixtures in the nuclear waste host phase without resorting to experimental measurements would make an important contribution to the modeling and optimization efforts in the plutonium and uranium disposition program. Hf-zirconolite is isostructural with zirconolite and would be expected to form a nearly ideal solution upon mixing. Heat capacity measurements on a solid solution of zirconolite and Hf-zirconolite would provide an important test for the feasibility of predicting the thermodynamic functions for some mixtures and provide an estimate of the potential uncertainties.

As part of an ongoing multi-laboratory collaboration, we have performed heat capacity measurements on  $\text{CaHfTi}_2\text{O}_7$  and on the solid solution  $\text{CaZr}_{0.26}\text{Hf}_{0.74}\text{Ti}_2\text{O}_7$  from  $T = 13$  K to  $T = 400$  K in order to determine the third-law entropy and enthalpy increments of the pure Hf-zirconolite and of the solid solution. Using a six-parameter fitting equation<sup>(4,7-9)</sup> the heat capacities and thermodynamic functions have been extrapolated to  $T = 1500$  K. The formation energetics will be reported separately.<sup>(10)</sup> The results show that the predicted entropy at  $T = 298.15$  K for the solid solution is high by 0.9 per cent of the measured value, and the zero-point

entropy of the mixture makes a substantial stabilization contribution implying the zero-point entropy for other mixtures in the plutonium disposition program will also have large stabilizing effects.

## 2. Experimental

The sample of  $\text{CaHfTi}_2\text{O}_7$  was synthesized from  $\text{CaCO}_3$  (Alpha Aesar),<sup>(11)</sup>  $\text{TiO}_2$  (cr, anatase) (Alpha Aesar, mass fraction > 0.9999),<sup>(11)</sup> and  $\text{HfO}_2$  (Alpha Aesar, mass fraction > 0.999).<sup>(11)</sup> Reactants were ground in a high density alumina mortar under ethanol, dried, and then sintered three times for 24, 48, and 96 h at  $T = 1573$  K in platinum crucibles. Between sinterings the samples were ground under ethanol in an alumina mortar. The resulting material was confirmed to be  $\text{CaHfTi}_2\text{O}_7$  with the zirconolite structure using powder X-ray diffraction. The solid solution,  $\text{CaZr}_{0.24}\text{Hf}_{0.76}\text{Ti}_2\text{O}_7$ , was synthesized using the same procedure but with the addition of  $\text{ZrO}_2$  (cr, baddeleyite) (Alpha Aesar, mass fraction > 0.999)<sup>(11)</sup> as a reactant. The zirconolite structure was also confirmed through powder X-ray diffraction.

The compositions of the Hf-zirconolite sample and the solid solution were verified using a Cameca SX-50 electron micro probe. The micro probe analysis revealed that both the Hf-zirconolite and the solid solution contained small amounts of perovskite,  $\text{CaTiO}_3$ . The presence of perovskite in synthetic samples of zirconolite has been reported previously,<sup>(12)</sup> and we have treated the perovskite as though it were present as a mechanical mixture with the phase of interest.<sup>(5,13)</sup> The composition of the two samples was determined to be  $(0.0684 \text{ CaTiO}_3 + 0.9315 \text{ CaHfTi}_2\text{O}_7)$  and  $(0.0637 \text{ CaTiO}_3 + 0.9363 \text{ CaZr}_{0.26}\text{Hf}_{0.74}\text{Ti}_2\text{O}_7)$  using energy dispersive spectroscopy (EDS) on the Cameca SX-50 and analyzing for the presence of Ca, Zr, Hf, Ti, and Al (from the grinding media). No aluminum was found to be present above the instrument background. Compositions were derived from the values of metals measured (Ca, Zr, Hf, Ti, and

Al) as a function of total metal concentration and represent the mean stoichiometry of the materials studied.

The heat capacity measurements were made using an adiabatic calorimeter; details of the apparatus have been published previously.<sup>(4,7,14,15)</sup> The mass of the  $\text{CaHfTi}_2\text{O}_7$  sample was 9.6612 g, corrected for buoyancy and for the  $\text{CaTiO}_3$  impurity, and the mass for the  $\text{CaZr}_{0.26}\text{Hf}_{0.74}\text{Ti}_2\text{O}_7$  sample was 11.0367 g, also corrected for buoyancy and the  $\text{CaTiO}_3$  impurity. Temperatures were measured using a Rosemont 25- $\Omega$  capsule thermometer calibrated on the ITS-90 temperature scale. The thermometer calibration provided by the company began at  $T = 13.8$  K, so our measurements were limited to temperatures above that minimum.

Measurements have been made on a standard sample of synthetic sapphire (NIST-SRM 720) to gauge the accuracy of our heat capacity results. Molar heat capacities calculated from a fit of our experimental results on sapphire have been compared to the smoothed values reported in Table 2 of Archer.<sup>(16)</sup> Our results on sapphire were found to be high by 2 percent at  $T = 15$  K, but they dropped systematically with increasing temperature to  $T = 50$  K. They were within  $\pm 0.15$  per cent for  $50 \leq T / \text{K} \leq 400$ .

### 3. Results

The experimental molar heat capacities, corrected for the heat capacities of the empty calorimeter, gold gasket, helium exchange gas, and the  $\text{CaTiO}_3$  impurity are listed in chronological order in Table 1 for  $\text{CaHfTi}_2\text{O}_7$  and in Table 2 for  $\text{CaZr}_{0.26}\text{Hf}_{0.74}\text{Ti}_2\text{O}_7$ . Both sets of data are displayed graphically in Figure 1, and the heat capacities below  $T = 50$  K are shown on an expanded scale in inset (a) of Figure 1. Corrections for curvature were made using conventional procedures, and the heat capacity contribution of the  $\text{CaTiO}_3$  impurity was taken

from Woodfield *et al.*<sup>(8)</sup> The contribution of both samples to the total heat capacity ranged from approximately 10 per cent at the lowest temperature to 25 per cent at the highest temperature.

#### 4. Discussion

In order to calculate the thermodynamic functions of  $\text{CaHfTi}_2\text{O}_7$  and  $\text{CaZr}_{0.26}\text{Hf}_{0.74}\text{Ti}_2\text{O}_7$ , it is necessary to fit the experimental heat capacities to a function that represents the results to within the experimental uncertainty. Recently, a function of the form

$$C_{p,m}^{\circ} = 3R \cdot \{m \cdot D(\theta_D/T) + n \cdot E(\theta_E/T)\} + A_1 \cdot (T/K) + A_2 \cdot (T/K)^2 \quad (1)$$

where  $D(\theta_D/T)$  and  $E(\theta_E/T)$  are Debye and Einstein functions, respectively, and the  $T$ - and  $T^2$ - terms represent an approximation to  $C_p - C_v$ , has been found to fit the heat capacity of  $\text{CaZrTi}_2\text{O}_7$  from  $T = 20$  K to  $T = 400$  K.<sup>(4)</sup> Equation (1) can represent the lattice heat capacity over a wide temperature interval using a small number of adjustable parameters, and it does not show the oscillations that may be associated with higher-order polynomial fits. More importantly, this function can be extrapolated beyond the experimental temperatures used to obtain it. However, the  $T$ - and  $T^2$ - terms, which are necessary to fit the high temperature data, cause a systematic deviation below  $T = 20$  K. An alternate equation must be used to represent the lattice heat capacity at low temperatures. We have found an acceptable equation to be the low-temperature expansion of the Debye function in the form

$$C_{v,m}^{\circ} = B_3 T^3 + B_5 T^5 + B_7 T^7 + \dots \quad (2)$$

where the required number of terms depends upon the upper temperature to which one wants to fit the data. We have combined the two equations into a single equation that can be fit in one process by the addition of a switching function,  $S$ , which turns off equation (1) and turns on equation (2).  $S$  has the form

$$S = 0.5 \cdot [1 - \tanh\{\alpha(T - T_S)\}], \quad (3)$$

where  $\alpha$  controls the sharpness with which one function is switched off and the other brought in at  $T = T_S$ . The equation used to fit the experimental heat capacity results is

$$C_{p,m}^{\circ} = S \cdot (B_3 T^3 + B_5 T^5 + B_7 T^7 + B_9 T^9 + B_{11} T^{11}) + (1 - S) \cdot [3R \cdot \{m \cdot D(\theta_D/T) + n \cdot E(\theta_E/T)\} + A_1 \cdot (T/K) + A_2 \cdot (T/K)^2] \quad (4)$$

This equation has been used successfully to fit the heat capacities of  $\text{CaTiO}_3$  and  $\text{ZrTiO}_4$ <sup>(8,9)</sup> to within the experimental error; however, in the case of  $\text{CaHfTi}_2\text{O}_7$  and  $\text{CaZr}_{0.26}\text{Hf}_{0.74}\text{Ti}_2\text{O}_7$  there was a small systematic deviation in the vicinity of  $T = 100$  K that could not be eliminated using various fitting conditions. Consequently, we have elected to fit our experimental heat capacities to orthogonal polynomials from  $T = 14$  K to  $T = 400$  K and have used the fit of the data to equation (4) for the low- and high-temperature extrapolations. The deviations from the orthogonal polynomial fits are generally within  $\pm 1$  per cent below  $T = 30$  K with a maximum deviation of 3 per cent but improve to  $\pm 0.15$  per cent from  $T = 50$  K to  $T = 400$  K with a maximum deviation of 0.2 per cent for just a few points. Deviations of the fit using equation (4) are comparable above  $T = 150$  K. Parameters obtained for the best fit to equation (4) for both  $\text{CaHfTi}_2\text{O}_7$  and  $\text{CaZr}_{0.26}\text{Hf}_{0.74}\text{Ti}_2\text{O}_7$  are found in Table 3.

The smoothed heat capacities generated from the fit to equation (4) and the orthogonal polynomials for  $\text{CaHfTi}_2\text{O}_7$  and  $\text{CaZr}_{0.26}\text{Hf}_{0.74}\text{Ti}_2\text{O}_7$  are given in Tables 4 and 5, respectively. Thermodynamic functions for  $\text{CaHfTi}_2\text{O}_7$  and  $\text{CaZr}_{0.26}\text{Hf}_{0.74}\text{Ti}_2\text{O}_7$  were calculated by numerical integration of the smoothed heat capacity curve and are also given in Tables 4 and 5. Two crystallographic studies on zirconolite<sup>(12,17)</sup> have established the existence of disorder at the Ti(2) site in the zirconolite structure. Thus, a contribution of  $\frac{1}{2}R \ln 2$  was added to the entropy values derived from the heat capacity measurements for both  $\text{CaHfTi}_2\text{O}_7$  and  $\text{CaZr}_{0.26}\text{Hf}_{0.74}\text{Ti}_2\text{O}_7$ . This quantity has been calculated according to the procedures outlined by Ulbrich and

Waldbaum<sup>(18)</sup> using the crystallographic data of Rossell,<sup>(19)</sup> Gatehouse *et al.*,<sup>(17)</sup> and Cheary *et al.*<sup>(12)</sup> with eight molecules per unit cell, a fourfold multiplicity of the Ti(2) site at which the Ti positional disorder occurs, and equal probability of having the Ti cation placed to either side of the expected site. For  $\text{CaZr}_{0.26}\text{Hf}_{0.74}\text{Ti}_2\text{O}_7$  we have also included an additional zero-point entropy contribution of  $4.765 \text{ J} \cdot \text{K}^{-1} \cdot \text{mol}^{-1}$  because of random mixing of the Hf and Zr at the Zr site, using the same procedure of Ulbrich and Waldbaum,<sup>(18)</sup> for a total zero-point entropy for the solid solution of  $7.646 \text{ J} \cdot \text{K}^{-1} \cdot \text{mol}^{-1}$ . We estimate an uncertainty of  $\pm 0.39 \text{ J} \cdot \text{K}^{-1} \cdot \text{mol}^{-1}$  on the entropy at  $T = 298.15 \text{ K}$  based on the deviations noted earlier for the heat capacity measurements made on NIST-SRM 720 sapphire using the same apparatus and analysis. We neglect any uncertainty arising from the effects on the entropy of an incomplete disorder in the crystal.

The previously published values for the thermodynamic functions of  $\text{CaZrTi}_2\text{O}_7$ <sup>(4)</sup> were calculated assuming the absence of a zero-point entropy contribution. In light of the more recent crystallographic data on zirconolite<sup>(12)</sup> which establishes the presence of residual disorder in the crystal, the thermodynamic functions of  $\text{CaZrTi}_2\text{O}_7$  have been updated to include a zero-point entropy contribution of  $\frac{1}{2}R \ln 2$  and are given in Table 6. The zero-point entropy for the unsubstituted zirconolite and Hf-zirconolite and the larger zero-point entropy for the solid solution suggest that entropic considerations are important for the stability of these compounds and, by extension, for the proposed plutonium and uranium solid solutions.

To extend the thermodynamic functions to the higher temperatures that are of interest for synthetic applications, we have extrapolated our heat capacity results from  $T = 400 \text{ K}$  to  $T = 1500 \text{ K}$  with equation (4). The extrapolated values of  $C_{p,m}^\circ$ , shown in inset (b) of Figure 1, have been used to calculate thermodynamic functions in this temperature range. These extrapolated thermodynamic functions are reported in Tables 4 and 5 and are represented by italics to

distinguish them from the values obtained in the region where there is experimental data. The validity of the extrapolated heat capacity curve for  $\text{CaHfTi}_2\text{O}_7$  has been checked by comparing with two enthalpy increments obtained by transposed temperature drop experiments<sup>(5,8,10)</sup> performed with  $T' = 973$  K and  $T' = 1073$  K. Integration of the extrapolated heat capacity yields  $\Delta_{298.15\text{K}}^{973\text{K}} H_m = 179.34$  kJ·mol<sup>-1</sup> and  $\Delta_{298.15\text{K}}^{1073\text{K}} H_m = 210.27$  kJ·mol<sup>-1</sup>. The calculated results are 7.5 and 5.9 per cent high compared to the experimental values of 166.89 kJ·mol<sup>-1</sup> and 198.50 kJ·mol<sup>-1</sup>.<sup>(10)</sup> Considering that they are calculated at temperatures in excess of 500 K from the highest heat capacity measurements, we consider the agreement to be acceptable. The extrapolation for  $\text{CaZr}_{0.26}\text{Hf}_{0.74}\text{Ti}_2\text{O}_7$ , as shown in Figure 1, is seen to be similar to the extrapolation for  $\text{CaHfTi}_2\text{O}_7$  as expected.

Shown in Figure 2 is a comparison of the measured heat capacity ( $C_{\text{meas}}$ ) of  $\text{CaZr}_{0.26}\text{Hf}_{0.74}\text{Ti}_2\text{O}_7$  versus a heat capacity ( $C_{\text{calc}}$ ) calculated as a weighted sum of the pure components of the solid solution,  $\text{CaZrTi}_2\text{O}_7$  and  $\text{CaHfTi}_2\text{O}_7$ . As can be seen, the difference between the measured and calculated heat capacities is oscillatory and systematically low but only on the order of 1 per cent for temperatures above  $T = 50$  K. Below  $T = 50$  K, the deviations are considerably larger. These negative deviations of the measured versus the calculated heat capacities, especially below  $T = 50$  K, show that the lattice of the mixture is actually more tightly bound than an ideal solution would suggest. Furthermore, a comparison of the entropy of the mixture obtained by integrating the experimental data versus a calculated entropy obtained from the entropy values of  $\text{CaZrTi}_2\text{O}_7$  and  $\text{CaHfTi}_2\text{O}_7$  at  $T = 298.15$  K shows that the measured entropy is 0.9 per cent lower than the calculated entropy value. If the zero-point entropy contributions of the three solids are excluded, however, this difference between the experimental entropy and the calculated entropy of the mixture increases to 1.4 per cent which we feel is a

more accurate gauge of the error associated with an estimation of the thermodynamic values of mixtures.

Funding was provided by the United States Department of Energy grant number DE-FG07-97ER45673. B. K. Hom and R. Stevens gratefully acknowledge financial support from the Office of Research and Creative Activities (ORCA) of Brigham Young University.

## REFERENCES

1. Lutze, W.; Ewing, R.C. *Radioactive Waste Forms for the Future*; North Holland: New York, 1988.
2. Ewing, R.C.; Lutze, W.; Weber, W.J. *Disposal of Weapons Plutonium*; Kluwer: Netherlands, 1996.
3. Ewing, R.C.; Lutze, W.; Weber, W.J. *J. Mater. Res.* **1995**, *10*, 243-246.
4. Woodfield, B.F.; Boerio-Goates, J.; Shapiro, J.L.; Putnam, R.L.; Navrotsky, A. *J. Chem. Thermodyn.* **1999**, *31*, 245-253.
5. Putnam, R.L.; Navrotsky, A.; Woodfield, B.F.; Boerio-Goates, J.; Shapiro, J.L. *J. Chem. Thermodyn.* **1999**, *31*, 229-243.
6. Putnam, R.L., PhD Thesis, Princeton University, **1999**.
7. Shapiro, J.L.; Woodfield, B.F.; Stevens, R.; Boerio-Goates, J.; Wilson, M.L. *J. Chem. Thermodyn.* **1999**, *31*, 725-739.
8. Woodfield, B.F.; Shapiro, J.L.; Stevens, R.; Boerio-Goates, J. *J. Chem. Thermodyn.* **1999**, *31*, 1573-1583.
9. Hom, B.K.; Stevens, R.; Woodfield, B.F.; Boerio-Goates, J.; Putnam, R.L.; Helean, K.B.; Navrotsky, A. In Press *J. Chem. Thermodyn.* .
10. Putnam, R.L.; Gutierrez, J.; Navrotsky, A.; Hom, B.K.; Stevens, R.; Boerio-Goates, J.; Woodfield, B.F. Submitted to *J. Chem. Thermodyn.* .
11. Chemicals *Alfa Aesar*; Ward Hill: 30 Bond Street; Vol. MA.
12. Cheary, R.W.; Coelho, A.A. *Phys. Chem. Minerals* **1997**, *24*, 447-454.
13. Putnam, R.L.; Navrotsky, A.; Woodfield, B.F.; Shapiro, J.L.; Stevens, R.; Boerio-Goates, J. *Mat. Res. Soc. Proc.* **1999**, *556*, 11-18.
14. Boerio-Goates, J.; Woodfield, B.F. *Can. J. Chem.* **1988**, *66*, 645-650.
15. Battley, E.H.; Putnam, R.L.; Boerio-Goates, J. *Thermochim. Acta* **1997**, *298*, 37-46.
16. Archer, D.G. *J. Phys. Chem. Ref. Data* **1993**, *22*, 1441-1453.
17. Gatehouse, B.M.; Grey, I.E.; Roderick, J.H.; Rossell, H.J. *Acta Cryst.* **1981**, *B37*, 306-312.
18. Ulbrich, H.H.; Waldbaum, D.R. *Geochim. Cosmochim. Acta* **1976**, *40*, 1-24.

19. Rossell, H.J. *Nature* **1980**, 283, 282-283.

TABLE 1. Experimental molar heat capacity,  $C_{p,m}$ , of  $\text{CaHfTi}_2\text{O}_7$ . ( $M = 426.3238 \text{ g}\cdot\text{mol}^{-1}$ .)

$T$ K	$C_{p,m}$ $\text{J}\cdot\text{K}^{-1}\cdot\text{mol}^{-1}$	$T$ K	$C_{p,m}$ $\text{J}\cdot\text{K}^{-1}\cdot\text{mol}^{-1}$	$T$ K	$C_{p,m}$ $\text{J}\cdot\text{K}^{-1}\cdot\text{mol}^{-1}$
Series 1		123.63	98.54	261.80	192.81
		128.68	103.42	266.97	195.19
14.32	0.61	133.73	108.29	272.14	196.87
15.57	0.72	138.80	113.01	277.31	199.02
16.92	0.91	Series 4		282.48	201.21
18.37	1.36			287.65	203.22
19.97	1.90	136.67	111.02	292.82	205.12
21.72	2.63	141.66	115.47	297.98	206.77
23.67	3.03	146.74	120.02	Series 7	
28.11	5.51	151.82	124.44		
32.60	8.19	156.92	128.76	292.53	204.96
35.12	9.72	162.02	133.20	297.69	206.69
38.13	12.09	167.14	137.24	302.87	208.85
41.45	14.91	172.25	141.00	308.04	210.42
45.13	18.15	177.36	144.81	313.22	212.30
49.24	21.81	182.49	148.69	318.40	213.91
53.62	25.83	187.62	152.50	323.58	215.39
58.08	30.09	192.75	155.90	328.75	216.63
62.64	34.55	197.89	159.00	333.93	218.30
				339.10	219.83
Series 2		Series 5		344.28	220.89
				349.46	222.35
56.96	29.03	192.56	155.53		
62.90	34.92	197.69	158.96	Series 8	
67.44	39.55	202.83	162.14		
72.14	44.51	207.98	165.27	343.08	220.17
76.90	49.60	213.12	168.37	348.26	221.54
81.70	54.79	218.28	171.23	353.45	222.76
86.54	60.06	223.42	174.18	358.63	224.29
91.43	65.38	228.57	176.95	363.81	225.49
96.34	70.69	233.73	179.60	368.99	226.77
101.28	76.03	238.90	182.01	374.18	228.20
		244.06	184.41		
Series 3		249.22	186.90	Series 9	
93.85	67.78	Series 6		372.74	227.08
98.67	72.98			377.92	228.15
103.62	78.43	241.18	183.29	383.10	229.41
108.60	83.49	246.31	185.73	388.28	230.01
113.59	88.56	251.48	188.23	393.47	231.77
118.60	93.68	256.64	190.57	398.02	232.60

TABLE 2. Experimental molar heat capacity,  $C_{p,m}$ , of  $\text{CaZr}_{0.26}\text{Hf}_{0.74}\text{Ti}_2\text{O}_7$ . ( $M = 404.5073$  g·mol<sup>-1</sup>)

$\frac{T}{\text{K}}$	$\frac{C_{p,m}}{\text{J} \cdot \text{K}^{-1} \cdot \text{mol}^{-1}}$	$\frac{T}{\text{K}}$	$\frac{C_{p,m}}{\text{J} \cdot \text{K}^{-1} \cdot \text{mol}^{-1}}$	$\frac{T}{\text{K}}$	$\frac{C_{p,m}}{\text{J} \cdot \text{K}^{-1} \cdot \text{mol}^{-1}}$
Series 1		118.56	93.22	278.90	199.33
		123.59	97.97	284.07	201.76
14.42	0.44	128.63	102.94	289.24	203.72
15.26	0.65	133.68	107.85	294.41	205.44
16.45	0.77	142.60	116.08	299.59	206.77
17.93	1.17	147.58	120.45		
19.64	1.61			Series 7	
21.50	2.16	Series 4			
23.56	3.09			292.52	204.69
25.85	3.93	152.67	124.91	297.66	205.99
28.39	5.11	157.76	129.28	302.83	207.73
31.20	6.50	162.87	133.47	308.00	210.11
34.32	8.53	167.98	137.53	313.18	211.61
37.79	11.04	173.09	141.51	318.35	213.35
41.69	14.21	178.21	145.32	333.88	218.34
45.87	17.74	183.34	148.97	339.07	218.95
50.14	21.66	188.47	152.60	344.24	220.56
54.53	25.62	193.60	156.06	349.42	221.81
59.01	30.04	198.73	159.12		
63.57	34.62			Series 8	
68.21	39.34	Series 5			
72.91	44.29			332.59	216.71
77.67	49.42	192.95	155.34	337.75	218.99
82.49	53.30	198.03	159.11	342.93	220.64
87.32	59.36	203.18	162.52	348.12	220.96
		208.33	163.97	353.30	223.09
Series 2		213.48	167.87	358.48	223.27
		218.63	171.04	363.66	224.93
65.09	36.03	223.78	173.93	368.84	227.22
70.33	41.61	228.93	176.81	374.02	225.92
75.03	46.43	234.09	179.15	379.17	228.74
79.81	51.79	239.24	182.00	384.36	230.30
84.64	56.81	244.39	183.78	389.57	229.66
89.50	62.77	249.55	186.80	394.77	232.27
94.40	67.26			398.67	232.81
99.32	71.99	Series 6			
				Series 9	
Series 3		242.85	184.12		
		247.93	186.63	312.68	211.45
93.74	64.83	253.09	188.41	317.84	213.20
98.64	72.13	258.24	190.86	323.02	214.87
103.59	77.24	263.40	193.22	328.20	216.45
108.56	82.92	268.56	195.44	333.38	217.77
113.55	84.87	273.73	197.30	338.56	219.03

TABLE 3. Coefficients obtained from fitting the experimental heat capacities to equation (4).

Parameters	Coefficients	
	CaHfTi <sub>2</sub> O <sub>7</sub>	CaZr <sub>0.26</sub> Hf <sub>0.74</sub> Ti <sub>2</sub> O <sub>7</sub>
$m$	4.3706	3.9013
$\theta_D / \text{K}$	375.20	375.13
$n$	4.8135	4.7645
$\theta_E / \text{K}$	659.82	625.81
$A_1 \times 10^{-3}$	82.730	116.29
$A_2 \times 10^{-7}$	3.2782	-201.46
$\alpha$	0.10000	0.50000
$T_S / \text{K}$	31.295	39.000
$B_3 \times 10^4 / \text{J} \cdot \text{mol}^{-1} \cdot \text{K}^{-2}$	1.8729	-0.14358
$B_5 \times 10^8 / \text{J} \cdot \text{mol}^{-1} \cdot \text{K}^{-4}$	3.4763	115.02
$B_7 \times 10^{12} / \text{J} \cdot \text{mol}^{-1} \cdot \text{K}^{-6}$	7.3455	-1909.7
$B_9 \times 10^{12} / \text{J} \cdot \text{mol}^{-1} \cdot \text{K}^{-8}$	0.0000	1.3138
$B_{11} \times 10^{16} / \text{J} \cdot \text{mol}^{-1} \cdot \text{K}^{-10}$	0.0000	-3.2585

TABLE 4. Standard molar thermodynamic properties of  $\text{CaHfTi}_2\text{O}_7$ , including a residual entropy of  $\frac{1}{2}R\ln 2$  to account for disorder on the Ti(2) site.<sup>(12)</sup> The italicized values at  $T > 400$  K are extrapolated using equation (4) with the coefficients in Table 3.  $\Phi_m^\circ \equiv \Delta_0^T S_m^\circ - \Delta_0^T H_m^\circ / T$  ( $M = 426.3238 \text{ g}\cdot\text{mol}^{-1}$  and  $p^\circ = 100 \text{ kPa}$ .)

$T$ K	$C_{p,m}^\circ$ $\text{J}\cdot\text{K}^{-1}\cdot\text{mol}^{-1}$	$\Delta_0^T S_m^\circ$ $\text{J}\cdot\text{K}^{-1}\cdot\text{mol}^{-1}$	$\Delta_0^T H_m^\circ / T$ $\text{J}\cdot\text{K}^{-1}\cdot\text{mol}^{-1}$	$\Phi_m^\circ$ $\text{J}\cdot\text{K}^{-1}\cdot\text{mol}^{-1}$
0	0	2.882	0	2.882
5	0.02564	2.891	0.006656	2.884
10	0.2020	2.950	0.05063	2.899
15	0.7014	3.112	0.1726	2.939
20	1.897	3.440	0.4218	3.018
25	3.958	4.076	0.9148	3.161
30	6.532	5.016	1.628	3.388
35	9.753	6.256	2.551	3.705
40	13.61	7.804	3.686	4.118
45	17.93	9.653	5.026	4.627
50	22.51	11.78	6.544	5.234
60	32.03	16.72	9.993	6.724
70	42.25	22.41	13.86	8.550
80	52.97	28.75	18.08	10.67
90	63.79	35.61	22.56	13.06
100	74.50	42.89	27.22	15.67
110	84.93	50.48	31.99	18.49
120	95.04	58.31	36.83	21.48
130	104.8	66.30	41.68	24.62
140	114.1	74.41	46.52	27.89
150	123.0	82.58	51.32	31.26
160	131.4	90.79	56.06	34.73
170	139.3	99.00	60.73	38.26
180	146.8	107.2	65.31	41.87
190	153.9	115.3	69.79	45.52
200	160.4	123.4	74.16	49.21
210	166.6	131.3	78.41	52.93
220	172.3	139.2	82.55	56.67
230	177.7	147.0	86.57	60.43
240	182.7	154.7	90.47	64.20
250	187.4	162.2	94.26	67.97
260	191.9	169.7	97.93	71.74
270	196.2	177.0	101.5	75.50
273.15	197.5	179.3	102.6	76.69
280	200.2	184.2	104.9	79.26
290	204.1	191.3	108.3	83.00
298.15	207.0	197.0	111.0	86.03
300	207.7	198.3	111.5	86.72

$\frac{T}{K}$	$\frac{C_{p,m}^{\circ}}{J \cdot K^{-1} \cdot mol^{-1}}$	$\frac{\Delta_0^T S_m^{\circ}}{J \cdot K^{-1} \cdot mol^{-1}}$	$\frac{\Delta_0^T H_m^{\circ}/T}{J \cdot K^{-1} \cdot mol^{-1}}$	$\frac{\Phi_m^{\circ}}{J \cdot K^{-1} \cdot mol^{-1}}$
320	214.3	211.9	117.8	94.12
340	219.8	225.1	123.6	101.4
360	224.5	237.8	129.1	108.7
380	228.8	250.0	134.2	115.8
400	233.7	261.8	139.1	122.8
420	237.7	273.3	143.7	129.7
440	241.5	284.5	148.0	136.5
460	245.0	295.3	152.2	143.1
480	248.4	305.8	156.1	149.7
500	251.5	316.0	159.9	156.2
550	258.8	340.3	168.5	171.8
600	265.3	363.1	176.3	186.8
650	271.4	384.6	183.4	201.2
700	277.1	404.9	189.9	215.0
750	282.5	424.2	195.9	228.3
800	287.7	442.6	201.5	241.2
850	292.7	460.2	206.7	253.5
900	297.6	477.1	211.6	265.5
950	302.4	493.3	216.3	277.1
1000	307.1	508.9	220.7	288.3
1100	316.3	538.7	229.0	309.7
1200	325.3	566.6	236.6	329.9
1300	334.2	593.0	243.8	349.2
1400	343.0	618.0	250.6	367.5
1500	351.7	642.0	257.0	385.0

TABLE 5. Standard molar thermodynamic properties of  $\text{CaZr}_{0.26}\text{Hf}_{0.74}\text{Ti}_2\text{O}_7$ , including a residual entropy of  $7.646 \text{ J}\cdot\text{K}^{-1}\cdot\text{mol}^{-1}$  to account for disorder on the Ti(2) site<sup>(12)</sup> and random mixing of the Hf and Zr on the Zr site. The italicized values at  $T > 400 \text{ K}$  are extrapolated using equation (4) with the coefficients in Table 3.  
 $\Phi_m^\circ \equiv \Delta_0^T S_m^\circ - \Delta_0^T H_m^\circ / T$  ( $M = 404.5073 \text{ g}\cdot\text{mol}^{-1}$  and  $p^\circ = 100 \text{ kPa}$ .)

$T$ K	$C_{p,m}^\circ$ $\text{J}\cdot\text{K}^{-1}\cdot\text{mol}^{-1}$	$\Delta_0^T S_m^\circ$ $\text{J}\cdot\text{K}^{-1}\cdot\text{mol}^{-1}$	$\Delta_0^T H_m^\circ / T$ $\text{J}\cdot\text{K}^{-1}\cdot\text{mol}^{-1}$	$\Phi_m^\circ$ $\text{J}\cdot\text{K}^{-1}\cdot\text{mol}^{-1}$
0	0	7.646	0	7.646
5	0.001653	7.646	0.0001320	7.646
10	0.08285	7.662	0.01332	7.648
15	0.5464	7.763	0.09749	7.666
20	1.710	8.062	0.3398	7.722
25	3.510	8.626	0.7841	7.842
30	5.937	9.471	1.431	8.039
35	9.042	10.61	2.289	8.322
40	12.77	12.06	3.360	8.695
45	16.98	13.80	4.636	9.162
50	21.49	15.82	6.094	9.725
60	30.99	20.57	9.445	11.12
70	41.22	26.11	13.25	12.86
80	51.81	32.30	17.40	14.90
90	62.59	39.03	21.83	17.20
100	73.36	46.18	26.44	19.74
110	83.97	53.67	31.19	22.48
120	94.30	61.42	36.02	25.40
130	104.2	69.36	40.89	28.48
140	113.7	77.44	45.76	31.68
150	122.7	85.60	50.59	35.01
160	131.2	93.79	55.37	38.42
170	139.1	102.0	60.06	41.92
180	146.5	110.2	64.66	45.49
190	153.5	118.3	69.16	49.10
200	160.0	126.3	73.54	52.76
210	166.1	134.3	77.80	56.45
220	171.8	142.1	81.94	60.17
230	177.2	149.9	85.97	63.90
240	182.3	157.5	89.88	67.64
250	187.1	165.1	93.67	71.39
260	191.6	172.5	97.35	75.13
270	195.9	179.8	100.9	78.88
273.15	197.2	182.1	102.0	80.05
280	199.9	187.0	104.4	82.61
290	203.7	194.1	107.8	86.33
298.15	206.7	199.8	110.4	89.35

$\frac{T}{\text{K}}$	$\frac{C_{p,m}^{\circ}}{\text{J} \cdot \text{K}^{-1} \cdot \text{mol}^{-1}}$	$\frac{\Delta_0^T S_m^{\circ}}{\text{J} \cdot \text{K}^{-1} \cdot \text{mol}^{-1}}$	$\frac{\Delta_0^T H_m^{\circ}/T}{\text{J} \cdot \text{K}^{-1} \cdot \text{mol}^{-1}}$	$\frac{\Phi_m^{\circ}}{\text{J} \cdot \text{K}^{-1} \cdot \text{mol}^{-1}}$
300	207.3	201.0	111.0	90.04
320	213.8	214.6	117.2	97.40
340	219.4	227.8	123.1	104.7
360	224.4	240.5	128.6	111.9
380	229.0	252.7	133.7	119.0
400	233.8	264.6	138.6	126.0
420	237.9	276.1	143.2	132.8
440	241.8	287.2	147.6	139.6
460	245.5	298.1	151.8	146.3
480	248.9	308.6	155.8	152.8
500	252.2	318.8	159.6	159.2
550	259.8	343.2	168.3	174.9
600	266.6	366.1	176.3	189.9
650	272.9	387.7	183.4	204.3
700	278.7	408.1	190.0	218.1
750	284.2	427.5	196.1	231.4
800	289.3	446.1	201.8	244.3
850	294.3	463.7	207.1	256.6
900	299.0	480.7	212.1	268.6
950	303.5	497.0	216.8	280.2
1000	307.8	512.7	221.2	291.5
1100	316.0	542.4	229.5	312.9
1200	323.5	570.2	237.0	333.2
1300	330.6	596.4	243.9	352.5
1400	337.2	621.1	250.3	370.8
1500	343.2	644.6	256.3	388.3

TABLE 6. Standard molar thermodynamic properties of  $\text{CaZrTi}_2\text{O}_7$ ,<sup>(4)</sup> updated for a residual entropy of  $\frac{1}{2}R\ln 2$  to account for disorder on the Ti(2) site.<sup>(12)</sup> The italicized values at  $T > 400$  K are extrapolated using equation (4) with the coefficients given reference (4).  $\Phi_m^\circ \equiv \Delta_0^T S_m^\circ - \Delta_0^T H_m^\circ / T$  ( $M = 339.10 \text{ g}\cdot\text{mol}^{-1}$  and  $p^\circ = 100 \text{ kPa}$ .)

$T$ K	$C_{p,m}^\circ$ $\text{J}\cdot\text{K}^{-1}\cdot\text{mol}^{-1}$	$\Delta_0^T S_m^\circ$ $\text{J}\cdot\text{K}^{-1}\cdot\text{mol}^{-1}$	$\Delta_0^T H_m^\circ / T$ $\text{J}\cdot\text{K}^{-1}\cdot\text{mol}^{-1}$	$\Phi_m^\circ$ $\text{J}\cdot\text{K}^{-1}\cdot\text{mol}^{-1}$
0	0	2.882	0	2.882
5	0.1321	3.001	0.06128	2.940
10	0.3778	3.158	0.1511	3.007
15	0.8491	3.391	0.2974	3.094
20	1.658	3.737	0.5282	3.209
25	2.917	4.233	0.8717	3.361
30	4.731	4.916	1.36	3.560
35	7.186	5.821	2.00	3.816
40	10.32	6.977	2.84	4.136
45	14.11	8.406	3.88	4.528
50	18.49	10.11	5.12	4.999
60	28.56	14.35	8.16	6.190
70	39.63	19.58	11.86	7.719
80	51.06	25.62	16.05	9.571
90	62.46	32.29	20.57	11.72
100	73.66	39.45	25.32	14.13
110	84.58	46.99	30.21	16.77
120	95.16	54.80	35.19	19.62
130	105.4	62.82	40.20	22.63
140	115.1	70.99	45.20	25.79
150	124.4	79.26	50.18	29.08
160	133.3	87.57	55.10	32.48
170	141.6	95.91	59.94	35.96
180	149.5	104.2	64.70	39.52
190	156.9	112.5	69.36	43.15
200	163.8	120.7	73.91	46.82
210	170.3	128.9	78.35	50.53
220	176.3	137.0	82.67	54.28
230	182.0	144.9	86.87	58.05
240	187.3	152.8	90.94	61.83
250	192.2	160.5	94.89	65.62
260	196.8	168.2	98.73	69.42
270	201.2	175.7	102.4	73.22
273.15	202.5	178.0	103.6	74.41
280	205.2	183.1	106.0	77.01
290	209.0	190.3	109.5	80.79
298.15	211.9	196.2	112.3	83.86

$\frac{T}{K}$	$\frac{C_{p,m}^{\circ}}{J \cdot K^{-1} \cdot mol^{-1}}$	$\frac{\Delta_0^T S_m^{\circ}}{J \cdot K^{-1} \cdot mol^{-1}}$	$\frac{\Delta_0^T H_m^{\circ}/T}{J \cdot K^{-1} \cdot mol^{-1}}$	$\frac{\Phi_m^{\circ}}{J \cdot K^{-1} \cdot mol^{-1}}$
300	212.6	197.5	112.9	84.56
320	219.1	211.4	119.3	92.05
340	224.8	224.9	125.4	99.47
360	230.0	237.9	131.1	106.8
380	234.7	250.4	136.4	114.0
400	238.9	262.6	141.4	121.2
420	242.8	274.3	146.1	128.2
440	246.3	285.7	150.6	135.1
460	249.6	296.7	154.8	141.9
480	252.6	307.4	158.9	148.5
500	255.5	317.8	162.7	155.1
550	262.0	342.4	171.4	171.0
600	267.7	365.5	179.2	186.3
650	273.0	387.1	186.2	200.9
700	278.0	407.5	192.6	214.9
750	282.7	426.9	198.5	228.4
800	287.4	445.3	203.9	241.4
850	291.9	462.8	208.9	253.9
900	296.4	479.6	213.6	266.0
950	300.9	495.8	218.1	277.7
1000	305.5	511.3	222.4	289.0
1100	314.7	540.9	230.3	310.5
1200	324.3	568.7	237.8	330.9
1300	334.2	595.0	244.8	350.2
1400	344.6	620.2	251.6	368.6
1500	355.4	644.3	258.1	386.2

## FIGURE HEADINGS

FIGURE 1. Experimental heat capacities,  $C_{p,m}$ , of  $\text{CaHfTi}_2\text{O}_7$  (●) and  $\text{CaZr}_{0.26}\text{Hf}_{0.74}\text{Ti}_2\text{O}_7$  (▲) corrected for the  $\text{CaTiO}_3$  impurity. Inset (a) shows the low-temperature data on an expanded scale, and inset (b) shows the high-temperature extrapolation to  $T = 1500$  K. The lines through the data (—) represent the fits to the data. The  $\text{CaZr}_{0.26}\text{Hf}_{0.74}\text{Ti}_2\text{O}_7$  (▲) results have been offset by  $20 \text{ J}\cdot\text{K}^{-1}\cdot\text{mol}^{-1}$  for clarity in the main figure and in inset (b) and  $10 \text{ J}\cdot\text{K}^{-1}\cdot\text{mol}^{-1}$  in inset (a).

FIGURE 2. The per cent deviations of the measured heat capacity for  $\text{CaZr}_{0.26}\text{Hf}_{0.74}\text{Ti}_2\text{O}_7$  ( $C_{\text{meas}}$ ) from the calculated heat capacity ( $C_{\text{calc}}$ ) using the results of  $\text{CaZrTi}_2\text{O}_7$  and  $\text{CaHfTi}_2\text{O}_7$ . See text for details.

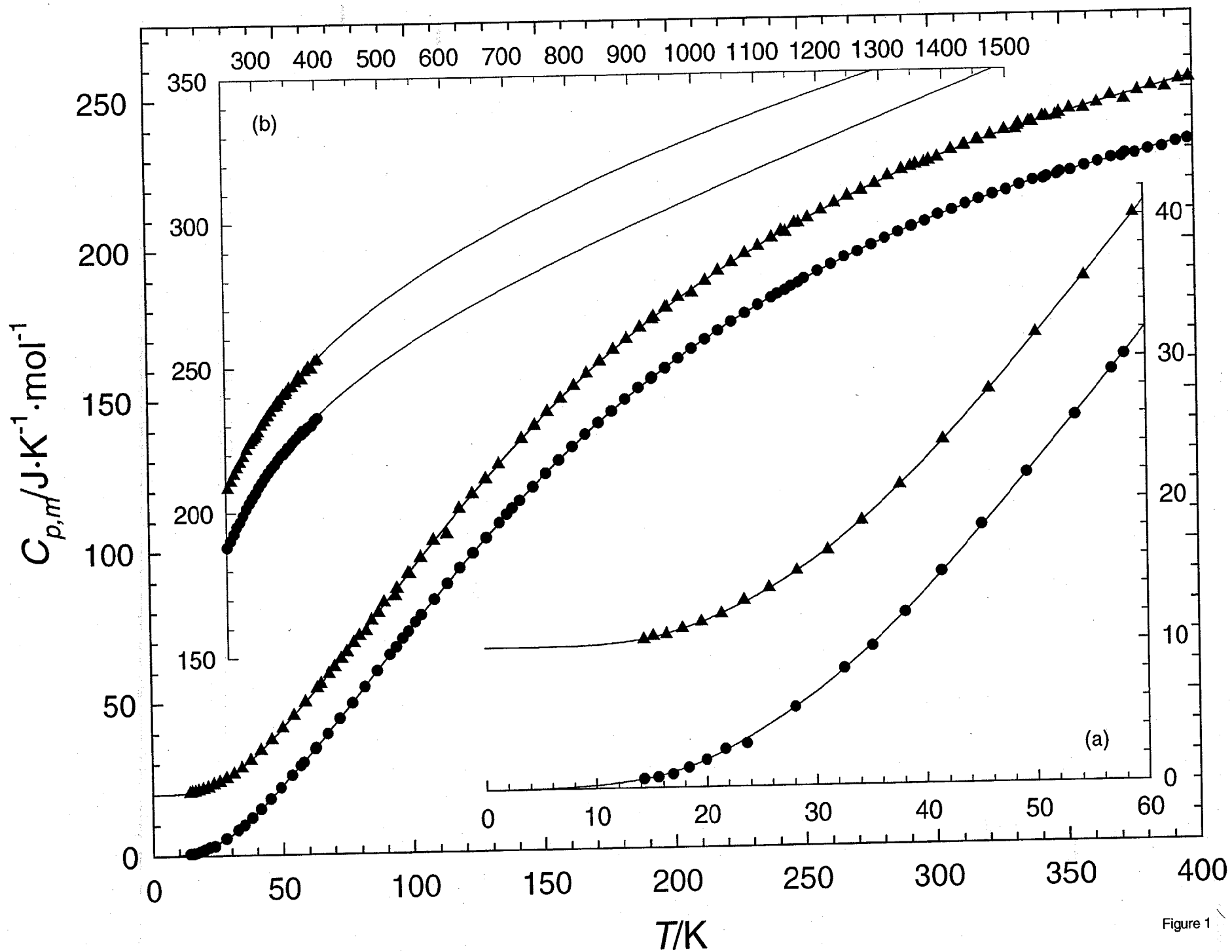


Figure 1

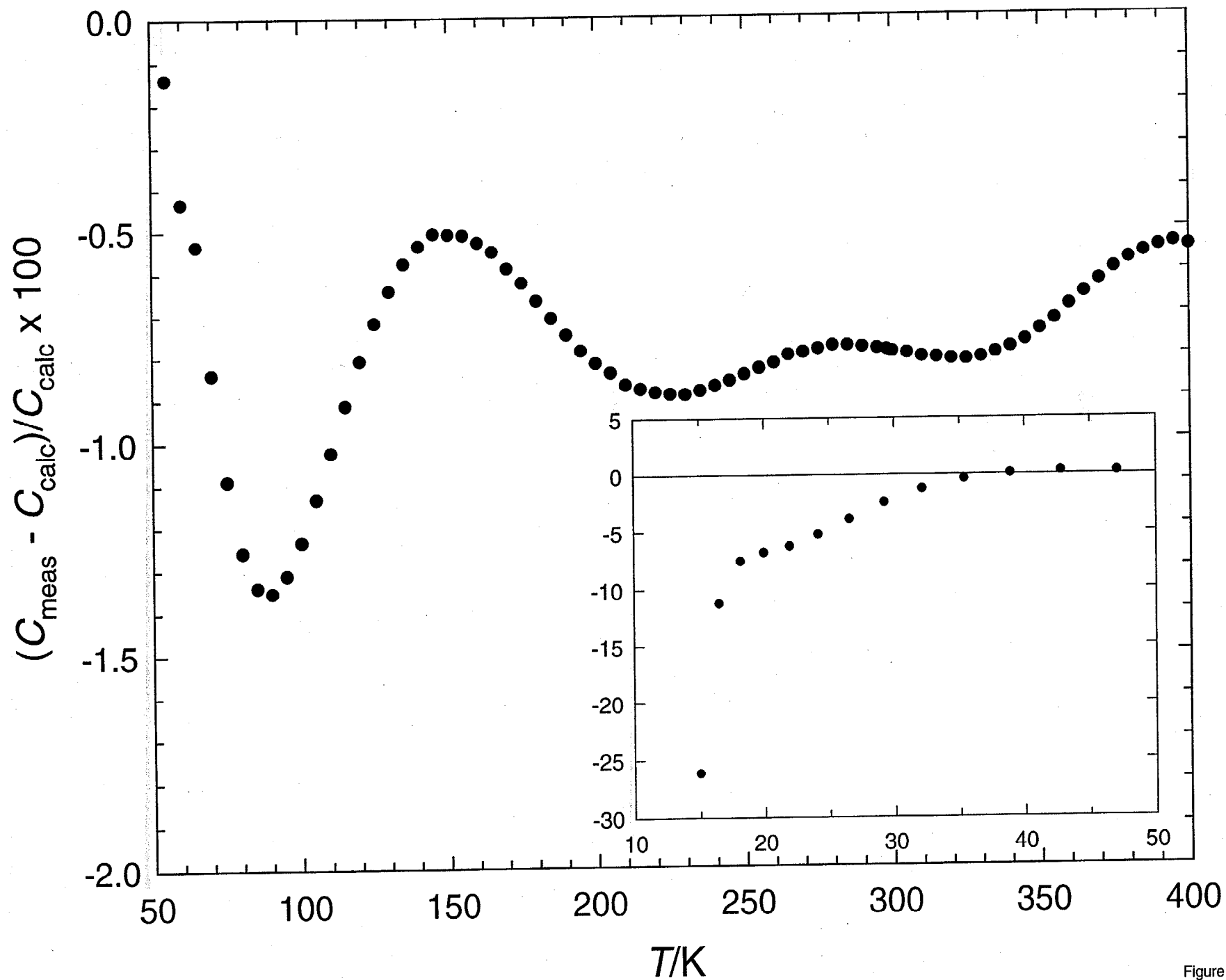


Figure 2

## ENTHALPIES OF FORMATION OF $Gd_2(Ti_{2-x}Zr_x)O_7$ PYROCHLORES

K.B. HELEAN<sup>1</sup>, B.D. BEGG<sup>2</sup>, A. NAVROTSKY<sup>1</sup>, B. EBBINGHAUS<sup>3</sup>, W.J. WEBER<sup>4</sup> and R.C. EWING<sup>5</sup>

<sup>1</sup> Thermochemistry Facility, Department of Chemical Engineering and Materials Science, The University of California at Davis, Davis, CA 95616, U.S.A.

<sup>2</sup> Materials Division, Australian Nuclear Science and Technology Organization, PMB 1, Menai, NSW 2234, Australia

<sup>3</sup> Lawrence Livermore National Laboratory, Livermore, CA 94550, U.S.A.

<sup>4</sup> Pacific Northwest National Laboratory, Richland, WA 99352, U.S.A.

<sup>5</sup> Department of Nuclear Engineering and Radiological Sciences, The University of Michigan, Ann Arbor, MI 48109, U.S.A.

### Abstract

A calorimetric investigation of the enthalpies of formation of  $Gd_2(Ti_{2-x}Zr_x)O_7$ , where  $0 \leq x \leq 2$  is underway. All samples exhibit pyrochlore ( $Fd3m$ ) peaks in their XRD patterns. However, where  $x=2$  significant local disorder is observed in the Raman spectra. Preliminary data for the enthalpies of formation from the oxides in kJ/mol are:  $x=0$ ,  $\Delta H_f = -113.4 \pm 2.7$ ;  $x=0.5$ ,  $\Delta H_f = -94.0 \pm 3.0$ ;  $x=1.0$ ,  $\Delta H_f = -74.2 \pm 4.9$ ;  $x=1.5$ ,  $\Delta H_f = -64.5 \pm 2.0$ ;  $x=2$ ,  $\Delta H_f = -52.2 \pm 4.8$ . Two additional samples,  $Gd_{1.80}Zr_{2.15}O_{7.00}$  (pyrochlore) and  $Gd_{2.15}Zr_{1.87}O_{7.00}$  (fluorite), were also studied. Their enthalpies of formation from the oxides in kJ/mole are  $-50.9 \pm 3.3$  and  $-46.4 \pm 3.4$  respectively. Replacing Ti with Zr, i.e. when  $x=2$ , destabilizes the pyrochlore in enthalpy by approximately 60 kJ/mol. The  $\Delta H_{mix}$  for the  $Gd_2(Ti_{2-x}Zr_x)O_7$  solid-solution series is positive and can be described by a regular solution formalism with an estimated interaction parameter,  $\Omega = +20$  kJ/mol. The results of this study suggest that the pyrochlore to fluorite transition enthalpy in  $Gd_2Zr_2O_7$  is small, of the order of the configurational entropy contribution due to cation disorder at the transition temperature,  $T\Delta S_{conf.} \approx 10$  kJ/mol.

### Introduction

Recent estimates indicate that the United States will designate approximately 13 metric tons of weapons plutonium for immobilization [1]. A crystalline ceramic waste form is under development, largely based on the SYNROC concept [2,3]. This ceramic lies in the pseudo-quaternary system consisting of  $CaHfTi_2O_7$ -  $CaPuTi_2O_7$ -  $CaUTi_2O_7$ -  $Gd_2Ti_2O_7$ . One consequence of incorporating plutonium into a crystalline matrix is the loss of long-range periodicity due to the accumulation of radiation damage, i.e. metamictization. The response of the ceramic to alpha-decay damage is, therefore, of interest.

Recent studies indicate that  $Gd_2Ti_2O_7$  pyrochlore ( $Fd3m$ ) becomes metamict under heavy ion irradiation [4,5,6,7]. The material becomes amorphous concurrent with a structural transformation of pyrochlore ( $Fd3m$ ) to an anion deficient fluorite ( $Fm3m$ ) due to cation disorder. The higher symmetry leads to a reduction of the lattice parameter,  $a$ , by a factor of two and the elimination of diffraction maxima associated with the pyrochlore super-cell. The substitution of Zr for Ti in  $Gd_2(Ti_{2-x}Zr_x)O_7$  was shown to increase the dose required for amorphization until, for pure  $Gd_2Zr_2O_7$ , the material remained crystalline under all experimental conditions [8,9,10,11,12]. The  $Gd_2Zr_2O_7$  end-member remained electron-diffraction crystalline up to a dose of 15 dpa.

In order to provide an energetic basis for the interpretation of the radiation damage mechanisms in Gd-pyrochlore, a calorimetric study is underway. This paper reports preliminary enthalpies of formation of  $\text{Gd}_2(\text{Ti}_{2-x}\text{Zr}_x)\text{O}_7$ , where  $0 \leq x \leq 2$ . The enthalpies of mixing of the solid-solution series are discussed.

### Experimental methods

Samples with the following nominal compositions,  $\text{Gd}_2(\text{Ti}_{2-x}\text{Zr}_x)\text{O}_7$ , where  $0 \leq x \leq 2$ , were prepared via an alkoxide route from a mixture of titanium iso-propoxide, tetrabutyl zirconate and gadolinium nitrate. Pellets of the dried products were sintered at 1600 °C for 50 hours in air. The details of sample preparation and characterization are reported elsewhere [10]. Two additional samples of nominal composition  $\text{Gd}_2\text{Zr}_2\text{O}_7$  were prepared by ball milling under methanol stoichiometric proportions of the binary oxides, pressing pellets and then sintering one sample at 1600 °C for 72 hours and then quenching in air. The second sample was sintered at 1500 °C for 480 hours in air.

Powder X-ray diffraction (XRD) data were collected using a Scintag PAD-V diffractometer with a 45 kV accelerating voltage and a Cu anode. Data were collected from 10 to 94 degrees  $2\theta$  with a 0.02 degree step size and a dwell time of 5 seconds. Lattice parameters were refined using Si as an internal standard.

Electron microprobe analysis was performed using a CAMECA SX-50 with an accelerating voltage of 20 kV and a spot size of 1  $\mu\text{m}$ . Quantitative chemical analyses were obtained using wave dispersive spectrometry (WDS) and  $\text{GdPO}_4$ ,  $\text{ZrO}_2$  and  $\text{TiO}_2$  (rutile) as standards. Back-scattered electron (BSE) imaging was used to assess sample homogeneity.

High temperature oxide melt solution calorimetry using a Tian-Calvet type calorimeter with a twinned design was used to measure the enthalpies of solution of the materials studied. The details of the calorimeter design and operation are described elsewhere [13,14]. Prior to calorimetry, powder samples were dried at 700 °C for a minimum of 1 hour. The solvent used in this study was sodium molybdate,  $3\text{Na}_2\text{O} \cdot 4\text{MoO}_3$ , at 975 K. Approximately 5 mg pellets were dropped from room temperature into the solvent. Calorimeters were calibrated using the heat content of  $\alpha\text{-Al}_2\text{O}_3$ . Oxygen was bubbled through the melt to aid in the dissolution of the pellets [14]. The measured values of drop solution were used in the appropriate thermodynamic cycles to calculate the enthalpy of formation from the oxides. Reference data for the enthalpies of formation from the elements for the binary oxides were used to calculate the enthalpies of formation from the elements for the compounds.

### Results

The samples used in this study deviate from their target compositions (Table 1). Both end-members,  $\text{Gd}_2\text{Ti}_2\text{O}_7$  and  $\text{Gd}_2\text{Zr}_2\text{O}_7$ , are considered stoichiometric for the purposes of interpreting the calorimetric data. The solid-solution samples prepared at PNNL are all slightly Gd-rich and Zr-poor. The two Gd-zirconate samples prepared at UCD deviate significantly from stoichiometry. The pyrochlore sample is Gd-poor:  $\text{Gd}_{1.80}\text{Zr}_{2.15}\text{O}_{7.00}$ . The fluorite sample is Gd-rich:  $\text{Gd}_{2.15}\text{Zr}_{1.87}\text{O}_{7.00}$  and contains approximately two mole percent unreacted  $\text{ZrO}_2$ , as estimated from analysis of BSE images.

Lattice parameters reflect a systematic increase in unit cell size with increasing Zr content. For the  $\text{Gd}_2\text{Zr}_2\text{O}_7$  prepared at PNNL, both the pyrochlore and fluorite cell parameters are reported. Poorly developed ( $\approx 1\%$  relative intensity) pyrochlore super-cell peaks are observed

in the X-ray diffraction pattern. Raman spectra show a distinct diminution of peaks associated with local order in  $Gd_2Zr_2O_7$  [10]. The lattice parameters reported here match, within error, values previously reported for the two end-member compositions [15].

TABLE 1. Sample descriptions of  $Gd_2(Ti_{2-x}Zr_x)O_7$ , where  $0 \leq x \leq 2$  plus two additional Gd-zirconate samples. Calculated stoichiometries are based on SEM-EDS or WDS quantitative chemical analyses. Errors are reported in parentheses.

Calculated stoichiometry	structure type P=pyro., F=fluorite	unit cell parameter <i>a</i> (nm)	source
$Gd_{2.01}Ti_{1.99}O_{7.00}$	P	1.0185(5)	LLNL <sup>1</sup>
$Gd_{2.03}Ti_{1.51}Zr_{0.47}O_{7.00}$	P	1.02827(6)	PNNL <sup>2</sup>
$Gd_{2.07}Ti_{1.01}Zr_{0.93}O_{7.00}$	P	1.03746(9)	PNNL
$Gd_{2.06}Ti_{0.51}Zr_{1.44}O_{7.00}$	P	1.04557(5)	PNNL
$Gd_{1.80}Zr_{2.15}O_{7.00}$	P	1.04907 (7)	UCD <sup>3</sup>
$Gd_{2.00}Zr_{2.00}O_{7.00}$	P	1.05352 (6)	PNNL
	F	0.52676 (3)	
$Gd_{2.15}Zr_{1.87}O_{7.00} +$ 2mol.% $ZrO_2$ impurity	F	0.52736 (8)	UCD

<sup>1</sup>sample provided by Lawrence Livermore National Laboratory

<sup>2</sup>samples prepared at Pacific Northwest National Laboratory

<sup>3</sup>samples prepared at the University of California at Davis

Calorimetric data are considered preliminary where the number of experiments is less than six (Table 2). The relatively large error in the enthalpy of drop solution for  $Gd_2TiZrO_7$  is a result of the very small heat effect obtained in each experiment due to the compensation of the heat content and the heat of solution which, for this sample, are approximately equal in magnitude but of opposite sign. Thermodynamic cycles are applied in order to calculate the enthalpies of formation from the oxides (Table 3). The thermodynamic cycles are corrected for stoichiometry and the  $\Delta H_{ds}$  values used in the cycles are corrected for impurities. Using reference data, standard  $\Delta H_f$ , i.e. formation enthalpies from the elements, were calculated (Table 4) [16].

## Discussion

The X-ray diffraction patterns show a diminution of pyrochlore ( $Fd3m$ ) peaks relative to the fluorite ( $Fm3m$ ) sub-cell when Zr is substituted for Ti in  $Gd_2(Ti_{2-x}Zr_x)O_7$  (Fig. 1). They also show substantial peak broadening. The Raman spectra show a diminution of the vibrational modes attributed to the pyrochlore structure [10]. Such effects may reflect an ingrowth of fluorite-structured material at the expense of pyrochlore or, alternatively, a gradual disordering of the pyrochlore phase. Further thermodynamic and structural studies, including HRTEM and Rietveld refinement of the X-ray diffraction patterns, are in progress to quantify these effects.

Table 2. Drop solution calorimetry data (kJ/mol). Errors are calculated as two standard deviations of the mean. N=number of experiments.

Phase	$\Delta H_{ds}$ (kJ/mol)	error	N
Gd <sub>2.01</sub> Ti <sub>1.99</sub> O <sub>7.00</sub>	82.71	2.11	12
Gd <sub>2.03</sub> Ti <sub>1.51</sub> Zr <sub>0.47</sub> O <sub>7.00</sub>	41.53	2.02	4
Gd <sub>2.07</sub> Ti <sub>1.01</sub> Zr <sub>0.93</sub> O <sub>7.00</sub>	1.90	4.01	4
Gd <sub>2.06</sub> Ti <sub>0.51</sub> Zr <sub>1.44</sub> O <sub>7.00</sub>	-30.02	0.77	2
Gd <sub>1.80</sub> Zr <sub>2.15</sub> O <sub>7.00</sub>	-40.45	1.33	3
Gd <sub>2.00</sub> Zr <sub>2.00</sub> O <sub>7.00</sub>	-56.96	3.74	3
Gd <sub>2.15</sub> Zr <sub>1.87</sub> O <sub>7.00</sub> *	-77.94	1.63	3
Gd <sub>2</sub> O <sub>3</sub>	-148.54	1.60	10
TiO <sub>2</sub>	58.95	1.34	12
ZrO <sub>2</sub> **	19.70	1.80	9

\*corrected for impurity;\*\*data taken from [17]

Table 3. Thermodynamic cycle used in calculating enthalpies of formation from the oxides (kJ/mol). Errors are propagated assuming independent, linear combinations.

	Reaction ( $0 \leq x \leq 2$ )
$\Delta H_1$	Gd <sub>2</sub> (Ti <sub>2-x</sub> Zr <sub>x</sub> )O <sub>7</sub> crystal, 298 K $\rightarrow$ {Gd <sub>2</sub> O <sub>3</sub> + (2-x)TiO <sub>2</sub> + xZrO <sub>2</sub> } solution, 975 K
$\Delta H_2$	Gd <sub>2</sub> O <sub>3</sub> crystal, 298 K $\rightarrow$ Gd <sub>2</sub> O <sub>3</sub> solution, 975 K
$\Delta H_3$	(2-x)TiO <sub>2</sub> crystal, 298 K $\rightarrow$ (2-x)TiO <sub>2</sub> solution, 975 K
$\Delta H_4$	xZrO <sub>2</sub> crystal, 298 K $\rightarrow$ xZrO <sub>2</sub> solution, 975 K
$\Delta H_f(\text{oxides})$	$= -\Delta H_1 + \Delta H_2 + \Delta H_3 + \Delta H_4$

Table 4. Calculated enthalpies of formation from the oxides and the elements (kJ/mol). Errors are calculated as two standard deviations of the mean.

phase	$\Delta H_f$ oxides (kJ/mol)	$\Delta H_f$ elements (kJ/mol)
Gd <sub>2.01</sub> Ti <sub>1.99</sub> O <sub>7.00</sub>	-113.4±2.7	-3822.5
Gd <sub>2.03</sub> Ti <sub>1.51</sub> Zr <sub>0.47</sub> O <sub>7.00</sub>	-94.0±3.0	-3884.8
Gd <sub>2.07</sub> Ti <sub>1.01</sub> Zr <sub>0.93</sub> O <sub>7.00</sub>	-74.2±4.9	-3935.2
Gd <sub>2.06</sub> Ti <sub>0.51</sub> Zr <sub>1.44</sub> O <sub>7.00</sub>	-64.5±2.0	-4005.3
Gd <sub>1.80</sub> Zr <sub>2.15</sub> O <sub>7.00</sub>	-50.9±3.3	-4054.8
Gd <sub>2.00</sub> Zr <sub>2.00</sub> O <sub>7.00</sub>	-52.2±4.8	-4072.9
Gd <sub>2.15</sub> Zr <sub>1.87</sub> O <sub>7.00</sub>	-46.4±3.4	-4060.5

Regardless of their structural state, all of the phases studied are stable with respect to the oxides (Table 4). As Zr substitutes for Ti in  $\text{Gd}_2(\text{Ti}_{2-x}\text{Zr}_x)\text{O}_7$ , the enthalpies of formation from the oxides becomes more endothermic (Fig. 2). Replacing Ti with Zr destabilizes the structure in enthalpy by approximately 60 kJ/mol. The data for the two off-stoichiometry Gd-zirconate samples are plotted for comparison (Fig. 2). The enthalpies of formation of the predominately fluorite-structured PNNL  $\text{Gd}_2\text{Zr}_2\text{O}_7$  and that of the UCD  $\text{Gd}_{1.80}\text{Zr}_{2.15}\text{O}_7$  sample which was sintered for 480 hours below the pyrochlore-to-fluorite transition temperature to maximize the cation ordering associated with the pyrochlore structure, are, within error, the same. The UCD fluorite sample,  $\text{Gd}_{2.15}\text{Zr}_{1.87}\text{O}_{7.00}$  is less stable in enthalpy than the other Gd-zirconate samples by  $5 \pm 3$  kJ/mol. No quantitative assessment of the enthalpy of the pyrochlore to fluorite transition ( $\Delta H_{p-f}$ ) can be made at this time. However, qualitatively, the magnitude of the transition appears to be small, of the order of the  $T\Delta S_{\text{conf}}$  contribution due to cation disorder at the transition temperature (1530 °C), approximately 10 kJ/mol.

There are two possible interpretations of the calorimetric data for the  $\text{Gd}_2(\text{Ti}_{2-x}\text{Zr}_x)\text{O}_7$  solid solution. If these samples are homogeneous single phase pyrochlores, then an enthalpy of mixing can be calculated as the difference between the calculated  $\Delta H_f$  and the calculated  $\Delta H_{\text{ideal}}$  which is represented as a dotted line on the plot of formation enthalpy (Fig. 2). The mixing of Zr and Ti in  $\text{Gd}_2(\text{Ti}_{2-x}\text{Zr}_x)\text{O}_7$  is positive and can be approximated by the regular solution formalism where the interaction parameter,  $\Omega$ , is approximately +20 kJ/mol (Fig. 3). Note the relatively large ( $\approx 5$  kJ/mol) errors on the calculated  $\Delta H_{\text{mix}}$ . These data are being refined. The value for  $\Omega$  will change in magnitude but not in sign.

Another interpretation is to assume that all of the samples in the Zr-Ti solid-solution series represent a mixture of pyrochlore and fluorite microdomains. The calorimetric data would then reflect the contributions of two domains which may have different compositions. Current work in progress focuses on the structural details of these samples so that the appropriate interpretation of the calorimetric data can be made.

### Acknowledgments

Financial support was provided by Lawrence Livermore National Laboratory, the Department of Energy EMSP grant number 60118 and grant number DE-FG07-97ER45673 and the University of California at Davis. RCE and WJW were supported by the Office of Basic Energy Sciences, DOE grants DE-FG02-97ER45656 and DE-AC06-76RL01830, respectively.

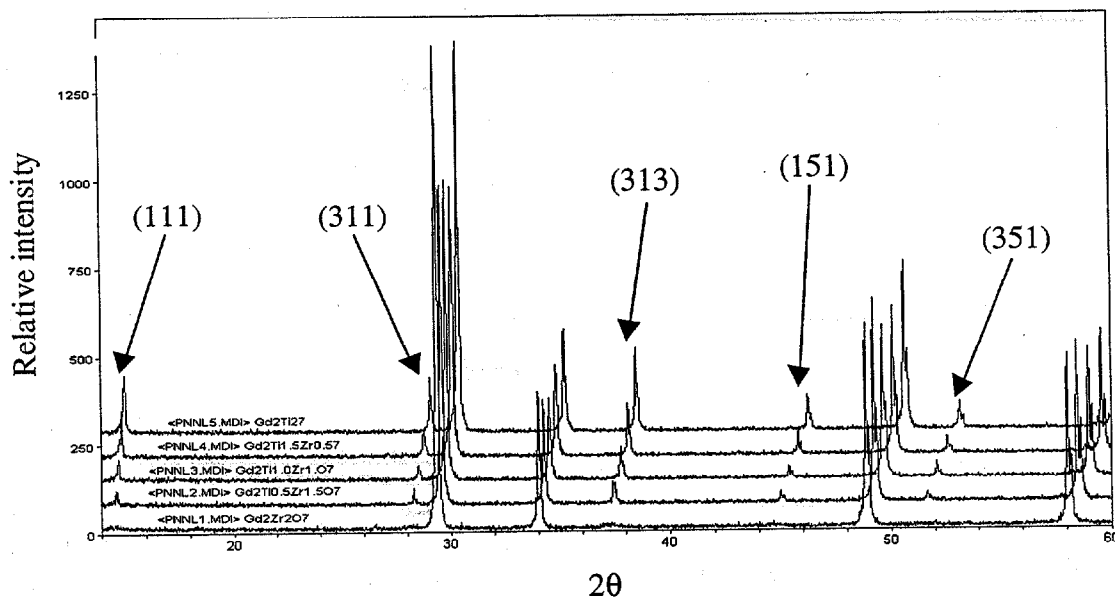


Fig. 1. XRD patterns for the  $\text{Gd}_2(\text{Ti}_{2-x}\text{Zr}_x)\text{O}_7$  solid solution series. Note the diminution of  $I/I_{\text{max}}$  of the peaks related to the pyrochlore super-structure when Zr replaces Ti.

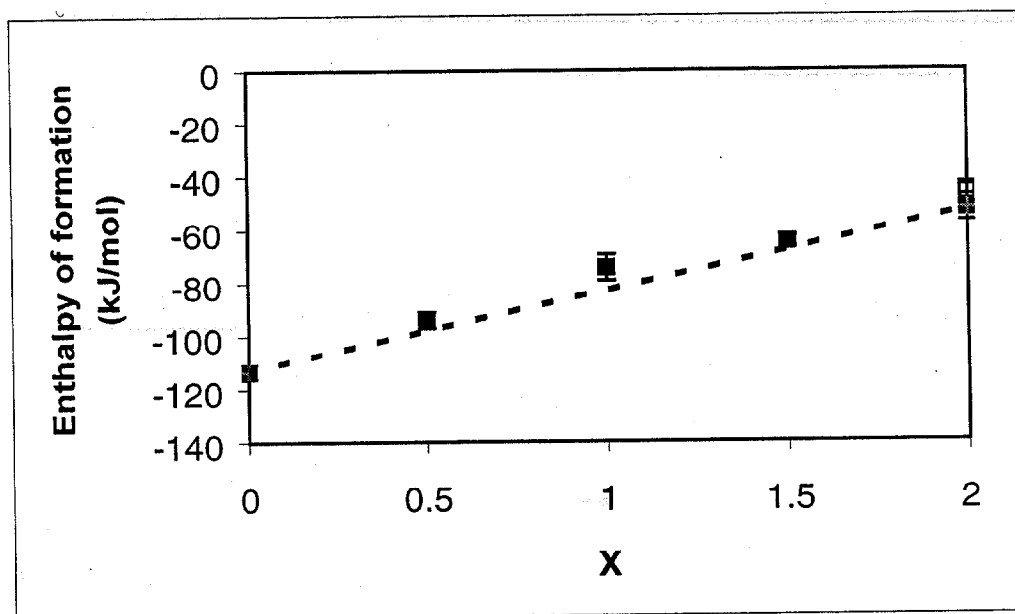


Fig. 2. Enthalpies of formation of  $\text{Gd}_2(\text{Ti}_{2-x}\text{Zr}_x)\text{O}_7$  where  $0 \leq x \leq 2$ . The ideal mixing curve is shown as a dotted line. Data for the two off-stoichiometry Gd-zirconate samples are plotted for comparison. The open symbol represents the UCD fluorite sample.

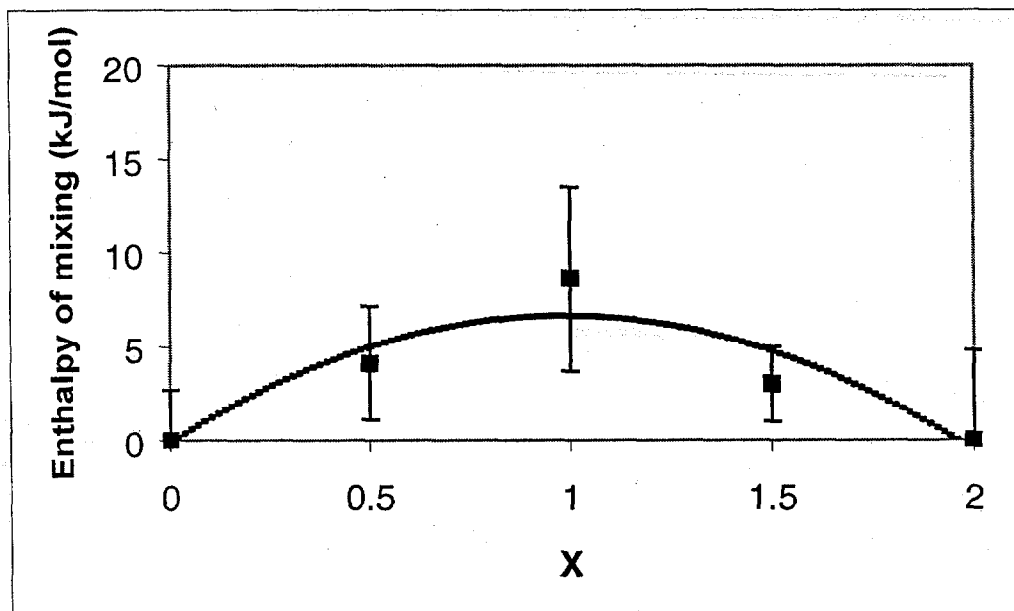


Fig. 3. Mixing enthalpy for  $Gd_2(Ti_{2-x}Zr_x)O_7$ . Within the error of the data, a regular solution model describes the trend with an interaction parameter,  $\Omega = +20$  kJ/mol.

## References

- [1] Record of Decision for the Storage and Disposition of Weapons-usable Fissile Materials, Final Programmatic Environmental Impact Statement, January 14, 1997, U.S. Department of Energy, Washington, D.C. 1997.
- [2] A.E. Ringwood (1978) Safe Disposal of High Level Nuclear Reactor Wastes: A New Strategy, ANU Canberra, Australia.
- [3] A.E. Ringwood, S.E. Kessen, K.D. Reeve, D.M. Levins and E.J. Ramm, in Radioactive Waste Forms for the Future, Eds. W. Lutze and R.C. Ewing, Elsevier, North-Holland, Amsterdam, Netherlands, pp 233-334 (1988).
- [4] W.J. Weber, J.W. Wald and H.J. Matzke (1985) Self-radiation damage in Cm-doped  $Gd_2Ti_2O_7$ , Materials Letters, 3, 173-180.
- [5] W.J. Weber, J.W. Wald and H.J. Matzke (1986) Effects of self-radiation damage in Cm-doped  $Gd_2Ti_2O_7$  and  $CaZrTi_2O_7$ , Journal of Nuclear Materials, 138, 196-209.
- [6] W.J. Weber and N.J. Hess (1993) Ion beam modification of  $Gd_2Ti_2O_7$ , Nuclear Instrumentation and Methods, B80/81, 1245-1251.
- [7] S.X. Wang, L.M. Wang, R.C. Ewing and K.V. Govidan Kutty (2000) Ion irradiation of rare-earth and yttrium-titanate pyrochlores, Nucl. Instrum. Methods Physics Res. B., 169, 135-140.
- [8] S.X. Wang, B.D. Begg, L.M. Wang, R.C. Ewing, W.J. Weber and K.V. Govidan Kutty (1999) Journal of Materials Research, 14(12), 4470-4473.

- [9] S.X. Wang, L.M. Wang, R.C. Ewing and K.V. Govidan Kutty (1999) Microstructural Processes in Irradiated Materials, edited by S.J. Zinkle G.E. Lucas, R.C. Ewing and J.S. Williams, Materials Research Society Symposium Proceedings, vol.540, 355-360.
- [10] B. D. Begg, N.J. Hess, D.E. McCready, S. Thevuthasan and W.J. Weber (2000) Heavy-ion irradiation effects in  $(\text{Gd}_2(\text{Ti}_{2-x}\text{Zr}_x)\text{O}_7)$  pyrochlores, American Ceramic Society Symposium Proceedings, 107, 553-560.
- [11] K.E. Sickafus, L. Minervini, R.W. Grimes, J.A. Valdez, M. Ishimaru, F. Li, K.J. McClellan and T. Hartman (2000) Radiation tolerance of complex oxides, Science, 289, 748-751.
- [12] W.J. Weber and R.C. Ewing (2000) Plutonium immobilization and radiation effects, Science, 289(5487), 2051.
- [13] A. Navrotsky (1997) Progress and new directions in high temperature calorimetry revisited, Phys. Chem. Minerals, 24, 222-241.
- [14] J.M. McHale, G.R. Kowach, A. Navrotsky and F.J. DiSalvo (1996) Thermochemistry of metal nitrides in the Ca/Zn/N system, Chem. Eur. J. 2, 1514.
- [15] Handbook on the physics and chemistry of rare earths, vol. 16, Eds. Gschneidner, K.A. and L. Eyring, Elsevier, North-Holland, Amsterdam, Netherlands, pp 589 (1993).
- [16] R.A. Robie, B.S. Hemingway, Thermodynamic Properties of Minerals and Related Substances at 298.15 and 1 Bar ( $10^5$  Pascals) Pressure and at Higher Temperatures (U.S. Government Printing Office: Washington, D.C. 1995).
- [17] I. Molodetsky (1999) Energetics of Zirconia Stabilized by Cation and Nitrogen Substitution, Ph.D. Dissertation, Princeton University.